AD-A090 028   RCA LABS PRINCETON NJ   F/G 11/6
CORROSION OF METAL FILMS WITH DEFECTIVE SURFACE PROTECTION LAYE--ETC(U)
JUL 80   R B COMIZZOLI, L K WHITE, W KERN   F30602-78-C-0276
UNCLASSIFIED   PRRL-79-CR-42   RADC-TR-80-236   NL

1 OF 2
AD A
090028

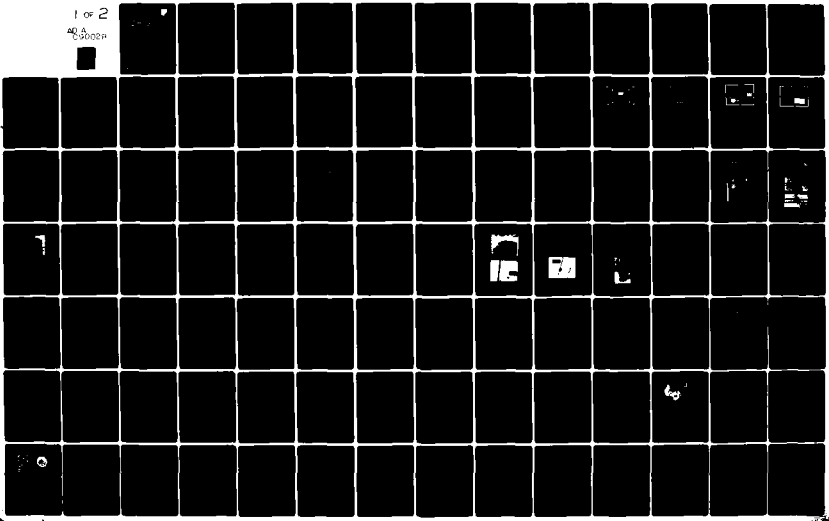

JL

LEVEL II

12

RADC-TR-80-236
Final Technical Report
July 1980

CORROSION OF METAL FILMS WITH DEFECTIVE SURFACE PROTECTION LAYERS

RCA Laboratories

R. B. Comizzoli
L. K. White
W. Kern
G. L. Schnable

APPROVED FOR PUBLIC RELEASE; DISTRIBUTION UNLIMITED

ROME AIR DEVELOPMENT CENTER
Air Force Systems Command
Griffiss Air Force Base, New York 13441

This report has been reviewed by the RADC Public Affairs Office (PA) and is releasable to the National Technical Information Service (NTIS). At NTIS it will be releasable to the general public, including foreign nations.

RADC-TR-80-236 has been reviewed and is approved for publication.

APPROVED: John J. Bart

JOHN J. BART
Project Engineer

APPROVED: David C. Luke

DAVID C. LUKE, Lt Col, USAF
Chief, Reliability & Compatibility Division

FOR THE COMMANDER: John P. Huss

JOHN P. HUSS
Acting Chief, Plans Office

SUBJECT TO EXPORT CONTROL LAWS

This document contains information for manufacturing or using munitions of war. Export of the information contained herein, or release to foreign nationals within the United States, without first obtaining an export license, is a violation of the International Traffic in Arms Regulations. Such violation is subject to a penalty of up to 2 years imprisonment and a fine of $100,000 under 22 U.S.C 2778.

Include this notice with any reproduced portion of this document.

If your address has changed or if you wish to be removed from the RADC mailing list, or if the addressee is no longer employed by your organization, please notify RADC (RBRP) Griffiss AFB NY 13441. This will assist us in maintaining a current mailing list.

Do not return this copy. Retain or destroy.

UNCLASSIFIED
SECURITY CLASSIFICATION OF THIS PAGE (When Data Entered)

⑲ **REPORT DOCUMENTATION PAGE**	READ INSTRUCTIONS BEFORE COMPLETING FORM
⑱ 1. REPORT NUMBER RADC-TR-80-236 2. GOVT ACCESSION NO. AD-A090 028	3. RECIPIENT'S CATALOG NUMBER
⑥ 4. TITLE (and Subtitle) CORROSION OF METAL FILMS WITH DEFECTIVE SURFACE PROTECTION LAYERS.	⑨ 5. TYPE OF REPORT & PERIOD COVERED Final Technical Rep[redacted]t, 1 Sep 78 — 31 Aug 79, ⑭ 6. PERFORMING ORG. REPORT NUMBER PRRL-79-CR-42
⑩ 7. AUTHOR(s) R. B. Comizzoli W. Kern L. K. White G. L. Schnable	⑮ 8. CONTRACT OR GRANT NUMBER(s) F30602-78-C-0276 new
9. PERFORMING ORGANIZATION NAME AND ADDRESS RCA Lab[redacted]s Princeton NJ 08540	10. PROGRAM ELEMENT, PROJECT, TASK AREA & WORK UNIT NUMBERS 61102F ⑯ 2306J401 ⑰ J4
11. CONTROLLING OFFICE NAME AND ADDRESS Rome Air Development Center (RBRP) Griffiss AFB NY 13441	⑪ 12. REPORT DATE Jul[redacted]980 13. NUMBER OF PAGES 137
14. MONITORING AGENCY NAME & ADDRESS (if different from Controlling Office) Same ⑫ 136	15. SECURITY CLASS. (of this report) UNCLASSIFIED 15a. DECLASSIFICATION DOWNGRADING SCHEDULE N/A

16. DISTRIBUTION STATEMENT (of this Report)

Approved for public release; distribution unlimited.

17. DISTRIBUTION STATEMENT (of the abstract entered in Block 20, if different from Report)

Same

18. SUPPLEMENTARY NOTES

RADC Project Engineer: John J. Bart (RBRP)

19. KEY WORDS (Continue on reverse side if necessary and identify by block number)

Thin Film Corrosion
Deposited Dielectric Layers
Aluminum Thin Films
Gold Thin Films
Contaminants
Electrochemical Measurements
Surface pH Measurements

20. ABSTRACT (Continue on reverse side if necessary and identify by block number)

Corrosion of thin-film aluminum and gold under defect-containing passivation layers of phosphorus-doped SiO_2 and plasma-deposited silicon nitride was investigated. Metal test patterns with corresponding passivation patterns, including deliberate passivation defects, made it possible to measure both corrosion current and corrosion rate. Measurements were done as a function of relative humidity and temperature. → next page

(Cont'd)

DD FORM 1 JAN 73 1473 EDITION OF 1 NOV 65 IS OBSOLETE

UNCLASSIFIED
SECURITY CLASSIFICATION OF THIS PAGE (When Data Entered)

299 000

Item 20 (Cont'd)

cont.

Electrochemical bias techniques were used to determine the relative corrosion stabilities of various metallized substrates. Fluoride and chloride contaminants produced greatly accelerated corrosion reactions for aluminized films. Alloying aluminum films improved their corrosion stability. The H_2 in the forming gas ambient during alloying further improved the corrosion stability. Measurements of film stress versus corrosion stability did not correlate well. However, films under compressive stress may exhibit an improved corrosion stability.

Fluorescent pH indicators were tested as a method of decorating IC devices. On aluminized IC devices in the presence of bias, some indicators exhibited fluorescence at localized sites.

The effect on corrosion current of various surface treatments such as heating, etching, storage, and surface chemical modification were examined. Application of hexamethyldisilazane reduced surface currents by a factor varying from 100X to 1000X.

PREFACE

This Final Report was prepared by RCA Laboratories, Princeton, NJ, under Contract No. F30602-78-C-0276. It describes work performed from 1 September 1978 to 31 August 1979 in the Integrated Circuit Technology Center, J. H. Scott, Director. The Project Supervisor was G. L. Schnable, and the Project Scientist was R. B. Comizzoli. Other Members of Technical Staff who participated in this program were C. A. Deckert, W. Kern, and L. K. White. Test device processing was done by D. A. Peters and R. D. Vibronek. J. Zelez contributed to the section on metal stress. Defect analysis was done by C. E. Tracy. A. W. Fisher, R. E. Allen, L. Jacobus, and W. Kurylo also assisted in certain areas. M. D. Coutts, J. H. Thomas, E. P. Bertin, B. L. Goydish, and H. H. Whitaker performed special analytical studies. The Air Force Technical Monitor was J. J. Bart of RADC.

Publication of this report does not constitute Air Force approval of the findings or conclusions. It is published only for the exchange and stimulation of ideas.

TABLE OF CONTENTS

Section Page

TABLE OF CONTENTS (Continued)

TABLE OF CONTENTS (Continued)

LIST OF ILLUSTRATIONS

LIST OF ILLUSTRATIONS (Continued)

LIST OF ILLUSTRATIONS (Continued)

LIST OF ILLUSTRATIONS (Continued)

LIST OF TABLES

EVALUATION

This final technical report describes the results of one of the initial studies performed under the Device Reliability Research task at the Rome Air Development Center. This is an Air Force Office of Scientific Research sponsored task directed toward the elucidation of the chemical and physical mechanisms which affect the reliability of solid state electronic devices.

This report covers an effort to quantitatively define the mechanisms of corrosion and electrochemical transport of thin metal fims used for interconnection of active areas in microelectronic devices. There is a critical need for this basic information.

Corrosion represents a severe hazard to fine line geometry microcircuits and there is a high degree of complexity involved with determining the kinetics of the various mechanisms on thin film structures.

Additional research will be pursued in thin film corrosion. Emphasis will be placed on developing approaches toward minimizing the severity of the corrosion of microcircuit metallization layers. Ultimately, the basic information gained on these studies will be transitioned to the exploratory development program in solid state device reliability. This latter program establishes procedures for assuring solid state device reliability through use of proper design and test procedures. These procedures are then documented in the specifications and standards for which RADC is the preparing activity.

John J. Bart

JOHN J. BART
Project Engineer

SECTION I

SUMMARY

Corrosion of thin-film aluminum and gold under defect-containing passivation layers of phosphorus-doped SiO_2 and plasma-deposited silicon nitride was investigated. Metal test patterns with corresponding passivation patterns, including deliberate passivation defects, made it possible to measure both corrosion current and corrosion rate. Measurements were done as a function of relative humidity and temperature. The humidity dependence agrees with that of adsorbed water film. Sputtered aluminum was more corrosion resistant than filament-evaporated aluminum. The presence of sodium contamination increased the aluminum corrosion rate by a factor of 5. The silicon nitride-passivated devices took much longer to corrode than did the phosphorus-doped SiO_2-passivated devices.

Electrochemical bias techniques were used to determine the relative corrosion stabilities of various metallized substrates. Fluoride and chloride contaminants produced greatly accelerated corrosion reactions for aluminized films. Alloying aluminum films [i.e., heating at 450°C for 20 minutes in nitrogen or forming gas (90% N_2 and 10% H_2)] improved their corrosion stability. The H_2 in the forming gas ambient during alloying further improved the corrosion stability. Measurements of film stress versus corrosion stability did not correlate well. However, films under compressive stress may exhibit an improved corrosion stability. Gold-trimetal (Au-Pt-Ti) films examined under electrochemical bias showed anodic-type reactions. Only small changes in the electrochemical behavior were observed in the presence of chloride contaminant for these films.

Methods for controlled sodium contamination were developed. Analysis of sodium motion indicated that the sodium penetrates aluminum layers during typical alloying treatments, and that the deposition of phosphorus-doped SiO_2 getters about 65% of the sodium from the thermal oxide and/or aluminum on the substrate. Ambient contamination effects with chlorine, HF vapor, and vapors outgassed from epoxy plastic were examined.

Fluorescent pH indicators were tested as a method of decorating IC devices. On aluminized IC devices in the presence of bias, some indicators

exhibited fluorescence at localized sites. Gold-metallized IC devices, coated with a fluorescent indicator solution actively exhibiting fluorescence, showed deactivation of the indicator at localized sites. These indicators appear to have the ability to detect localized corrosion sites on ICs and may be able to identify the specific defects that produce corrosion processes.

The effect on corrosion current of various surface treatments such as heating, etching, storage, and surface chemical modification were examined. Application of hexamethyldisilazane reduced surface currents by a factor varying from 100X to 1000X.

SECTION II

INTRODUCTION

A. CORROSION AND PASSIVATION LITERATURE

This section outlines selected published information [1-252] on the corrosion of thin metal films of the type used to fabricate solid-state electronic devices. References have been provided to indicate the type of information available in the published literature on corrosion studies, analytical methodology, and related relevant topics. In general, we have included fairly recent references rather than extensive citations of early literature, since the earlier literature has been cited in a number of recent reviews [4,59,67,76,84,95,114,117,118,120,136,155,158,163,177,197, 198,201,203,222,233,235,243]. No attempt has been made to present a complete survey of this field; instead, we have selected examples that illustrate the problems and the general approaches to the applicable analytical methodology.

A considerable amount of pertinent published information exists on the corrosion of aluminum metal in silicon devices in both hermetic and plastic packages [20,47,65,117,158,165,167,180,247-249], on defects in passivation layers [15,22,23,48,110,114,137,201], and on general corrosion phenomena [58,67,120,175,176,197,234].

A vast amount of information is also available on methods of studying corrosion [47,58,67,111,118,129,175,176,213,234] and on the corrosion of aluminum [4,26,136,175] and gold [175,197]. Corrosion studies of aluminum and aluminum alloys [14,27,225,232] have been performed on bulk samples and on thin-film samples immersed in various electrolyte solutions.

There also exists a large number of studies of the corrosion of thin-film metallization in test structures with patterned metal electrodes. Cathodic corrosion of aluminum metal in semiconductor devices has been studied extensively [20,47,65,84,118,120,165,168,201,239]. The effects of moisture [34,47,118,158,165], of sodium ions [168], of chloride ions [120], and of the phosphorus content of the overlying phosphosilicate glass [11, 47,167] have been reported. In a variety of devices the formation of gold dendrites at cathodes has been noted [22,82,141,143,203,210]. In several studies, failure was attributed to moisture-induced conduction at the interface between two dielectrics [32,206].

B. CORROSION AND DEVICE FAILURE

1. Types of Corrosion

Corrosion effects may be classified as chemical (no bias involved), electrochemical (electrodes serve as cathode and anode when bias is applied), and galvanic (dissimilar metals).

The scope of this program of study is essentially limited to electrochemical corrosion at metal electrodes in liquid or gaseous ambients and in localized liquid sites (such as capillaries). The test patterns also include areas designed for chemical as well as for electrochemical corrosion tests. One reason for determining chemical corrosion rates is their usefulness as controls against which to compare electrochemical corrosion rates. Another reason for desiring information about chemical corrosion is that, in improper environments, the chemical corrosion of exposed metal in bonding-pad areas can be the ultimate cause for device failure. Even 25-μm aluminum bond wires have corroded under certain conditions [17].

2. Defects in Metal Protection Layers

Structural defects in inorganic glassy passivation layers include cracks, pinholes, inadequate edge coverage of metal lines, and other localized defects [15,22,48,94,114,201]. Cracks originate because of excessive tensile stress in the deposited film, or because of tensile stresses when the device is subjected to elevated temperatures during subsequent device processing, since the thermal coefficient of expansion of the aluminum or gold film is considerably higher than that of phosphosilicate glass or of plasma-deposited nitride. Cracks can also be caused by the recrystaliization of aluminum at elevated temperatures (particularly over large metal areas), by contact printing, and by impact during chip handling [15,22,109, 110,114,201].

Pinholes in dielectric films can be formed during the process of etching open the bonding pads. They may be caused by pinholes in the resist film as spun on, inadequate coverage of the resist over the edges of topological steps, dust or defects in the photomask, or wafer handling or contact printing [110,114,115,244].

Most chemically vapor deposited SiO_2 or phosphosilicate passivation glass films [114,201] and certain plasma-deposited silicon nitride passivation films [112,216] are in tensile stress at room temperature and at device usage conditions. When the passivation layer is strongly adherent to the underlying metal, the tensile stress is distributed uniformly. If, however, a crack forms in the dielectric, then the tensile stress in the passivation layer exerts a localized tensile force on the underlying metal at the bottom of the crack. This might cause stress corrosion cracking and could therefore enhance corrosion. Somewhat similarly, when the area of dielectric is removed by etching, and adjacent areas are protected by photoresist, the tensile stress in the dielectric film may result in the application of a tensile force to the underlying metal at the edge of the delineated area of the passivation layer. This happens when the passivation layer is removed from bonding-pad areas, and occurs in the circuit itself because of any defects that may be present in the photoresist film or photomask and that permit the localized etching of pinholes over metal lines in the circuit [15,110,111,114].

Generally, deposited passivation layers adhere well to thermally grown SiO_2 *and to aluminum*, but have limited adhesion to gold metallization. In regions where the Au metallization lines go over topological steps in the underlying dielectric, tensile stresses in the deposited passivation film would tend to cause localized lifting of the passivation film.

Plasma-deposited silicon nitride samples, which frequently contain appreciable amounts of dissolved as well as chemically bonded hydrogen, are sometimes susceptible to blistering effects during life testing at elevated temperatures [112].

3. Aluminum Metallization and Its Corrosion

Aluminum metal is the material most commonly used for the metallization of silicon devices. It finds wide application in integrated circuits and small-signal transistors, as well as in many silicon power devices.

Aluminum films on integrated circuits are in tension at room temperature, and also under most conditions of use. Since aluminum metal is known to undergo stress corrosion cracking, tensile stress in the aluminum film may be a factor in the rate at which an aluminum line corrodes to an electrical open or becomes reduced in cross-sectional area to the point of failure due to electromigration (current-induced mass transport) or some other mechanism.

In many cases, devices fail because of the corrosion of aluminum metal in regions near bonding pads. In such devices, localized defects in the passivation glass are the sites at which the corrosion begins. The exposed metal at the defect serves as one electrode; an adjacent bonding pad of opposite polarity serves as the opposite electrode. Obviously, anode and cathode currents are equal. However, since the defects in the glass are small, whereas adjacent areas of exposed metal at the bond pads are large, the current density at the exposed metal at the defect is very high. At such high current densities, localized increases in pH at the cathode may result in appreciable current efficiency for the dissolution of aluminum metal.

The most commonly encountered failure mode due to chemical interaction of dielectric with metallization is metal corrosion at the glass-aluminum interface. This is brought about by the leaching of P_2O_5 from phosphosilicate glass, or of B_2O_3 from borosilicate by moisture, especially during pressure-cooker testing or life tests under electrical bias in high humidity. These oxides react with moisture, forming phosphoric or boric acid, respectively. These acids readily attack the aluminum, especially the phosphoric acid. To remedy this, the glass composition or the densification may need to be changed, or a protective interlayer of SiO_2 or Si_3N_4 may have to be deposited.

It should be recalled that aluminum is extremely prone to corrosion in the presence of certain impurities (such as sodium ions and chloride ions), even during its deposition and processing. Although serious problems of aluminum corrosion occur in plastic-encapsulated devices, especially during life testing at high humidity, even hermetic packages can be problematic. Thus, hermetic packages may contain leaks, entrapped moisture or other ionizing impurities from inadequate sealing processing, or, for chip attach or conformal coatings, epoxy adhesives that release polar contaminants. All of these materials may contribute to metal corrosion.

4. Gold Metallization and Its Corrosion

Gold is widely used in discrete transistors and certain integrated circuits as the top layer in beam-lead-type metallization systems consisting of Au-Pt-Ti or Au-Pd-Ti, and in systems such as Au-Mo-Pt. The primary gold layer is usually deposited by vacuum evaporation or sputtering and is then built up by electroplating to a thickness of typically several micrometers (or, in the case of beam leads, a larger fraction of a millimeter).

While the basic failure mechanism in gold metallization systems is a result of dendrite formation at the cathode, a study of anode reactions in gold-metallized devices is important because reactions at the anode are the source for gold-containing ions that are ultimately reduced to elemental gold at the cathode. The presence of contaminants such as chloride ions (or other complexing agents for gold such as bromide ions, iodide ions, or cyanide ions) [197,212], determine whether the anode reaction results in the dissolution of gold metal rather than the evolution of oxygen; the latter would occur in an aqueous system free of complexing agents for gold.

The cathodic formation of dendrites may lead to a type of failure mechanism of gold-metallized devices known as migratory resistive shorts [82,210]. Several authors have reviewed the mechanisms leading to failures characteristic of beam-lead sealed-junction semiconductor devices [33,70, 86,143,193].

SECTION III

EXPERIMENTAL METHODS

A. TEST DEVICE STRUCTURE

In this section the design of the two test device structures is described. For measurement of corrosion current, a comb pattern is used and, for measurement of corrosion rate by resistance change, a line pattern. "Comb" and "line" refer to the main feature of each metal pattern. In addition, each pattern has its own over-metal passivation pattern which simulates passivation defects. The details of each pattern are described below.

1. Line Resistance Structure

The metal pattern for the line resistance measurements is shown in Fig. 1. This pattern permits biasing between the line pairs, spaced 12 and 24 μm apart, and measurement of the line resistance. The line width is 12 μm, and length is 2000 μm (0.2 cm). Under certain conditions, it may also be possible to measure corrosion currents with this pattern. Basic design considerations were to furnish a line with convenient electrical resistance and yet not excessively long so that anomalous defects would not be a factor in the corrosion rate measurements. Based on our previous work, we believe that a 2000-μm-long line is suitable. This yields a line resistance of approximately 5-10 Ω for aluminum.

Two other masks accompany the metal mask M2 shown in Fig. 1. One is a substrate dielectric mask that provides steps in the oxide under one metal line pair, as shown in Fig. 2. The steps consist of 50-μm-wide rectangles, spaced 50 μm from edge to edge, providing a total of 30 oxide steps under a metal line pair. The other in this set, which is the final mask, is also shown in Fig. 3. As can be seen, it provides a series of 7-μm-diam holes over each line of the two line pairs, to simulate passivation defects, and also provides bond pad openings. There are 32 holes, spaced 50-μm apart, over each line.

The pattern of two line pairs with bonding pads at one end only and a third line opposite the end of the two lines in Fig. 1 is a special

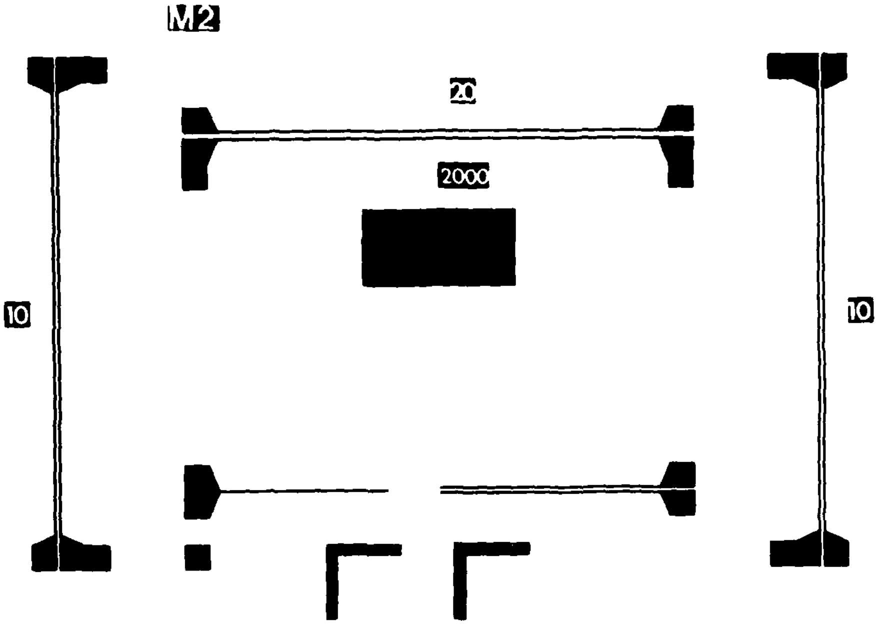

Figure 1. Metal line pattern for corrosion rate measurements by line resistance change.

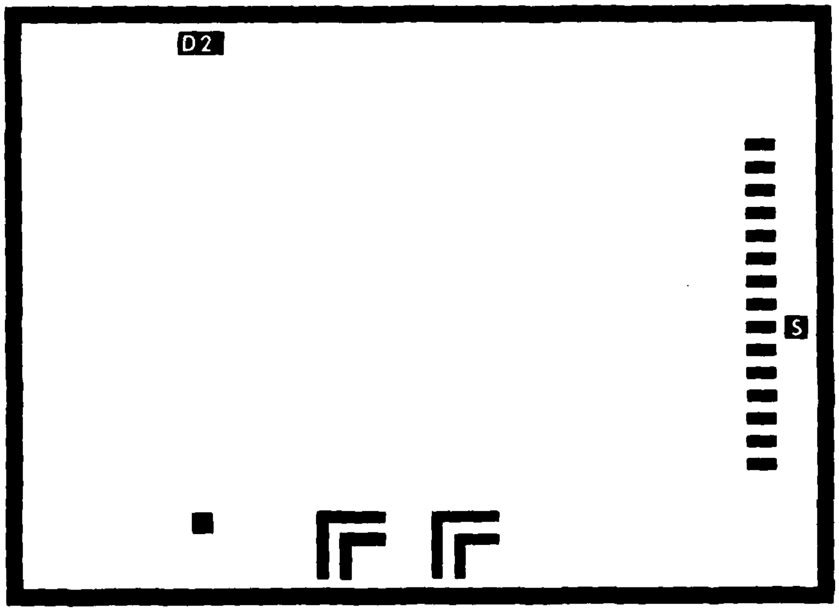

Figure 2. Substrate dielectric mask for metal line pattern of Fig. 1, providing stepped insulator pattern.

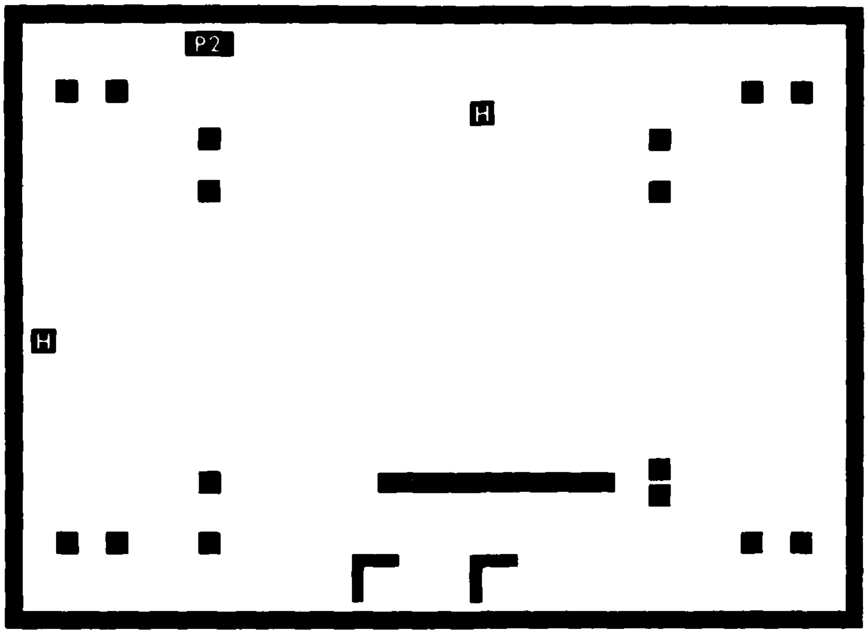

Figure 3. Passivation mask for metal line pattern providing holes over two line pairs and removal of passivation over potential profile structure.

structure designed to explore the possibility of potential profile measurements. If a voltage is applied between the line pair, and the third line is allowed to float electrically, then the floating line is expected to reach eventually a potential equal to one-half that of the line-pair potential difference, provided the electrical field is constant across the 12-μm-wide space between the lines. If the electrical field is not constant across this gap, because of, for example, a potential drop at one electrode, then the potential of the solitary line will deviate from this value, and a simple measurement of charge on this line will indicate the voltage. Thus, it may be possible to infer the presence of electrode potential drops.

2. Metal Comb Pattern

The metal comb pattern is shown in Fig. 4. This pattern consists of four pairs of identical combs. Each comb of each pair has 32 interdigitated

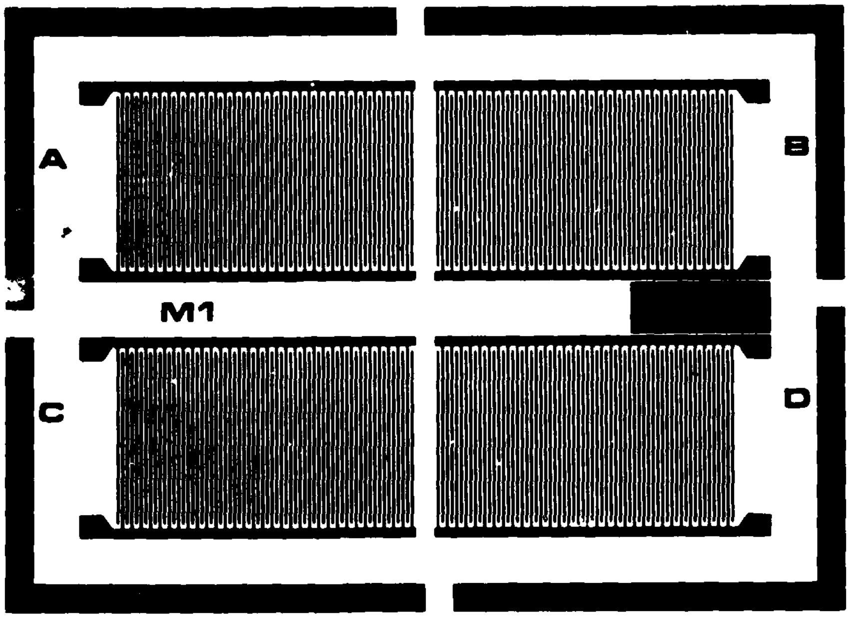

Figure 4. Metal comb pattern with four identical metal comb pairs for corrosion current measurements.

lines. The line width is 12 µm; the line spacing, 12 µm. The length of each line is 770 µm. Thus, for each comb pair the ratio of spacing to line length is 2.52×10^{-4}. Surface resistance can then be calculated from

$$\rho_s = 4.0 \times 10^3 \text{ V/I}$$

where ρ_s is surface resistance in ohms per square (Ω/□), V is the applied potential in volts (V), and I is the measured current in amperes (A).

The passivation pattern, shown in Fig. 5, is different for each of the four comb pairs. Thus, comb pair A has continuous passivation over the entire comb pair. Comb pair B has 7-µm holes in the passivation over every line of both combs; there are 13 holes over each line, and they are spaced 50 µm along the length of the line. Comb pair C has the same hole pattern as B over the comb whose connecting bar is near the center of the test device; an open line in the passivation of 7-µm width is oriented over each metal line of the outer comb of comb pair C. The line or slot extends 25 µm beyond the end of the hole pattern on the opposite lines. Comb pair

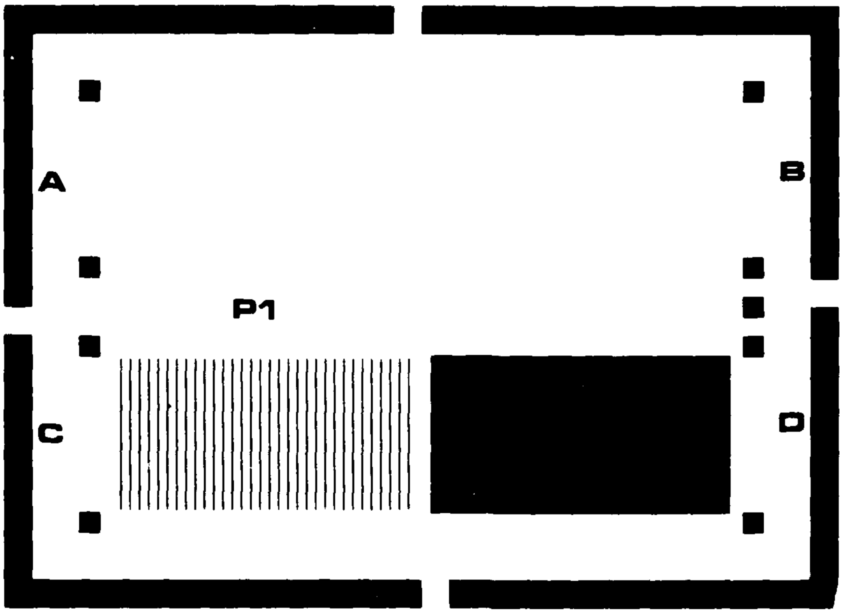

Figure 5. Passivation pattern for comb pairs A, B, and C, providing continuous passivation, holes, and holes plus slots, respectively, and no passivation over comb pair D.

D has the passivation completely removed in a rectangular pattern over all the lines; essentially, all the line pattern is exposed.

B. DEVICE PROCESSING

1. Terminology

Several terms relevant to device processing are described below.

Except for the thermal SiO_2 layers, all dielectric layers studied were formed by chemical vapor deposition (CVD).

The phosphosilicate glass (PSG) layers were formed from silane, oxygen, and phosphine, with nitrogen as a carrier gas [111].

A plasma-assisted CVD process with silane and ammonia in nitrogen carrier gas is used to deposit a "silicon nitride" layer. This material, which actually consists of silicon, nitrogen, oxygen, and hydrogen [112], is referred to as SINCAP.

For the gold-trimetal (gold, platinum, titanium) process, detailed descriptions are available [116,117]. Standard procedures were used for aluminum deposition.

2. Dielectric Layers

The starting wafers were (100), n-type, 1-10 Ω·cm. Wafer size varied from 3.8 to 5.6 cm in diameter. After standard cleaning, the wafers were oxidized in HCl-steam to a thickness of approximately 6000 Å. In the case of line pattern devices, the oxide was patterned with the step mask D2 (Fig. 2) and oxidized again in the same manner. Thermal-oxide thicknesses were monitored by ellipsometry, visible interference reflectance, and step etching followed by stylus surface profiling.

In some cases, a phosphorus-doped oxide was formed over the thermal oxide by CVD. The conditions for this CVD oxide were a substrate temperature of 450°C, a deposition rate of 1490 Å/min, and an oxygen/total hydride ratio of 20:1. The oxide was then densified in N_2 at 800°C for 15 minutes. Etch rate analysis, used for all CVD oxides, indicated a thickness of 6000 Å and a phosphorus content of 8.2% by wt. For gold-trimetal structures a CVD silicon nitride layer was deposited over the thermal oxide. This was deposited at 800°C from NH_3 plus 3% SiH_4 to a thickness of 1200 Å. Thickness and P content of PSG layers were determined by etch rate analysis. SINCAP thickness was determined by stylus profiling at an etched step.

3. Metallization

The next step in device fabrication is the metal deposition process. Aluminum and gold-trimetal were investigated. Aluminum (five 9s pure) was deposited by filament evaporation, electron-beam evaporation, and S-gun sputtering. The conditions for each process are given in Table 1.

The deposition process for the gold-trimetal involved the following steps: First, 1000 Å of titanium was deposited by magnetron sputtering. Then, 1000 Å of platinum was deposited in the same manner. Photoresist

TABLE 1. ALUMINUM DEPOSITION PARAMETERS

Process	Parameters		
	Pressure (Torr)	Deposition Rate (Å/s)	Substrate Temperature (°C)
Filament Evaporation	5×10^{-6}	30-40	35-50
E-Beam Evaporation	5×10^{-6}	100-150	25-35
S-Gun Sputtering	2×10^{-3} (argon)	6	35

was applied and patterned. Aqua regia was used to remove the platinum down to the titanium. Photoresist was reapplied and patterned to cover the areas where the platinum had been etched away. Gold was then electroplated to a thickness of 12 μm and used as a mask for removal of the titanium.

After deposition and patterning of aluminum films, the samples received a metal-alloying treatment. This consisted of a 20-minute treatment at 450°C with forming gas (90% N_2 and 10% H_2).

4. Passivation Layer Deposition

The standard PSG layer (4% P by wt) was deposited at a substrate temperature of 450°C and a rate of 1000 Å/min. Normally, the thickness was approximately 8000 Å, although thicker layers were also prepared and studied. In all cases the oxygen/total hydride ratio was 20:1. For an extensive description of PSG deposition processes, a previous study [111] may be consulted.

The SINCAP layer was deposited by plasma-assisted CVD [112]. The substrate temperature was 300°C, the standard thickness 8000 Å, and the deposition rate approximately 200 Å/min. Thicker layers were prepared as well.

5. Layer Patterning

All metal films were patterned with photoresist and wet chemical etching, except for the gold in the trimetal process, as described in Section III.B.3. PSG layers were patterned with photoresist and etched in buffered HF. SINCAP layers were patterned with photoresist and plasma etched.

6. Device Packaging

After wafer dicing, the test devices were inspected for metal bridging, metal opens, and passivation and dielectric defects. Only devices with the intentional defects open to the metal were selected. The chips were mounted in packages with a gold-silicon eutectic bond. Note that the final wafer processing step was gold deposition on the back of the wafer by evaporation. The packages chosen were 16-lead dual-in-line ceramic (DIC). After chip mounting, the devices were ultrasonically wire bonded with aluminum wire 25 μm in diameter.

7. Device Cleaning

Initially, devices were tested without cleaning after assembly. During measurements of the current dependence on relative humidity and temperature, it was found necessary to introduce a cleaning step to avoid unusual hysteresis effects that made the interpretation of the data extremely difficult. This cleaning step involved rinsing five times in deionized water with ultrasonic agitation followed by vapor degreasing with trichlorotrifluoroethane for 20 minutes. Finally, a 1-h bake at 200°C in room ambient was applied.

C. EXPERIMENTAL APPARATUS

In this section the principal experimental equipment is described. This includes a room-temperature, controlled-humidity probing station; a temperature-humidity cabinet with associated sample-monitoring circuitry; a controlled-ambient contamination chamber and sample circuitry; and an electrochemical corrosion cell for cyclic voltammetry.

Apparatus used only occasionally will be described as needed. Analytical methods and equipment will be described in Section III.D.

1. Probing Station

The probing station consisted of a cylindrical housing with three electrical feedthroughs connected to three tungsten probes. The probes enter the station through small ports whose cross-sectional area is so small that a total flow rate of 20 ft^3/h of conditioned gas is sufficient to maintain the relative humidity constant. The aluminum cylinder is capped with a transparent, conductively coated glass plate, which is removable for sample access. The desired relative humidity is obtained by mixing proper proportions of dry nitrogen with water-saturated nitrogen. The humidity is monitored constantly, and the calibration is checked by diverting the flow to wet- and dry-bulb thermometers.

2. Humidity Cabinet and Electrical Apparatus

The humidity chamber is commercially available. Separate heaters for the vapor and liquid phases are proportionally controlled. Conditions are monitored with wet- and dry-bulb thermometers. These are calibrated with thermocouples and an electronic hygrometer. The system is capable of temperature control from 50 to 100°C and relative humidity control from 50 to 98%. A port in the side wall of the chamber provides routing for electrical cables.

The electronic system for applying a corrosion potential to samples in the humidity chamber consisted of a stainless-steel socket holder with five polytetrafluoroethylene (PTFE) sockets mounted in the chamber with wires brought out to a switching system. This switching system permitted application of bias voltage, measurement of corrosion current, measurement of metal line resistance, and detection of substrate shorts for the 15 line pairs involved in one test run of the line pattern devices. For the comb devices, the system permitted application of bias, current measurement between comb pairs, and detection of shorts to the substrate for four test devices mounted in PTFE sockets on a stainless-steel board. A sensitive electrometer was used for current measurements; a digital ohmmeter, for line resistance measurements. A schematic of the measurement system is shown in Fig. 6. Dry-nitrogen flow used in the switching box served to decrease leakage currents. By use of this equipment and ceramic packages without sample chips, leakage currents of 5×10^{-11} A were measured at 20 V and 85°C/85% rh.

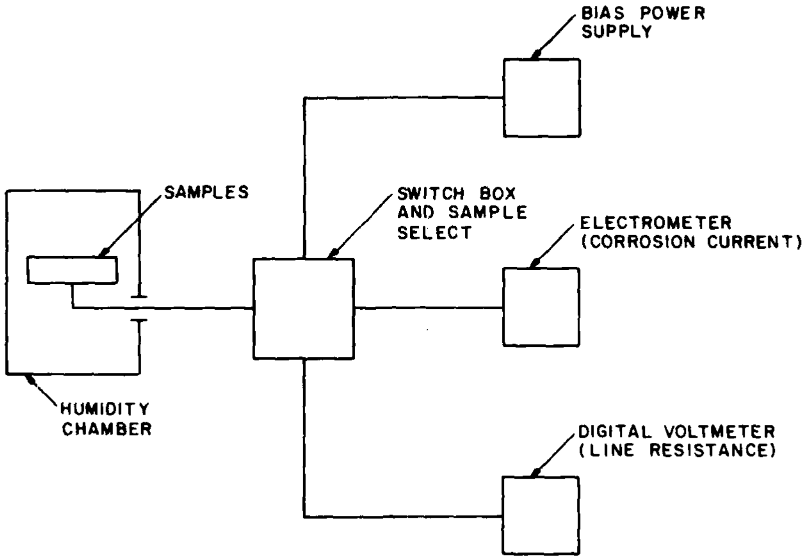

Figure 6. Schematic of electrical apparatus for measurement of devices in humidity cabinet.

3. Contamination Chamber

The contamination chamber was designed to expose the devices to a known concentration of contaminant gas under controlled conditions of humidity and temperature. The chamber apparatus is shown in Fig. 7; it was modeled after the apparatus described by Sbar [192,195]. The contaminant and the rh-control gas flows enter the chamber separately. Permeation tubes were used to control the contaminant gas concentration, while a controlled-temperature water bubbler supplied constant relative humidity. Permeation tube techniques [164] can be used to reproducibly generate nanogram quantities of a wide range of materials (i.e., Cl_2, SO_2, NO_2, NH_3, etc). To prevent precipitation of moisture from the rh-control gas, heating tape was supplied for the tubes entering the oven. In addition, the bubbler was maintained at a temperature lower than the chamber temperature to prevent condensation within the chamber. A level controller for the bubbler lets the corrosive gas apparatus run without interruption for long periods of time.

For temperature control, the entire reaction chamber was contained within a forced-air oven. To minimize spurious contaminants and corrosion,

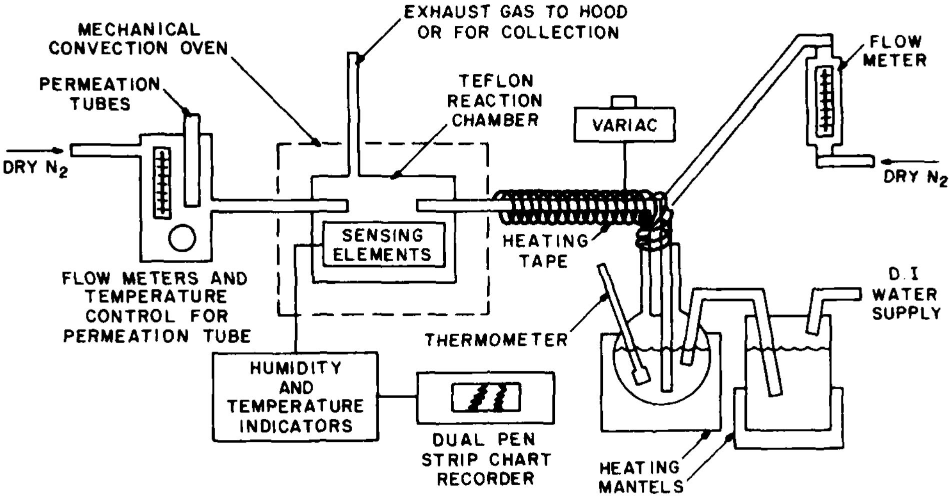

Figure 7. Schematic of controlled-contamination apparatus.

PTFE was used to construct the chamber and its hardware. The temperature and humidity of the reaction chamber were monitored by electronic sensors.

Circuit boards and current measuring apparatus used for the contamination chamber are similar to those used for the humidity chamber (see Section III.C.2).

4. Electrochemical Corrosion Cell

The corrosion cell monitors reaction rate as a function of the electrochemical potential. In this apparatus cyclic voltammetry is used as a rapid method to evaluate corrosion stability. To accelerate the corrosion process the experiments were conducted under conditions more strenuous than those typically encountered for electronic devices. The metallized test substrate was in direct contact with an aqueous solution containing a substantial concentration of electrolyte. A variable potential was applied to the surface of the metallized substrate undergoing testing. To determine corrosion stability, corrosion currents were monitored, while the potential of the test electrode surface was varied with respect to the reference electrode. The current generated by the reactions at the surface of the test electrode is an instantaneous measure of the corrosion reaction rate. The potential at which current is generated by reactions on the test electrode and the current magnitude and direction can be used to characterize the type of corrosion reactions on the surface of the test electrode. Comparison of the magnitude of the corrosion rates under various test conditions and for various test electrodes is indicative of the relative corrosion stability.

A circuit diagram of our corrosion cell apparatus is displayed in Fig. 8. Many valuable aspects of this design were supplied to us by the late G. S. Lozier. A significant feature of this circuit is the summing op-amp. The driving electrochemical potential (i.e., a triangular wave and offset voltage) is applied to the inverting input. Since the feedback loop containing the corrosion cell is attached to the inverting input, and

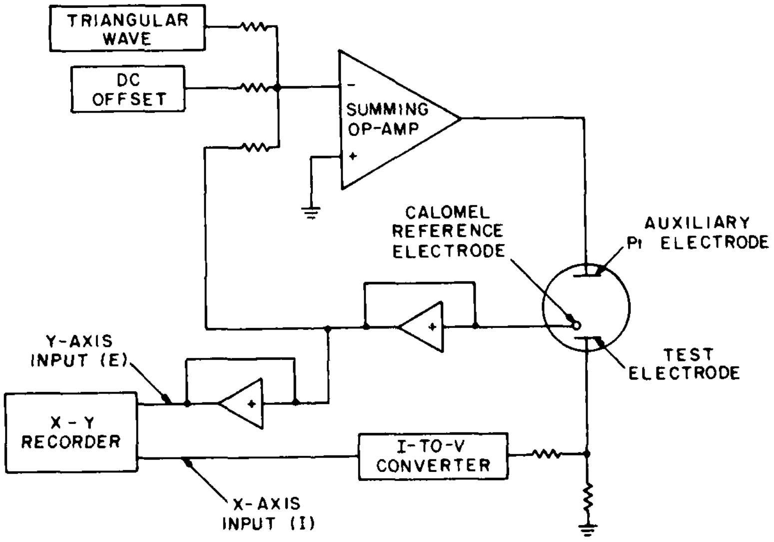

Figure 8. Schematic of corrosion-monitoring electrochemical-cell circuitry for cyclic voltammetry.

the noninverting input is grounded, the potential applied to the test electrode is of a polarity opposite to that of the input potential on the summing op-amp. A calomel reference electrode in close proximity to the test electrode surface essentially monitors the chemical potential at the metal surface. Voltage followers are provided in the feedback loop to drive the y axis of the recorder and to supply the feedback input to the summing op-amp.

The design of the corrosion cell shown in Fig. 9 is also noteworthy. The test electrode (i.e., the metallized substrate) is placed over the hole on the side of the cell opposite the auxiliary platinum electrode. A threaded rod and plastic plate hold the test electrode in place. Circuit contacts for the test electrode are made with the tantalum foil on both sides of the hole. This design ensures that a reproducible surface area is exposed to the electrolyte for every test electrode, allowing the comparison of the relative magnitude of the corrosion current between test samples. The capillary design for the reference electrode holder near the exposed test electrode hole facilitates measurement of the potential at the test electrode surface.

Selection of the electrolyte composition for these aqueous solution experiments can be critical. The salt electrolyte must be relatively stable over the potential range studied for the test electrode. For our experiments, the potential on the platinum auxiliary electrode was varied from +1.3 to -0.5 V with respect to the calomel reference electrode. In this electrochemical potential range, electrolysis of the aqueous solution is minimal in the near-neutral pH range (pH 4-9). Alkylammonium, alkali-metal, and alkali-earth cations are relatively stable electrolyte species. Acetate, sulfate, and halide anions also afford some stability in the desired electrode potential range. Although the halides are stable in solution, with respect to aluminum metallization their presence (notably that of Cl^-) increases the corrosion rate. Some pH control can be obtained by buffering the solution with suitable electrolyte salts and their conjugate acids or bases.

A typical test for corrosion stability was done in the following manner: A selected test electrode (i.e., an aluminized substrate corrosion sample)

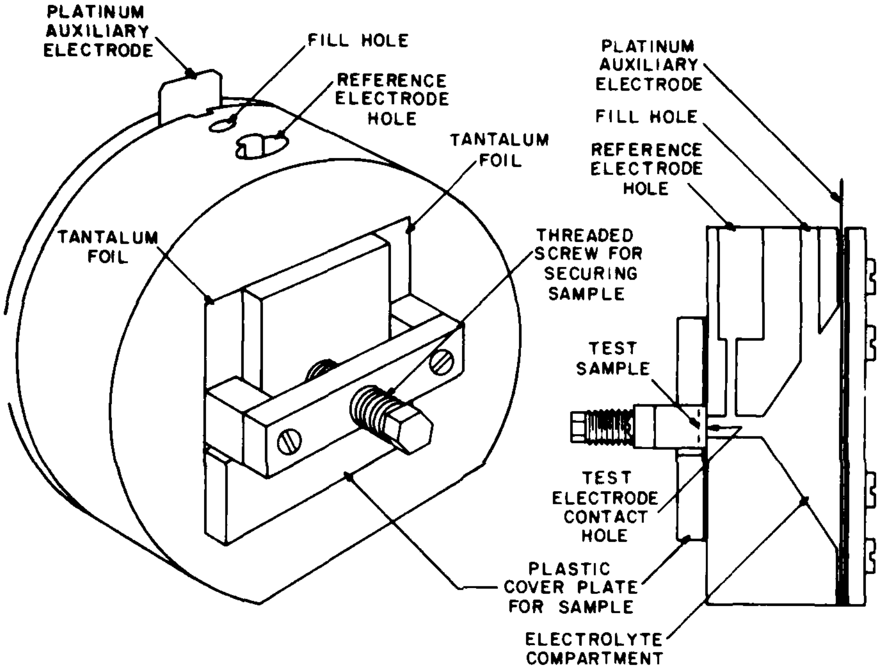

Figure 9. Electrochemical cell.

was attached to the cell. The cell was filled with the appropriate electrolyte (∿60 ml) of known pH and/or contaminant concentration. The reference electrode was inserted, and appropriate connections to the auxiliary platinum and test electrodes were made. Voltage-vs-current (E vs I) curves were recorded for each electrochemical corrosion cycle. The cycles and E-vs-I curves were repeated until corrosion was complete or a steady state was reached. Relative corrosion stability of a test electrode was obtained by comparison of the E-vs-I curves with other test samples and electrolyte compositions.

D. ANALYTICAL METHODS

1. Physical Analysis Methods

Physical methods of analysis included optical microscopy (bright-field, dark-field, differential interference contrast, polarizing, and monochromatic), scanning electron microscopy, x-ray diffractometry, and x-ray Laue ring analysis for determining the physical structure of corrosion products and film structure.

Ellipsometry, interferometry, and reflectance spectrophotometry were used to determine the thickness and refractive index of dielectric films. The step height of metal films was measured by stylus profilometers.

Residual stress in deposited metal and insulator films was determined by measuring the radius of curvature of uniformly thin and circular substrates (such as glass discs and silicon wafers) before and after film deposition. Details of this technique were reported in a previous paper [114].

2. Techniques for the Detection of Localized Structural Defects

Pinholes in passivation layers over aluminum are difficult to observe in an optical microscope because of the rough texture of the underlying metal. This texture is the result of the recrystallization by heating that occurs during contact alloying or during deposition of the passivation layer. The pinholes are made readily visible and are recorded photographically by selective chemical metal etching. The techniques we used had been developed and reported by us under a previous program [48,109,110].

3. Microchemical Analysis Methods

Quantitative analysis of isolated (extracted) corrosion products was performed by standard microchemical methods including gravimetric analysis of reacted products, atomic absorption analysis for specific elements, and atomic emission spectroscopic analysis for the rapid scanning of most elements. Conductometric measurements of extracts with high-purity water allowed determination of water-soluble ionizable salts.

4. Instrumental Methods for Thin-Film and Surface Analysis

The chemical composition of the surfaces, the bulk, and the interfaces of thin insulator and metal films was analyzed on an atomic level by a variety of analytical methods, in which photons, electrons, atoms, molecules, or ions serve as the reactive species. In combination with sputtering techniques these methods have provided quantitative information of not only the surface chemical composition but also of the film bulk as a function of layer depth, including film interfaces. The use of microprobes of the reactive species in combination with scanning electron microscopy permits analysis of microscopic areas for the purpose of identifying microcrystallites, particles, precipitates, and other corrosion products in localized sample areas. The instrumental methods we employed most frequently in the present project have included electron-beam microanalysis, x-ray fluorescence spectrometry, scanning Auger microanalysis, Auger electron spectroscopy, and secondary ion mass spectroscopy.

SECTION IV

MEASUREMENTS AND ANALYSES

A. EVALUATION OF PASSIVATION LAYER DEFECTS

In the interpretation of corrosion data for test patterns with intentional passivation defects, it is important to know that the local defects present are actually those which are patterned. Confusion might result if either the intentional defects were not completely etched through down to the metal, or if a substantial number of random defects masked the effects of the intentional defects.

Both gold-trimetal- and Al-metallized test samples passivated with either SINCAP or PSG of different thicknesses were etched selectively to reveal the presence of passivation pinholes intentionally produced by photolithography. Aluminum samples were etched in Al-etchant (60 H_3PO_4: 1 HNO_3:12 CH_3COOH:4 H_2O; by vol) for 3 minutes at 50°C; gold samples were etched in C-35 Semiconductor Etchant (a KI-based solution, from Film Microelectronics, Inc.) for 3 minutes at 40°C. Microscopic examination of metallized wafers and discrete IC pellets confirmed complete removal of the passivation layer in the 7-µm holes as well as proper alignment accuracy, evidenced by the fact that all the holes overlapped metal lines (see Figs. 10 and 11).

A small percentage of both Au-trimetal- and Al-metallized samples exhibited characteristic processing defects associated with wafer fabrication and handling, namely, pinholes, poor step coverage, and edge-related microcracks. Gross cracking of the PSG layer or blistering of the SINCAP layer, which can result from large tensile or compressive stresses, respectively, were absent.

Al-metallized corrosion test samples with PSG passivation were also subjected to sequential etching in buffered HF, followed by selective metal etching to determine the density of hidden or buried defects that extend only partially into the insulator layer. Figure 12 illustrates a typical distribution of partial pinholes after removal of more than 50% of the passivant.

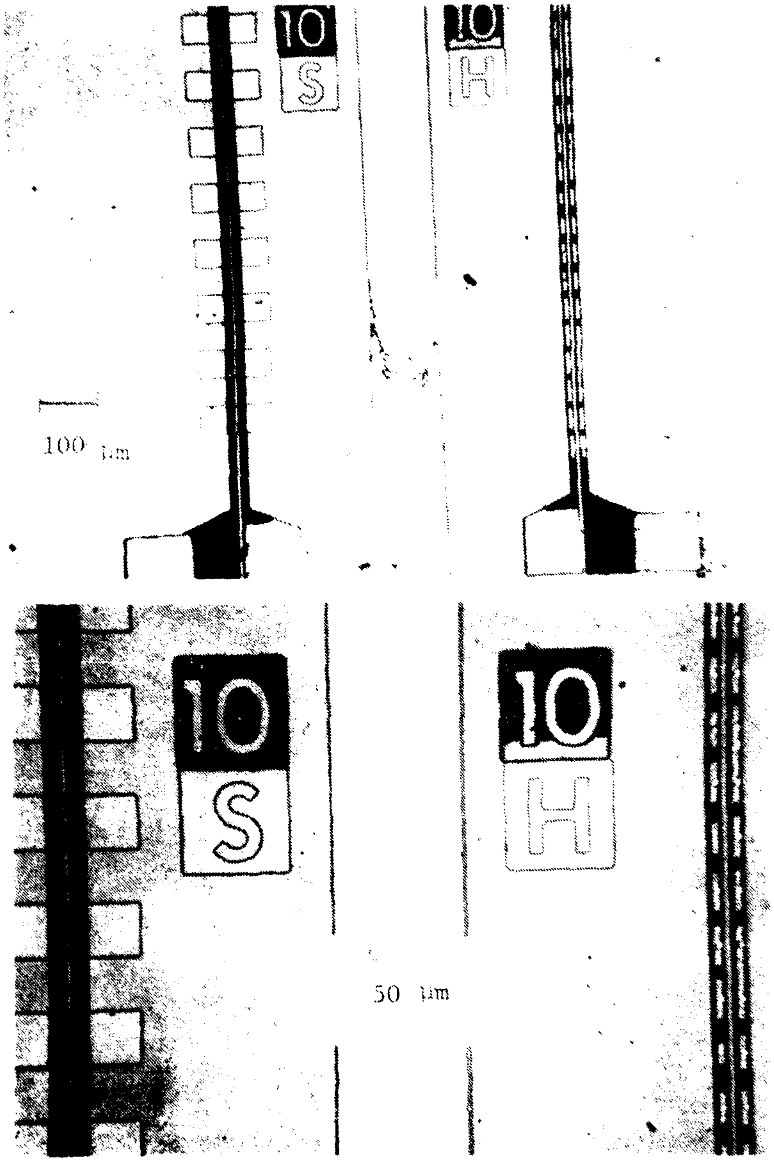

Figure 10. Elucidation of intentional pinholes on gold-trimetal corrosion test sample passivated with 5000 Å of SINCAP after selective etching in KI-based etchant.

REMARKS: White dots on 10H lines are actual pinholes; gray areas surrounding the pinholes are selectively etched metal regions beneath the passivation layer; dark areas are remaining, unetched gold metal beneath the passivant. Note the excellent step coverage on 10S lines to the left and two unintentional pinholes on the 10H line to the right.

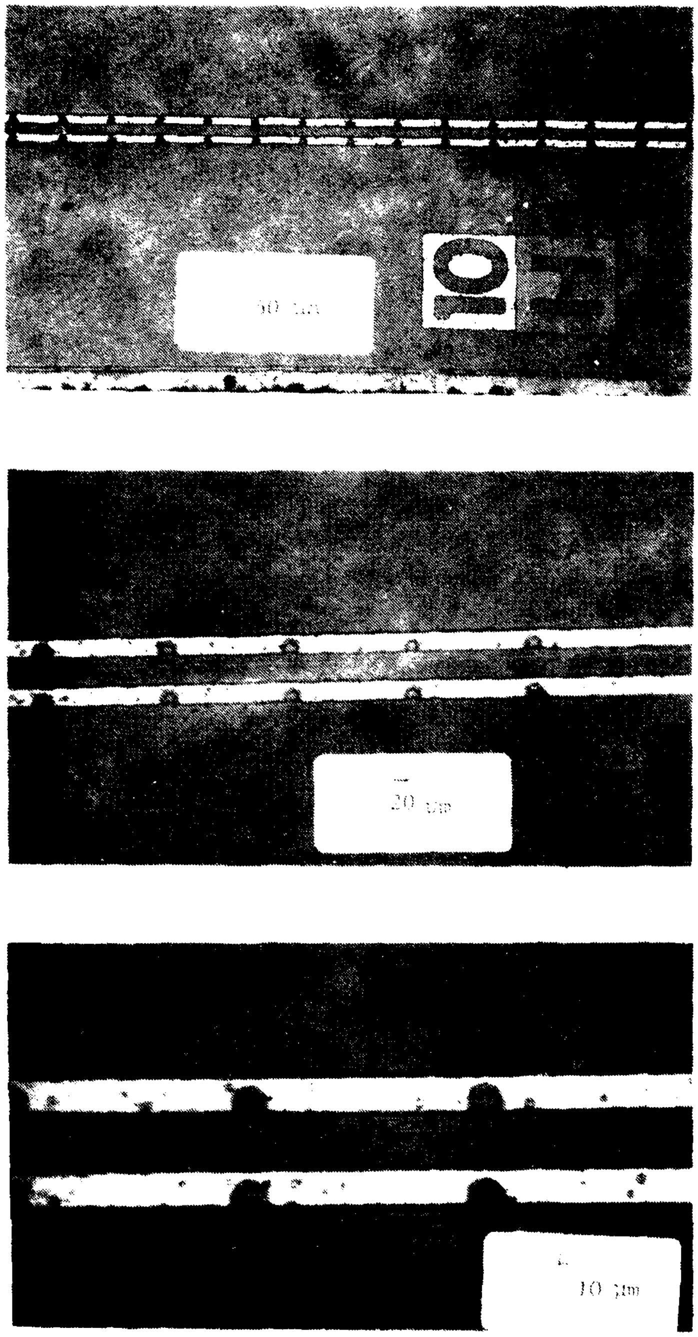

Figure 11. Selective etching of Al-metallized corrosion test sample passivated with 7500 Å of 4.2% PSG. Note that intentional pinholes are slightly misaligned to one edge, but still intersecting the metal.

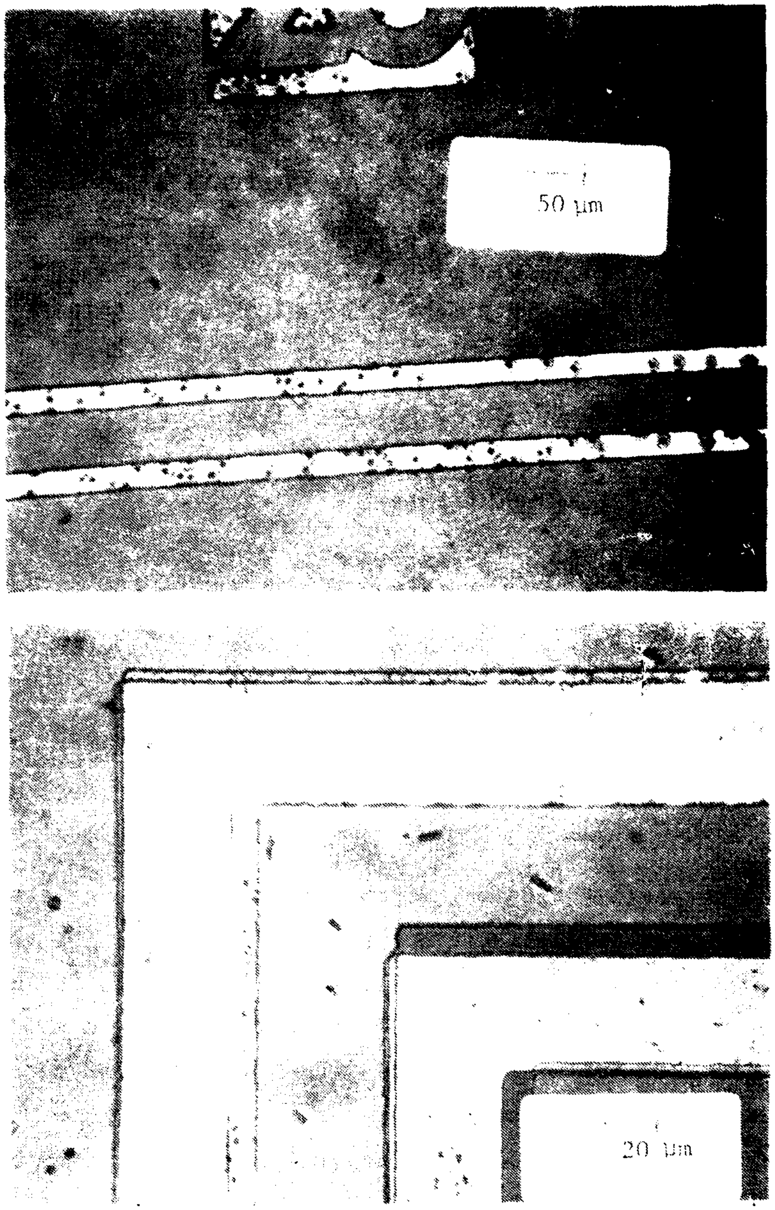

Figure 12. This Al-metallized sample was originally passivated with 8350 Å of 4% PSG. Sequential etching for 30 s in buffered HF removed 60% of the dielectric; subsequent selective metal etching revealed a number of partial pinholes. Note the step-related increase in the pinhole density along the upper edge of the metal line in the lower photo.

B. CORROSION RATE MEASUREMENTS

1. Corrosion Rate of Aluminum

A series of measurements were done with aluminum line pattern samples to assess the dependence of corrosion rate on parameters such as the method of metal deposition, passivation type, and presence of sodium contamination. The test matrix is shown in Table 2.

TABLE 2. SAMPLE PARAMETERS FOR CORROSION RATE TEST

	Parameters				
Wafer No.	Contaminant	Metal	Type	Thickness, Å	P, % by wt
10	$NaHCO_3$	Filament-evaporated Al	PSG	7,500	4.2
11	None	Filament-evaporated Al	PSG	8,300	4.0
16	None	Filament-evaporated Al	SINCAP	7,900	-
26	None	Sputtered Al	PSG	7,800	4.1
30	None	Sputtered Al	PSG	13,600	3.8

The sodium contamination was accomplished by immersing sample no. 10 in a 0.1 g/100 ml distilled water solution of $NaHCO_3$ for 5 s, followed by a 2-s rinse in alcohol. This was done immediately prior to PSG deposition.

These devices were placed in the humidity chamber and maintained at 85 ± 1°C and 85 ± 2% relative humidity. These samples had received no initial cleaning. After about 16 hours of exposure to these conditions, a constant dc potential of 100 V was applied to one line (the outer one) of each pair of lines on the chip. Current between lines and line resistance were monitored at intervals. In one case, the potential was reversed after a certain time.

Cathodic corrosion was observed after voltage application times ranging from several hours to days. This was manifested as an increase in aluminum line resistance. The fractional change in line resistance ΔR_f was calculated as

$$\Delta R_f(t) = \frac{R(t) - R_o}{R_o}$$

where R(t) is the resistance at the measurement time and R_o is the resistance at the time of voltage application (t = 0).

A comparison of the corrosion rate, ΔR_f vs time, for the various samples of Table 2, yields several interesting observations. These are discussed below.

Figures 13 and 14 show typical cathodic corrosion rates for sodium-contaminated samples from wafer no. 10. The last point plotted was the last measurement before the particular line became an open circuit. The even-numbered lines are for the 20-μm-spaced pair, and the odd-numbered lines refer to the 10-μm-spaced pair. There is little difference in corrosion rate for these two spacings. The data in the two figures include

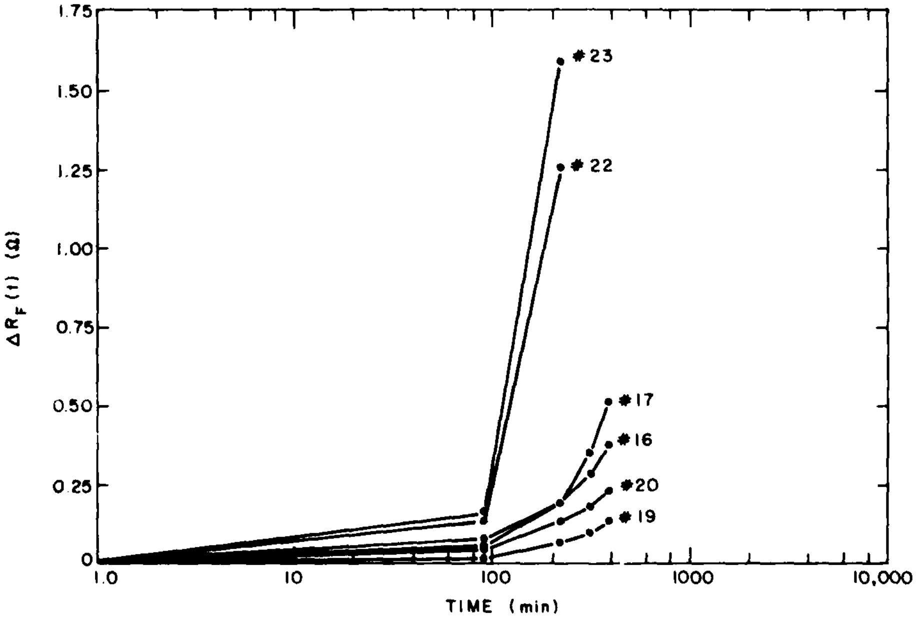

Figure 13. Cathodic corrosion rate for sodium-contaminated sample. Line resistance fractional change is plotted vs time. Sample is PSG over aluminum.

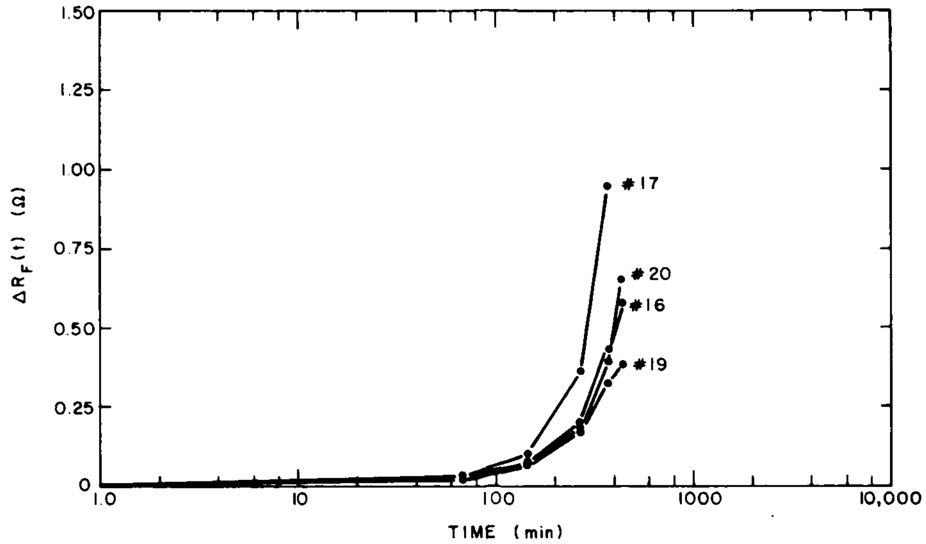

Figure 14. Cathodic corrosion rate in a second test for sodium-contaminated sample. Line resistance fractional change is plotted vs time. Sample is PSG over aluminum.

several test devices in each figure, and separate 85°C/85% rh runs for Figs. 13 and 14. The corrosion times are quite closely spaced from 200 to 450 minutes, indicating reasonable uniformity and control of temperature and humidity. There was very slight anodic corrosion of wafer no. 10 samples, as shown in Fig. 15. Upon voltage reversal, the previous anodes corrode quickly as cathodes, as shown in Fig. 16, where the corrosion times are within a factor of 3 of the initial cathodic corrosion. The time scale in Fig. 16 begins at the time of voltage reversal. Microscopic examination of the line pairs associated with the data marked 1 and 2 in Fig. 16 showed that the initial cathodic corrosion had been so severe that the initial cathode essentially ceased to exist. Thus, little further corrosion took place after voltage reversal.

Wafer no. 11 is from the same lot as wafer no. 10, except that no sodium contamination was added. Processing was identical up to and including metal definition. PSG deposition was done in two successive runs under identical conditions to eliminate cross-contamination by sodium. For wafer no. 11, the corrosion times are substantially longer than for no. 10.

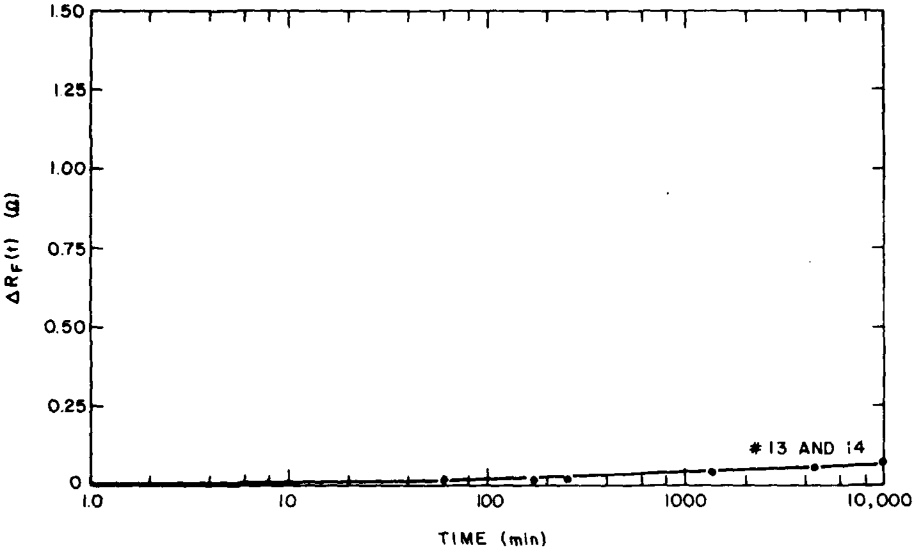

Figure 15. Anodic corrosion rate for sodium-contaminated sample. Sample is PSG over aluminum.

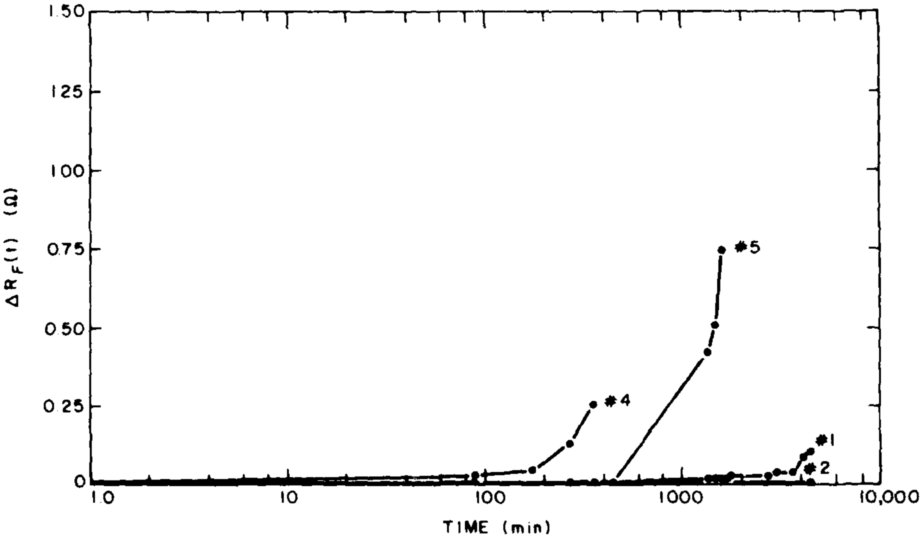

Figure 16. Cathodic corrosion rate of electrodes which were previously the anodes in Fig. 15.

Figure 17 shows that corrosion time to open circuit is about 2000 minutes, about five times longer than for no. 10. This indicates that the presence of sodium enhances cathodic corrosion. As shown in Fig. 18, the anodic corrosion occurs at approximately the same rate as for no. 10, indicating that sodium does not enhance anodic corrosion.

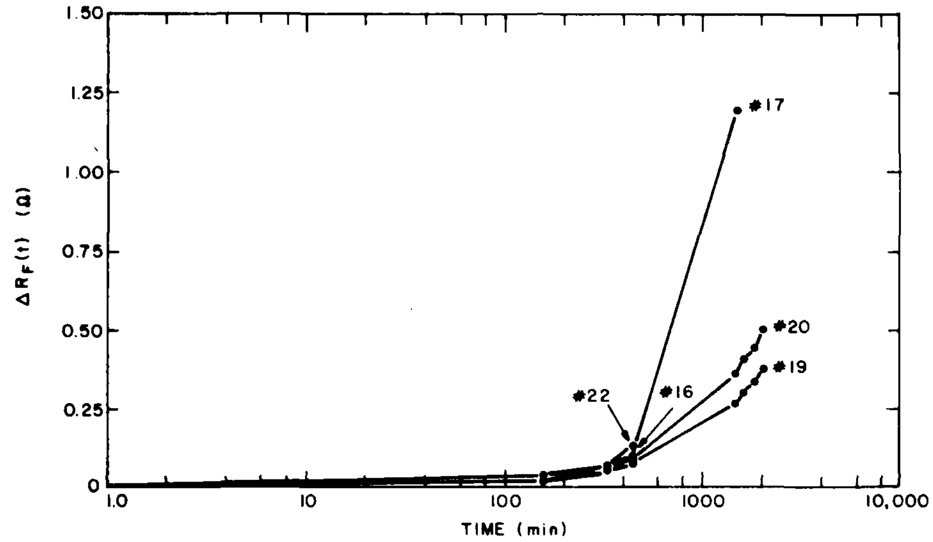

Figure 17. Cathodic corrosion rate for sample without any intentional contamination. Sample is PSG over aluminum.

Initial corrosion currents for both samples no. 10 and no. 11 were approximately equal, and both decreased similarly with time. Thus, the difference in corrosion rates is not reflected in a corresponding difference in the total current measured.

Wafer no. 16 was produced by the same process as nos. 10 and 11, except that SINCAP passivation was used instead of PSG. The anodic corrosion of these samples was not detectable. There was a slight decrease in line resistance after 5000 minutes. The cathodic corrosion rate, shown in Fig. 19, is much slower than for wafer no. 11. Only one aluminum line out of four went to open circuit at 5000 minutes. At this point, the voltage was reversed. Subsequently the corrosion rate of the cathodes (which had been anodes) was much slower than that shown in Fig. 19. At

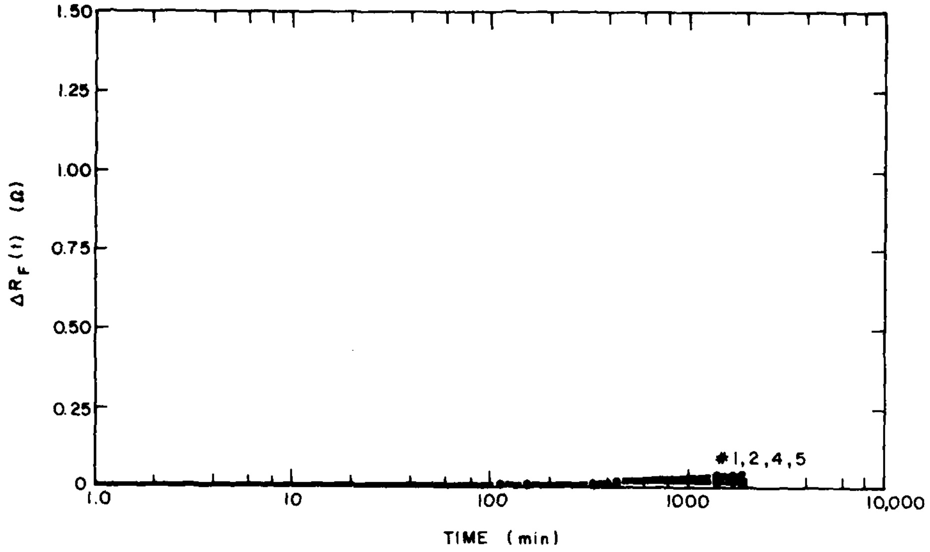

Figure 18. Anodic corrosion rate for same sample type as shown in Fig. 17.

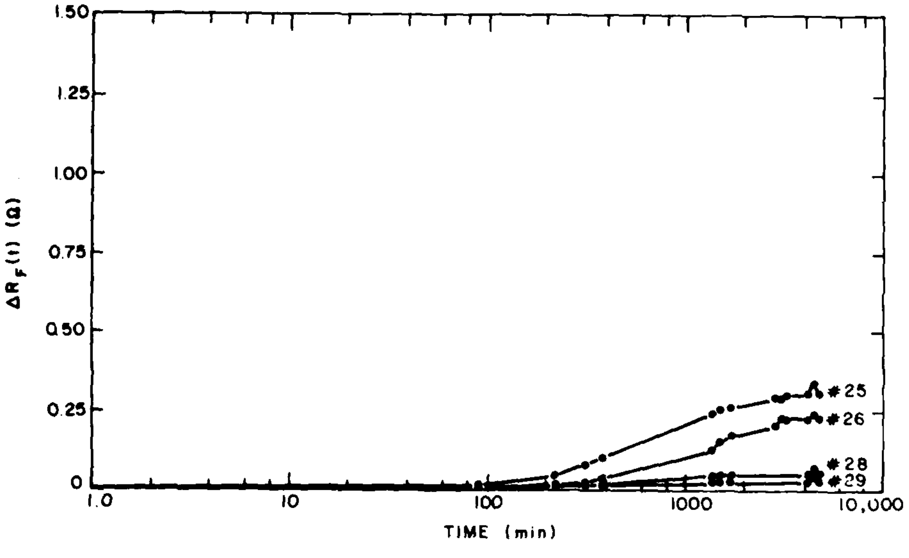

Figure 19. Cathodic corrosion rate for aluminum with SINCAP passivation.

5000 minutes, essentially no corrosion had taken place on these cathodes. The resistance changes were less than 1%. This suggests that the oxide formed at the anode is not readily decomposed upon voltage reversal with SINCAP passivation. Measurements of corrosion rate on samples of types 26 and 30 indicated a very slow corrosion rate. With exposure to 85°C/85% rh at 100 V, these samples showed very low corrosion rates out to 12,800 minutes. The value of $\Delta R_f(t)$ at $t = 12{,}800$ minutes was about 0.05 or less for both positively and negatively biased lines.

2. Measurements on Gold Line Patterns

For the gold-trimetal devices, the line resistance was too low for accurate measurement with our apparatus. Therefore, only line-to-line current was monitored. These devices, with SINCAP passivation over gold trimetal, were placed in 85°C/85% rh ambient for 432 hours at 20 V. Currents ranged from 1×10^{-10} to 1×10^{-9} A and were fairly constant (within a factor of 2) throughout the test, except for one line pair which intermittently exhibited surges of current. Microscopic examination was done at 250X: neither any dendrites nor any corrosion product could be seen.

The devices were put back into the humidity chamber under the same ambient conditions but with 100 V applied. Under the bias, large decreases in current occurred with time. The amount of decrease varied from 10X to 10,000X. No line-to-line shorts were detected. The samples were than removed and examined by optical microscopy and SEM (see Section IV.B.3 below).

3. Corrosion Product Analysis

All of the sample types listed in Table 2 were examined by optical microscopy after exposure to 85°C and 85% rh. Several devices of wafer types 10, 11, and 16 were selected for examination by scanning electron microscopy (SEM) and by energy-dispersive x-ray analysis (EDXRA). Figure 20 shows a wafer no. 10 sample (sodium contaminated, PSG passivation) after the 85°C/85% rh test. Initially, the heavily corroded line was biased negatively with respect to the other line; after 400 minutes, the polarity was reversed. The black appearance of the corrosion product is characteristic of cathodic corrosion. No metallic aluminum was observable on the heavily corroded line except at certain isolated locations which appear

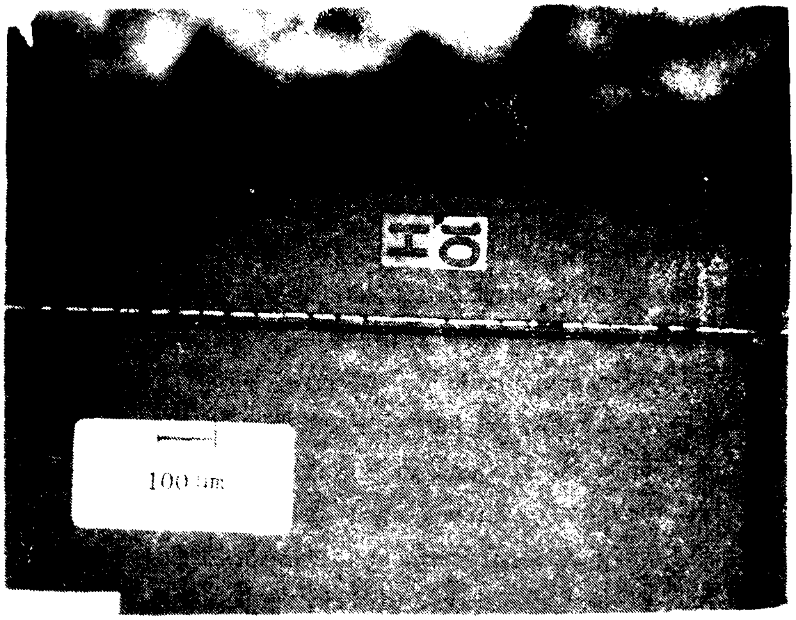

Figure 20. Optical micrograph of aluminum line pair on sodium-contaminated device after corrosion at 85 °C and 85% rh. The lower line was the cathode.

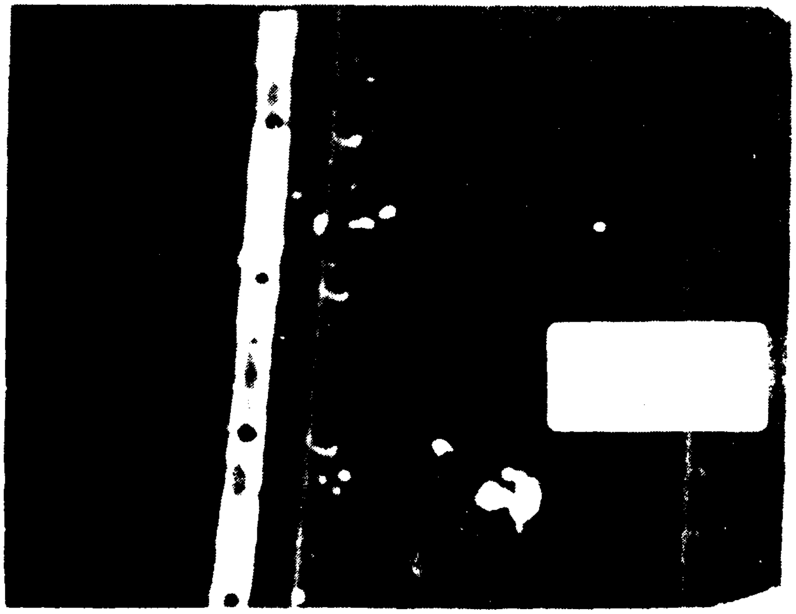

Figure 21. Low-voltage SEM of portion of line pair of Fig. 20. Line on left is lower line of Fig. 20.

bright in the micrograph. Figure 21 shows a portion of the line pair of Fig. 20 under low-voltage SEM. With low beam voltages, there is marked contrast between insulators and conductors; the more insulating regions appear brighter. The line on the left in Fig. 21 is the more heavily corroded line of Fig. 20. EDXRA determined the presence of aluminum in those regions where metallic aluminum was not present. The ratio of Si to Al in these regions ranged from 0.4 to 0.7, indicating aluminum as a major component. This, coupled with the insulating nature of the material, indicates that Al_2O_3 was the corrosion product. Similar results were obtained for all PSG-aluminum samples examined by SEM and EDXRA. Figure 22 shows a line pair on a wafer no. 16 sample, which was passivated with SINCAP. Here, an isolated outgrowth at a cathodic intentional defect site is insulating. This outgrowth registered higher aluminum than silicon activity, while the surrounding region had higher silicon activity. Again, the corrosion product appears to be Al_2O_3.

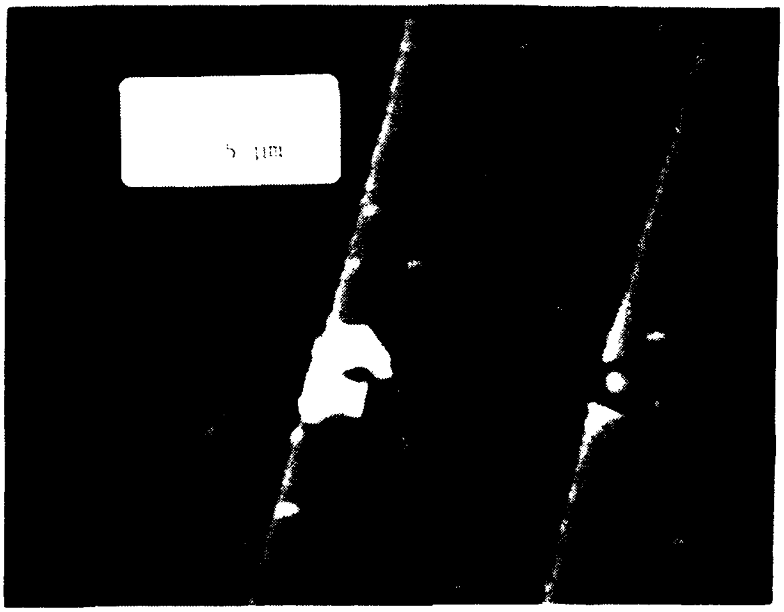

Figure 22. Low-voltage SEM of aluminum line passivated with SINCAP after corrosion at 85°C and 85% rh. Line at left was the cathode.

The gold-SINCAP devices discussed in Section IV.B.2 were examined by optical microscopy. This indicated that large regions of SINCAP overcoat had flaked off, but only at biased line pairs. Thus, the line pair used for the floating electrode measurement and the large metal rectangle showed no SINCAP delamination.

The gold at intentional SINCAP pinholes appeared black or red-brown on all the positively biased lines with 10-µm gap. One sample had this black appearance also at the negative 10-µm line. This was the line pair that had the current increase during the 180 hours of bias. The positive lines with 20-µm gap had this same black appearance at the pinholes on four of the five samples; x-ray energy analysis in the SEM revealed only gold at these sites. These observations agree with a known corrosion mechanism of positively biased gold in acid media. The gold can be converted to a gold oxide under positive bias and then coverted back again. The reconversion to gold causes a disruption of the gold habit, creating a red-brown or black appearance [102]. The typical appearance of this corrosion result is shown in Fig. 23.

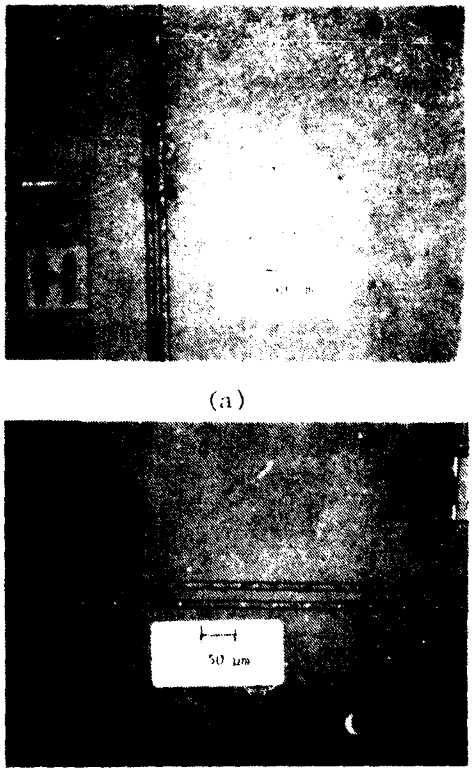

(a)

(b)

Figure 23. Typical black appearance of gold corrosion with positive bias. (a) 10-µm gap; (b) 20-µm gap.

SEM inspection did not show any dendrites. Several possible dendrites had been observed optically, but EDXRA indicated they were not composed of gold. SEM analysis revealed no treelike shape. These initial SEM studies were done on nonconductively coated specimens. After carbon was deposited on these devices, the topology of the black-appearing product was examined. The product appears as a porous or powdery aggregate, as would be expected from the oxide conversion process described above [102].

4. Discussion

During the analysis of passivation layer defects of Section IV.A, it was found that coverage of the line pattern over the intentional steps was generally excellent. In agreement with these findings, during corrosion testing no open circuits were produced on any of the stepped patterns.

Cathodic corrosion was much more prevalent than anodic in all tests of corrosion rate. This is related to the basic corrosion mechanism for aluminum [118,167]. In the presence of water, H^+ and OH^- ions are formed [118,167] according to the following reactions:

Anode: $2\ H_2O \rightarrow O_2 + 4\ H^+ + 4\ e^-$

Cathode: $2\ H^+ + 2\ e^- \rightarrow H_2$

Water: $H_2O \rightleftarrows H^+ + OH^-$

These reactions cause an increase in pH at the cathode and a decrease at the anode. Aluminum will corrode at either low or high pH, but normally only cathodic corrosion occurs since the anodic corrosion product, Al_2O_3, forms an insulating barrier.

The cathodic corrosion process proceeds as follows:

$$2\ Al + 6\ H^+ \rightarrow 2\ Al^{3+} + 3\ H_2$$

$$2\ Al^{3+} + 6\ H_2O \rightarrow 2\ Al(OH)_3 + 3\ H_2$$

The aluminum hydroxide formed has the characteristic black or dark-gray appearance we observed on corroded lines.

An increase in pH at the anode and a decrease at the cathode has been proposed [167]. For our structures, the cathode pH actually increases during corrosion, as described in Section IV.G.

In the presence of sodium deposited before PSG deposition, there was a fivefold increase in the corrosion rate of aluminum. The PSG getters sodium, and Koelmans [118] postulated that the sodium is released when phosphoric acid is leached from the PSG by water. Na^+ then migrates to the cathode and the following reaction takes place [168]:

$$Na^+ + e^- \rightarrow Na$$

$$2\ Na + 2\ H_2O \rightarrow 2\ Na^+ + 2\ OH^- + H_2$$

This reaction increases local pH and thus enhances corrosion.

The much slower corrosion rate of SINCAP-passivated filament-evaporated aluminum is probably related to the absence of phosphoric acid and moisture, both of which are present together when PSG is used. For the PSG layer samples the acid lowers the pH, thus enhancing corrosion rate.

Aluminum deposited by S-gun sputtering had a much lower corrosion rate than filament-evaporated aluminum. As will be seen in Section IV.F.3, the S-gun aluminum after alloying has a much larger grain size than the filament-evaporated aluminum. Since corrosion rate can be enhanced at grain boundaries by the microsegregation of impurities at these boundaries [29], the comparison of corrosion rates indicates the advantage of large grain size.

From the measurements of current described in Section IV.B.1 and from microscopic analysis, current efficiencies for corrosion were calculated. This was done by obtaining the approximate total charge by linear integration of the current measured at intervals during the corrosion test; the total volume of aluminum corroded is determined by microscopic observation at 150X. The current efficiency is given by

$$\varepsilon = nF\rho V/mQ$$

where

ε = current efficiency,
n = valence (3 for aluminum),
$F = 9.65 \times 10^4$ C,

ρ = density (2.7 g/cm^3 for aluminum),
V = volume corroded, cm^3,
m = molecular weight (27 g/mole for aluminum), and
Q = integrated current, C.

For aluminum, the above equation reduces to

$$\varepsilon = 2.90 \times 10^4 \, V/Q$$

Current efficiencies were calculated for several types of test devices. The devices chosen were typical in both current magnitude and amount of corrosion observed. The results are given in Table 3.

TABLE 3. CURRENT EFFICIENCY FOR CORROSION

Sample* Passivation	Efficiency
PSG, 4% P, 8300 Å	0.03, 0.08
PSG,** 4% P, 7500 Å	0.01, 0.07
Plasma SINCAP, 7900 Å	0.004, 0.003

---

*All samples had 10,000 Å of filament-evaporated aluminum.
**$NaHCO_3$ applied just prior to passivation.

Neither in the testing of gold patterns in the humidity chamber nor in the contamination chamber with chlorine could any evidence of gold deplating or dendrite formation be found. In previous work, dendrites were found with sputtered quartz passivation [83,210] and on hybrid circuits with Al_2O_3 substrates [44,141]. We know of no gold dendrite formation with SINCAP passivation. In all of these previous cases, either a crack at the metal edge or poor edge coverage was involved. For pinholes over the metal line, dendrite growth may be much less likely.

C. CORROSION CURRENT MEASUREMENTS

Several methods were used to determine the dependence of the corrosion current on relative humidity and temperature. The comb pattern test device was employed each time. In the first series of tests, devices were placed in the humidity chamber after cleaning and baking. Measurements were taken as relative humidity was decreased from 90 to 65% at each temperature, in the order of decreasing temperature. Temperatures were 85, 70, and 57°C. After each temperature and humidity condition was established, a potential of 20 V was applied, and the current was recorded after two hours. Previous tests had shown that a reasonably steady state was established in about two hours. Figure 24 shows the typical time dependence.

In addition to being very time consuming, this type of measurement produced anomalous results in that current readings for a constant humidity were larger at the lower temperatures than at the higher temperatures. This indicates that some sort of conditioning effect occurs at the higher temperature-humidity conditions which affects the current at the lower temperatures. This effect has been found by others [192,196].

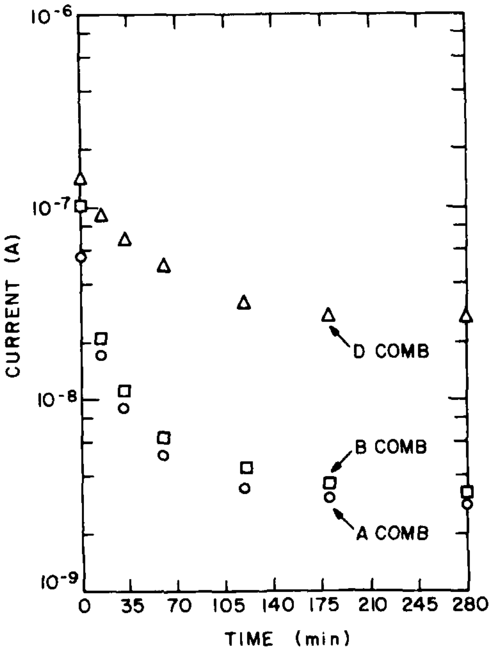

Figure 24. Time dependence of current for comb patterns at 85°C and 85% rh. Voltage of 100 V applied at time = 0. Sample is aluminum with standard PSG layer.

In the next experiment, measurements were taken as temperature and humidity were increased. Again, it was found that current increased as temperature decreased. After several further measurements, a method was adopted that yielded a positive dependence of current on temperature. This measurement technique is described below.

Initially, the devices were cleaned and baked as described in Section III.B.7. Measurements were taken as an increasing function of humidity at constant temperature. The same result was obtained for increasing as for decreasing temperature. At each temperature and humidity setting, the devices were allowed to equilibrate for 60 minutes after reaching constant temperature and humidity. Then, voltage was applied and the current was read after one minute. The voltage was then turned off. After each series of measurements as a function of increasing humidity at a given constant temperature, the devices were removed from the chamber and baked at 200°C in room ambient before being put back into the humidity chamber for measurement at the next temperature.

This procedure enabled us to obtain reproducible data in which current increased with increasing temperature at a given humidity, in contrast to our previous anomalous results in which current decreased with increasing temperature. Since voltage is applied only when current readings are made, we expect our results to apply to practical situations where a large, renewable supply of moisture and contaminant is present. Specific examples would include plastic-packaged devices, hermetic devices with leaks in a humid ambient, or hermetic devices with gross sealed-in contamination.

The procedure just described was applied to aluminum comb pattern devices of two types that were identical except for the passivation layer. The device parameters are given in Table 4.

1. Voltage Dependence

The dependence of current on voltage is approximately linear up to about 30 V, and sublinear (exponent of 0.9 on log-log plot) from 30 to 100 V. This sublinear dependence probably reflects ionic sweep-out.

TABLE 4. TEST DEVICE STRUCTURE

Structure	Passivation	
	PSG	SINCAP
Oxide	6200 Å, HCl-steam	Same
Aluminum	11,000-Å filament	Same
Heat treatment	450°C, 20 min, FG*	Same
Passivation	8200 Å, 4.4% P	8000 Å
Passivation etch	Buffered HF	Plasma

---

*Forming gas.

2. Relative Humidity and Temperature Dependence

The dependence of the log of the corrosion current on relative humidity was approximately linear at the three temperatures examined (87.5, 73.5, and 60.0°C). The current at 100 V was converted to an effective surface resistance as shown in Section III.A.2, and the typical humidity dependence for a PSG device is shown in Fig. 25. Note that the A comb has the highest surface resistance, and the D comb the lowest, as expected. Figure 26 shows the corresponding result for a SINCAP-passivated device. From the raw current data from which the surface resistance was calculated, the constant b in the term

$$I = I_o \exp (b \times rh)$$

was calculated. Here, I is current (A) and rh is relative humidity (%). For the PSG-passivated devices, values of b ranged from 0.10 to 0.20 over a voltage range of 10-100 V. Calculations for the SINCAP-passivated devices yielded similar values for b, but the range of slopes was greater, varying from 0.10 to 0.30.

Figure 27 shows the temperature dependence at rh = 90% for the B and D combs of the PSG sample. The activation energies are 1.2 and 1.4 eV for the B comb (passivation with pinholes) and D comb (passivation removed), respectively. Figure 28 shows similar data for the SINCAP samples. Here

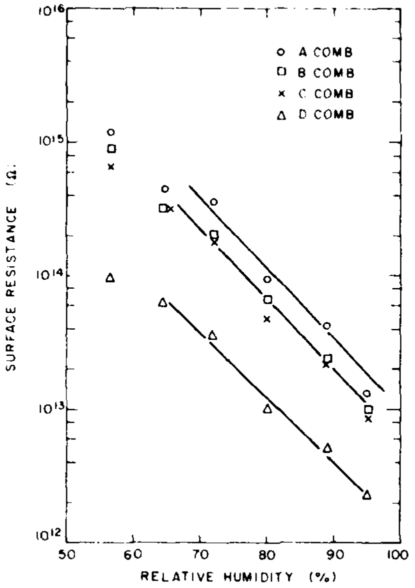

Figure 25. Dependence of initial surface resistance at 100 V on relative humidity at 87.5°C for aluminum combs passivated with PSG.

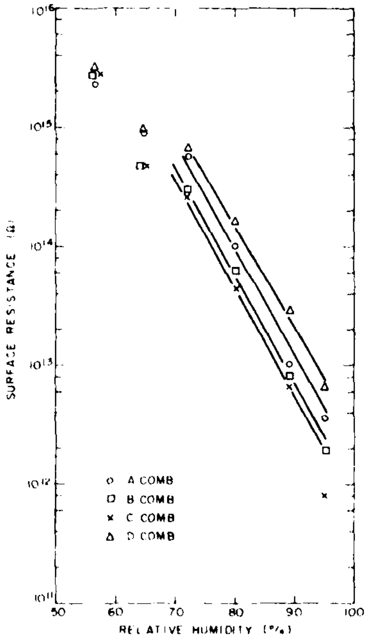

Figure 26. Dependence of initial surface resistance at 100 V on relative humidity at 87.5°C for aluminum combs passivated with SINCAP.

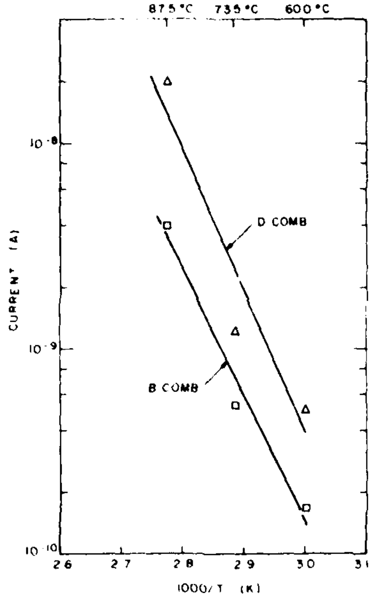

Figure 27. Temperature dependence of corrosion current at 90% rh for PSG-passivated aluminum combs.

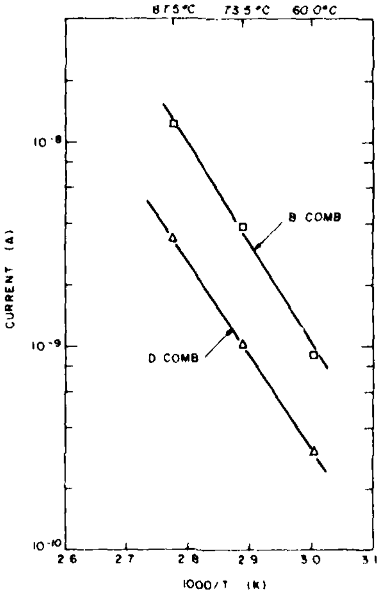

Figure 28. Temperature dependence of corrosion current at 90% rh for SINCAP-passivated aluminum combs.

the activation energies are 1.0 and 0.90 eV for the B and D combs, respectively.

During this series of measurements, corrosion was found in the initial tests when voltage was applied for the total time in the humidity chamber. The corrosion produced by 100-V bias at t = 86°C, rh = 90% on aluminum comb patterns with PSG passivation occurred principally at the negatively biased metal, as expected. A comparison of cathode corrosion for identical cathode geometry but different amounts of exposed anode showed that the anode area is related to the amount of cathode corrosion. This was done by comparing the number of corrosion sites on combs B and C on the same chips. Both cathode combs had identical intentional pinholes in the passivation. The anode of comb B has an identical hole pattern, while the anode of comb C has long open slots in the passivation over the anode. Cathode corrosion on comb C occurred at about four times the number of locations as on comb B, and the corrosion at each site was greater.

3. Interface Currents

The comb test device was used to investigate the possible presence of ionic current flow at the interface between the thermal oxide and the deposited PSG passivation layer. Currents between aluminum combs on patterns A and D were measured at 100 V and 23°C in dry N_2 as a function of autoclave exposure (15 psig, 121°C) for samples with 27,000-Å-thick PSG and with 12,000-Å-thick PSG. The phosphorus contents were both 4.7% by wt. As seen in Fig. 29, the D comb without passivation shows only a slight increase in current due to autoclave exposure, as anticipated, since it is over a thermal oxide. For the passivation-covered A pattern there is a large increase in current. For times greater than 20 hours there was little or no additional increase. Because the measurements are done in dry N_2 ambient, these currents are not surface related and thus flow in the bulk of the PSG or at the PSG-SiO_2 interface. If this interface were a large factor in this autoclave-induced current, then the current for the thick PSG sample (27,000 Å) would be comparable to that of the thin PSG sample. Since there is, however, a large dependence on PSG thickness, we conclude that most of the current induced by moisture penetration

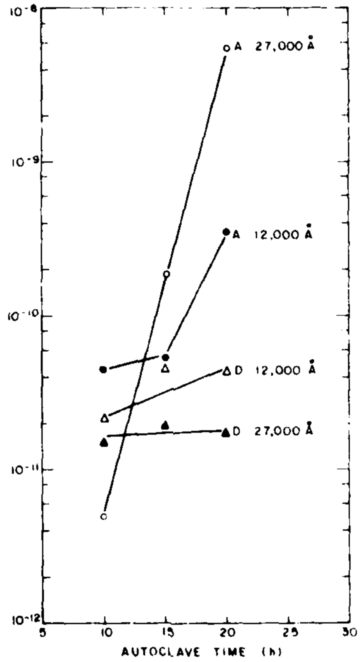

Figure 29. Current at 100 V on comb patterns in dry ambient after autoclave exposure for two PSG thicknesses.

in PSG films over thermal SiO_2 flows in the bulk of the film, with little contribution from the PSG-SiO_2 interface.

4. Potential-Profile Measurements

The special structure described in Section III.A.1 that consists of a closely spaced line pair with a potential-measuring electrode opposite the end of the line pair was intended as an exploratory structure to attempt detection of nonuniform potential profiles at corroding electrodes. Aluminum patterns with either PSG or SINCAP passivation were studied. The silicon substrate was grounded and the single potential-profiling electrode was left floating. While bias was applied for times ranging from 10 to 30 minutes across the closely spaced line pair with an ambient relative humidity of about 70%, the current between the lines of the pair was monitored. With bias still applied, dry N_2 was admitted to the probe station. When the relative humidity had decreased to about 20% and the monitored current was less than 1 pA, a probe connected to an electrometer in the charge-measuring mode was brought down onto the previously floating potential-profile electrode. This made it possible to measure the charge on this electrode. The capacitance to the substrate was calculated from the line area and oxide thickness. From this and the measured charge, the potential of the line with respect to the substrate was determined. This experiment was done with the following bias conditions on the closely spaced electrodes: One line was always grounded and the other line was made +50, -50, or 0 V with respect to the grounded line. With zero bias, the potential detected on the test electrode was near zero, as expected, and was no more than 0.1-0.2 V. For the case of +50-V bias, voltages of about 2-3 V were measured. This might indicate, since the test electrode is very close to the potential of the negative closely spaced line, that there is a large potential drop at the positively biased electrode. If this were the case, then with -50 V on the line pair, a potential on the test electrode near to -50 V should be detected. This was not the case, however, as voltages of approximately -2 to -3 V were detected. This indicates that the test electrode potential is essentially governed by leakage paths to the grounded substrate.

In addition, tests were done with a high-impedance voltmeter connected to the potential-profile electrode. Measurement of the potential during application of bias to the line pair under humid and dry conditions indicated again that leakage paths to the substrate governed the potential of the test electrode.

5. Discussion

The measurements of corrosion current described in this Section (IV.C) represent the first report, we believe, of corrosion current measurement in the presence of a passivation layer over the metal. Previous studies [45,118,196,213] measured corrosion current only in the absence of a hard passivation over the metal. In one case, the author stated that corrosion currents could not be measured in the presence of SiO_2 passivation [213].

The dependence on relative humidity was found to be exponential for both PSG and SINCAP passivation, and for the D comb where passivation was etched away. The constant of proportionality between the natural logarithm of current and relative humidity ranged from 0.10 to 0.20 for PSG, and from 0.10 to 0.30 for SINCAP. This can be compared with data of Anderson and Kempton [6], quoted by L. Holland [97]. Anderson and Kempton measured the surface water adsorbed by silica as a function of the partial pressure of water. From their data, a similar proportionality factor can be calculated to be 0.060, when rh is expressed in percent. This agrees reasonably well with our current-dependence data, and indicates that the magnitude of current is directly proportional to the amount of water adsorbed on the surface of the phosphosilicate glass or SINCAP passivation. Others have also found an exponential dependence of current on vapor pressure [8,118,141,196]. For gold metal and SINCAP, the proportionality constant was about 0.07 [196]. A proportionality constant of 0.3 can be calculated for the aluminum corrosion rate with PSG passivation [167]. Since the dependence on relative humidity is approximately the same for the corrosion rate as it is for the amount of adsorbed water, the current-limiting step is the transport through the water film connecting the two electrodes. Thus, a high-field region is expected to exist everywhere between the two closely spaced electrodes, and diffusion is unimportant. This is reflected in the fluroescent dye experiments discussed in Section IV.G. As evidenced by the fluorescence, the change in pH occurred immediately when voltage was applied. When bias was removed, the fluorescence decayed slowly (within minutes).

The activation energies found for the currents are in the range of 0.9-1.4 eV. This is higher than the previously reported values, which range from about 0.34 [118] to 0.75 [213]. This difference may be related to differences in the measurement method, as the current values in Section IV.C were obtained immediately after voltage application, while those in the previous work were measured a few hours after voltage application. Also, there may be real differences in kinetics between the corrosion current flowing over an insulator between large metal electrodes and the corrosion current flowing between small regions of electrodes with overlying passivation.

The fact that corrosion was more likely to occur on the C comb (with a large anode) than on the B comb (with a relatively small anode) proves the importance of anode passivation. Since the formation of a passivating oxide limits the current flow, the presence of a large anode induces greater corrosion on a given cathode.

In none of these experiments - the corrosion rate measurements with line patterns, the corrosion current measurements with comb patterns, and contamination tests - were any sites of purely chemical corrosion found. Unbiased metal regions, whether passivated or not, were unaffected.

D. EFFECTS OF CONTAMINANTS

The effect of sodium contamination prior to PSG deposition was discussed in Section IV.B.1. The sodium produced a large increase in aluminum corrosion rate. In this section some further electrical measurements of contaminant effects are discussed, and an analysis of the effect of sodium motion on test devices is presented.

1. Electrical Measurements

Fluoride ion produces large and unique corrosive effects on an aluminum film in contact with the electrolyte in an electrochemical cell (see Section IV.E). The following experiment shows that sodium fluoride has a smaller effect than sodium chloride on the surface conduction of oxides. Thus, any special effect of fluoride ion on aluminum in an IC will be due only to the reaction at the corroding electrode, and the reduced effect on oxide surface conduction by fluoride will act to decrease possible fluoride-induced corrosion as compared with chloride-induced corrosion.

The tests were done at room temperature in the controlled-humidity probe station. Comb patterns of aluminum passivated with a standard PSG layer (8200 Å, 4.4% P) were used.

Current at 100 V was measured on A, B, C, and D combs of 10 test devices at a relative humidity of 25, 45, 60, and 70%. Five of the devices were then contaminated with a 0.01M/L solution of NaCl, and five with NaF of the same concentration. This was done by dipping the samples into the solutions for 5 s, draining, and air drying. Then the device surface currents were measured again, as described above. Results within each group of NaCl and NaF devices agreed closely and can be illustrated by considering the data for one device at 60% rh. The results, shown in Table 5, indicate that the effect on corrosion current of contamination by NaF is much smaller than that of NaCl.

TABLE 5. EFFECTS OF CONTAMINATION ON CURRENT (A)

	Condition		
Comb	Initial	NaCl	NaF
A	1×10^{-12}	5×10^{-11}	1×10^{-12}
B	1×10^{-12}	3×10^{-9}	2×10^{-11}
C	1×10^{-11}	5×10^{-8}	2×10^{-10}
D	5×10^{-11}	3×10^{-6}	5×10^{-8}

The controlled contamination chamber was used for exploratory studies of vapor-carried contaminants. The effects of Cl_2 gas, HF gas, and possible vapor from a silver-containing chip-mounting epoxy (uncured) were introduced separately to the sample chamber. The concentration of each gas, Cl_2 and HF, in the sample chamber was approximately 10 ppm. The identity and concentration of vapors from the epoxy were not known. The uncured epoxy was heated at temperatures up to 150°C in N_2 flow to generate vapor that was carried to the sample chamber. Conditions in the chamber were maintained at 75°C, 75% rh. Samples tested included aluminum comb patterns passivated with PSG and SINCAP, and gold-trimetal line patterns passivated with SINCAP. Increases in corrosion current due to contaminant vapor were observed only with chlorine, and only on aluminum passivated with PSG. A tenfold increase was observed when Cl_2 vapor was introduced, and a corresponding decrease occurred after the flow of Cl_2 was stopped.

All samples exposed to the contamination were examined by optical microscopy. The cathodic corrosion product on the aluminum PSG devices had a typical black appearance and, at the anodes, the aluminum was missing.

The gold-SINCAP devices had a black corrosion product on the anodes, similar to that discussed in Section IV.B.3. Even after 240 hours at 75°C/75% rh with 10 ppm Cl_2, no dendrite formation was detected. The aluminum-SINCAP comb devices had an unusual-looking corrosion product. Microscopic examination of the test devices revealed a black, sooty product, predominantly cathodic in origin, over all of the four Al comb patterns (see Figs. 30 and 31). The extent of Al corrosion on each comb pattern appeared inversely proportional to the degree of SINCAP coverage; patterns A, B, C, and D, ranging from completely passivated to partially passivated to unpassivated, exhibited a correspondingly increasing amount of corrosion. The test devices were decapsulated and submitted for compositional analysis of the corrosion product by scanning Auger microanalysis. The results of this analysis are shown in Table 6.

TABLE 6. SCANNING AUGER ANALYSIS (ATOMIC %) SAMPLING OF 100-Å SURFACE DEPTH

	Element						
Comb	Cl	C	N	O	F	Al	Si
A	0.8	33.8	4.9	26.0	0.2	4.1	34.2
B	0.6	26.1	7.6	28.9	0.2	3.0	41.2
C	1.8	47.8	1.0	27.2	0.3	7.2	12.1
D	1.2	17.0	-	32.5	0.7	14.4	26.5

The presence of Si, Al, O, and N as components of the metal or passivation layer was expected. The chlorine was adsorbed from the contamination chamber ambient. The fluorine and carbon were not expected to be present. A possible source for fluorine may have been the degreasing process with trichlorotrifluoroethane just prior to measurement. Residual photoresist after passivation layer patterning may have been a source for carbon. This sooty corrosion product was found only with chlorine present in the ambient; devices exposed to bias in the humidity chamber did not have this appearance.

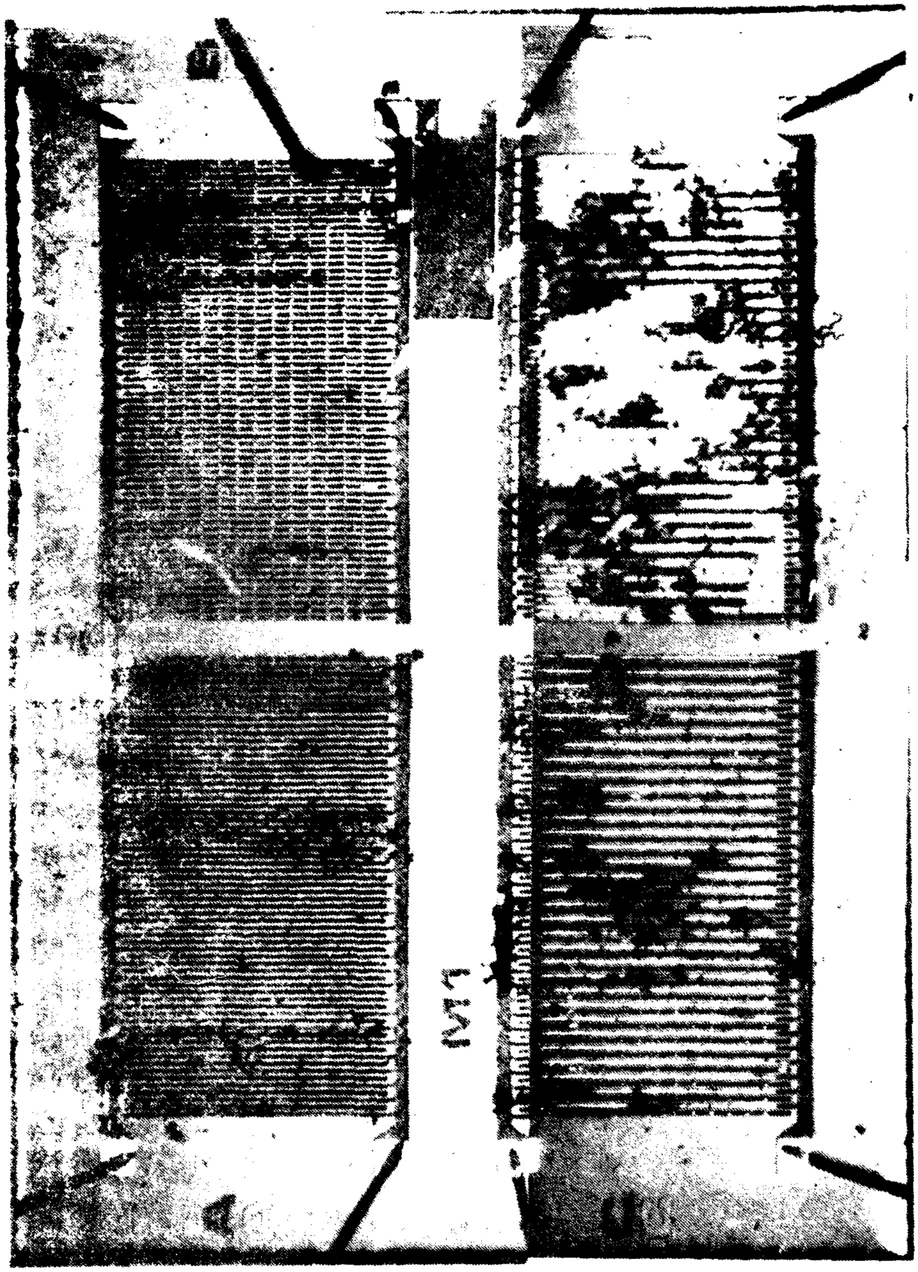

Figure 30. Composite photomicrograph of the black, sooty, corrosion product on an Al comb-patterned device passivated with SINCAP after Cl_2 gas treatment at 75°C and 75% rh.

Note the progressively increasing amount of corrosion in patterns A, B, C, and D, which represent correspondingly decreasing degrees of passivation.

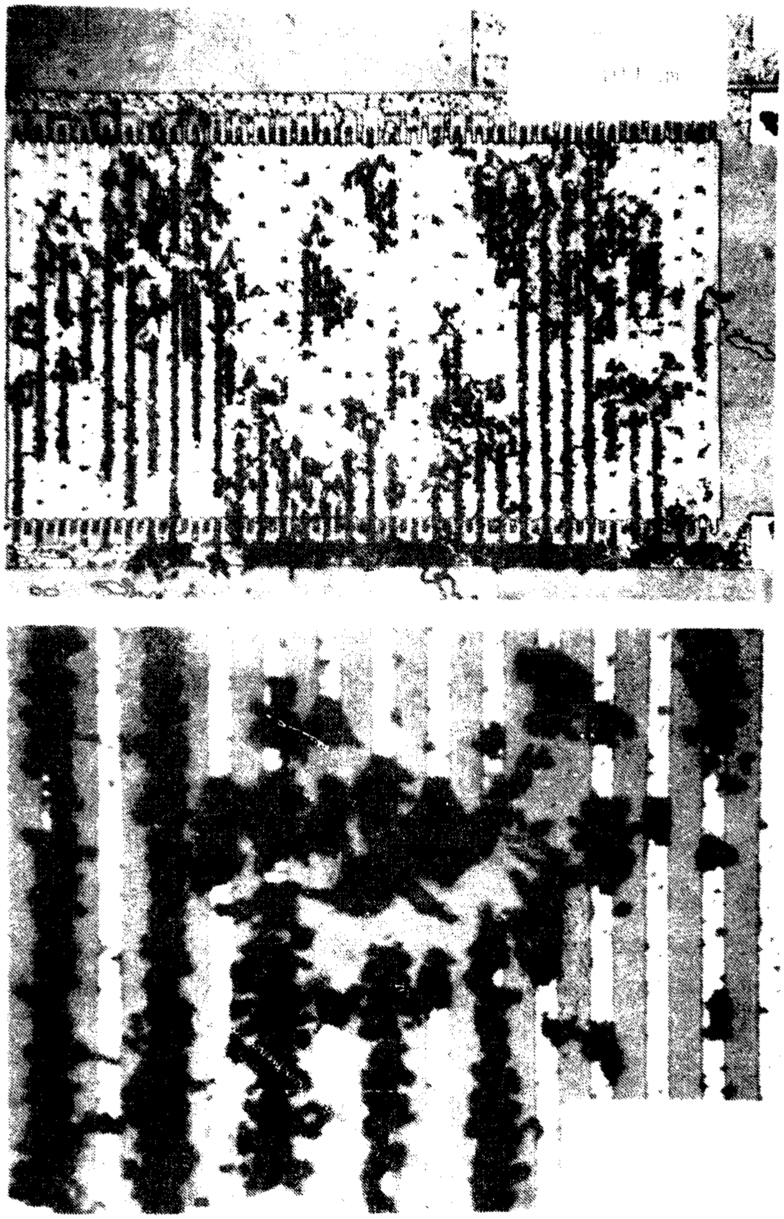

Figure 31. Higher magnification of the corrosion product on the unpassivated Al-comb pattern D of Fig. 30, which exhibited the most severe degradation.

2. Technique for Attaining Uniform Ion Distribution on Surfaces

Instrumental analysis of samples purposely contaminated with sodium ion by dipping in aqueous-alcoholic solution showed nonuniform surface distribution. It became clear that a technique needed to be established for attaining controlled and uniform surface contamination of device test wafers so that the effects of ionic impurities, such as sodium ions, on metal corrosion could be studied.

The test samples used consisted of patterned and unpatterned electron-beam-evaporated aluminum films on both polished, single-crystal silicon slices, and on thermally grown SiO_2 films on silicon slices. Sodium ion in the form of Na_2CO_3 in aqueous solutions was chosen as the contaminant species. Electron probe microanalysis was employed as the test method for examining the distribution of Na^+ on the surfaces before and after alloying heat treatments for 20 minutes at 450°C in N_2. Simultaneous scans of the NaK_α and the SiK_β radiation intensities vs surface distance were strip-chart-recorded for subsequent evaluation. The SiK_β radiation from the substrate was effectively shielded by the Al patterns, revealing the exact location of the pattern in the synchronized chart recordings. We have demonstrated that uniform surface distribution can be attained on SiO_2 and on unpatterned and patterned aluminum, whether unalloyed or alloyed. Higher concentrations result on Al surfaces than on extremely smooth SiO_2. The concentration on SiO_2 remains uniform to the very edge of the Al patterns. However, to achieve the uniformity we report it is necessary to prepare the sample surface for optimal wetting with the carefully applied contaminant solution. The best results for organically contaminated (during normal storage) SiO_2 and Al surfaces (without removing more than a thin surface layer of Al) were obtained with the following procedure:

(1) Immerse in NH_4OH(28-30% by wt NH_3)-H_2O_2(30%)-H_2O (DI)* solution (1:1:5 by vol) for 2 minutes at 95°C. Rinse with water.

(2) Immerse in HNO_3(70%)-H_2O (DI) solution (1:10 by vol) for 10 s at room temperature and rinse with water.

---

*DI = deionized.

(3) Immerse in absolute C_2H_5OH for 30 s.

(4) Without allowing to dry from step 3, immerse for 30 s in the contaminant solution consisting of 0.010, 0.10, or 1.0% by wt of Na_2CO_3 in H_2O-C_2H_5OH (1:1 by vol), containing 0.01% by vol of FC-93 fluorocarbon surfactant (3M Company).

(5) Remove the sample without rinsing and place it on wafer spinner for drying at high centrifugal speed.

The resulting surface concentration on SiO_2 from the three solutions is shown graphically in Fig. 32. These data were obtained by quantitative atomic absorption spectrometry of an HF-H_2O (1:20 by vol) extract which removed SiO_2 to a depth of 240 Å from the wafer front surface. Prior to analysis the wafer edges were removed by cutting to eliminate any edge buildup of contaminant; the surface of the wafer was protected with a thick layer of acrylic spray coating.

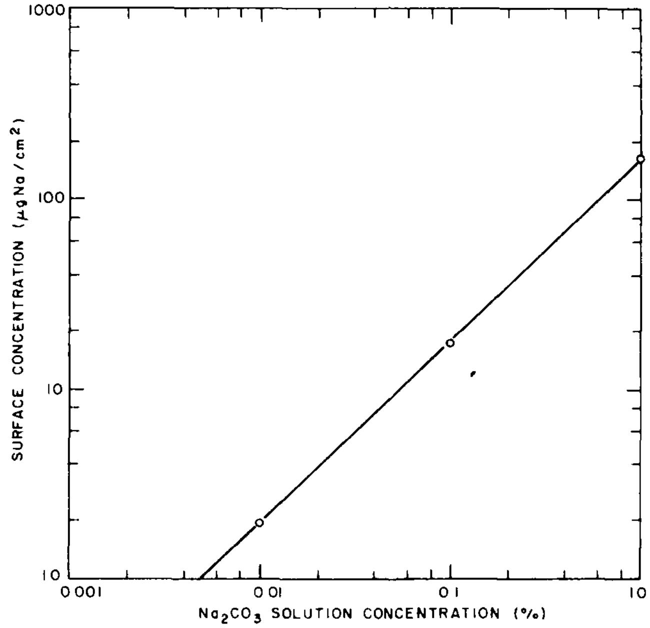

Figure 32. Surface quantity of sodium ions on SiO_2 vs Na_2CO_3 solution concentration.

3. Depth Distribution of Sodium Ions in Oxide and Metal Films

Unexpected results were obtained in preliminary tests that indicated rapid diffusion of sodium ions into aluminum. Repeat tests and additional analyses confirmed these findings. The results obtained in the present detailed set of experiments are summarized in Table 7 for SiO_2 and in Table 8 for aluminum.

The substrate materials used for these tests consisted of polished silicon wafers of 7.5-cm diameter. For the oxide tests, one wafer with a thermally steam-grown SiO_2 layer of 1-μm thickness was used. For the metal tests, one wafer with an electron-beam-evaporated Al-1%Si alloy layer of 1-μm thickness was used. A section was cut from each wafer to serve as a blank in the film dissolution tests. The wafers were then chemically cleaned and contaminated with Na_2CO_3 solution by the technique outlined in Section IV.D.2. Next, the back surface of the wafers was protected with a double layer of acrylic plastic to seal in sodium and thereby prevent its removal during the dissolution treatments.

Mechanically captive and physically adsorbed Na^+ ions were removed by rinsing for 2 minutes in deionized and distilled water. Chemisorbed Na^+ was then desorbed from the surface by immersion for 2 minutes in HNO_3-H_2O (1:10) without etching of the SiO_2 or Al. Diffused Na^+ was isolated by the sequential removal of layer sections (i.e., 10 and 20% of total thickness) with highly selective chemical etchants especially formulated for this purpose (for details see Tables 7 and 8). All dissolution tests were conducted at 25°C with 25 mL of etchant, followed by water rinsing and adjustment to 100 mL. The Na^+ concentrations were determined by atomic absorption spectrometry corrected for blank values obtained from the uncontaminated layers, and expressed as net μg Na^+/cm^2 surface or layer section. The results are also expressed as percent per layer of the total quantity of Na^+ recovered.

The results from Tables 7 and 8 and from previous tests are summarized as follows:

1. Controlled contamination of thermally grown SiO_2 films with Na_2CO_3 solution by the technique described in Section IV.D.2 shows that 52% of the sodium is mechanically and physically adsorbed on the surface, 25% is chemically adsorbed, and 23% diffuses at room temperature into SiO_2 to a depth of 2000 Å.

TABLE 7. DISTRIBUTION OF SODIUM IONS IN SiO_2 FILMS BEFORE AND AFTER ANNEALING AND GLASSING*

		Treatment								
		No Heat Treatments			Annealed for 20 min at 450°C in N_2			Annealed and Glassed at 450°C		
Layer Dissolved (%)	Etchant Solution	Sample (#)	Net Na^+_2 ($\mu g/cm^2$)	Dissolved (%)	Sample (#)	Net Na^+_2 ($\mu g/cm^2$)	Dissolved (%)	Sample (#)	Net Na^+_2 ($\mu g/cm^2$)	Dissolved (%)
PSG Top (800 Å)			None			None				
80	BHF**							G-1	18.5	24
10	BHF							G-2	19.0	24
10	BHF							G-3	11.8	15
SiO_2 (10,000 Å)										
0	H_2O	N-1	19.2	52	A-1	8.64	37			
0	HNO_3, 6.4%	N-2	9.30	25	A-2	3.91	17			
10	BHF	N-3	5.43	15	A-3	3.10	13	G-4	3.86	4.9
10	BHF	N-2	2.85	7.7	A-4	4.52	19	G-5	13.2	17
20	BHF	N-5	0	0	A-5	3.11	13	G-6	10.1	13
20	BHF	N-6	0	0	A-6	0	0	G-6	2.10	2.7
Total			36.8	100		23.3	99		78.6	101

---

*Explanations are given in text.

**Buffered HF composition: 80 mL HF, 49%; 300 mL H_2O, 200 g NH_4F (cryst.); 360 mL CH_3COOH, 99%; at 25°C.

TABLE 8. DISTRIBUTION OF SODIUM IONS IN ALUMINUM FILMS BEFORE AND AFTER ANNEALING AND GLASSING*

		Treatment								
		No Heat Treatments			Annealed for 20 min at 450°C in N_2			Annealed and Glassed at 450°C		
Layer Dissolved (%)	Etchant Solution**	Sample (#)	Net Na^+ ($\mu g/cm^2$)	Dissolved (%)	Sample (#)	Net Na^+ ($\mu g/cm^2$)	Dissolved (%)	Sample (#)	Net Na^+ ($\mu g/cm^2$)	Dissolved (%)
PSG Top (8000 Å)			None			None				
80	BHF							G-11	0	0
10	BHF							G-12	9.69	44
10	BHF							G-13	1.56	7.2
Al-1%Si (10,000 Å)										
0	H_2O	N-11	3.31	16	A-11	0.35	1.8			
0	HNO_3, 6.4%	N-12	8.39	40	A-12	0.62	3.1	G-14	3.03	14
10	Al-Etchant	N-13	6.78	32	A-13	1.71	8.6	G-15	5.83	27
10	Al-Etchant	N-14	2.59	12	A-14	2.69	13	G-16	0.87	4.0
20	Al-Etchant				A-15	2.93	15	G-17	0	0
20	Al-Etchant				A-16	2.84	14	G-18	0.83	3.6
40	Al-Etchant				A-17	Est. 9	Est. 45			
Total			21.1	100		20	100		21.8	100

---

*Explanations are given in text.

**Special high-selectivity etchant compositions are as follows:

BHF (Buffered HF): 80 mL HF, 49%, 300 mL H_2O, 200 g NH_4F (cryst.); 360 mL CH_3COOH, 99%; at 25°C.

Al-Etchant: 40 mL H_3PO_4, 85%; 40 mL CH_3COOH, 99%; 10 mL HNO_3, 70%; 10 mL H_2O; at 25°C.

2. A simulated alloying heat treatment at 450°C for 20 minutes in N_2 caused 45% of the Na^+ to diffuse to a depth in SiO_2 of 4000 Å.

3. Annealing followed by glassing at 450°C caused gettering of the Na^+ by PSG to the extent of 64%, the bottom 20% layer of the PSG containing 39% of the Na^+ and the balance being distributed in the SiO_2 beneath.

4. Contamination of electron-beam-evaporated Al-1%Si on Si substrate by the same technique noted above (see 1) caused 16% of the Na^+ to be lightly adsorbed, 40% chemisorbed, and 44% to penetrate at room temperature to a depth of at least 2000 Å.

5. Alloying at 450°C for 20 minutes in N_2 caused most of the Na^+ to penetrate throughout the 10,000-Å-thick metal layer. Only 3.9% remained on the surface. Similar results were obtained with electron-beam-evaporated 100% Al, alloyed before or after contamination, where Na^+ became distributed more or less uniformly throughout the layer.

6. Annealing followed by glassing at 450°C caused the Na^+ to be redistributed in the PSG to the extent of 51%, most of which is concentrated in the second 10%-layer near the Al. The other half of the Na^+ remains in the top 20% of the Al.

In conclusion we report that during alloying at 450°C, surface-adsorbed Na^+ diffused extremely rapidly to a depth of 0.4 μm in the SiO_2, and throughout a 1-μm-thick layer of 100% Al or Al-1%Si alloy. Subsequent deposition of a PSG layer effectively gettered more than half of the Na^+ from the SiO_2 or Al sublayers.

E. ELECTROCHEMICAL MEASUREMENTS

Corrosion is an electrochemical phenomenon. On IC devices, corrosion is difficult to characterize because of the small scale of electrodes and the complexity of the process. Current paths, transport mechanisms, electrode potentials, and corrosion products are difficult to determine. In spite of these unique problems encountered in IC device corrosion processes, some information about general corrosion processes can be gained by examining the electrochemical processes on a relatively large scale and within the confines of a well-defined electrochemical system. The evaluations of corrosion stability discussed in this section are measurements of this kind. A test electrode with an area of 0.49 cm^2, large by IC device standards, is used. The electrolyte composition, applied electrochemical bias, and test electrode characteristics are experimentally controlled by the apparatus described in Section III.C.

Current paths and the transport of reaction product are dominated by the highly conductive electrolyte in contact with test electrode surfaces. This situation may be significantly different from that encountered on a metallized IC substrate. However, the electrolyte is expected to speed up the corrosion processes of the thin-film test electrodes studied here. In addition, the electrochemical characteristics of the corrosion process are better defined under these circumstances.

The discussion of these electrochemical measurements is organized as follows: An initial section is devoted to outlining the experimental procedure and the various methods by which relative corrosion stability is evaluated. Specific evaluations of corrosion stabilities are described in subsequent subsections. They include the effect of contaminants on the corrosion processes of aluminized substrate, effects of alloying on the corrosion stability of aluminized substrates, corrosion processes on gold-trimetal substrates, and a determination of film stress effects on corrosion stability. The final subsection is devoted to a discussion of the methods of electrochemical evaluation and the major experimental results.

1. Methods of Evaluating Relative Corrosion Stability

Most of the evaluations described in this section are qualitative. Comparisons between various aluminum and gold substrates were made to determine if there were any significant differences in their corrosion stabilities. A combination of visual comparison of the samples and of the electrochemical E-vs-I curves described in Section III.C were employed. On aluminized substrates, because the breakthroughs of corrosion pits through the Al film to silicon or SiO_2 substrate are easily seen, the relative number and size of corrosion pits were used for visual comparisons. E-vs-I curve measurements of corrosion stability involved comparing the magnitude of the recorded current at a given potential for the samples of interest. Also, the relative shapes and sizes of the curves provide a general comparison of the corrosion reaction mechanism.

Another type of evaluation related to the E-vs-I curve measurements correlated well with the above tests for corrosion stability. It is a measurement of what in this report is termed an "open-circuit corrosion current." Before the voltage supply was turned on to run an E-vs-I curve, a current reading was recorded on some samples. This current is associated with corrosion current. Since the operational amplifier drives the potential of the test electrode to +0.0 V [standard calomel electrode (SCE)], the electrochemical potential of the electrode has been altered from its corroding potential. This change can in fact alter the corrosion characteristics of the test electrode, but if the reading is taken rapidly after applying appropriate leads to the corrosion cell (i.e., within one minute), an approximate measure of the corrosion current is obtained. This "open-circuit corrosion current" corresponds to measurements of the current at +0.0 V (SCE) when no external electrochemical bias has been applied to the test electrode.

Typically, the test electrodes to be compared were mounted in separate corrosion cells. Addition of the appropriate electrolyte to each cell, from the same bottle, was followed usually by a 24-hour equilibration period. Then electrochemical measurements were made on each cell. In general, these tests were repeated at least three times before any conclusions were drawn. Comparisons were made between test samples that had run the same day. Basically, this electrochemical technique allows the corrosion process to begin and proceed during the 24-h equilibration period. Then, the E-vs-I curve and open-circuit corrosion current measurements are determined as a means of rapidly characterizing the reaction and its relative rate. This method suffers from the difficulty that the relative rate at the time of measurement may differ from that at another time. We did encounter this difficulty in some cases. Overnight some samples had completely corroded, and no corrosion currents were present. In these cases, visual inspection of the sample took precedence over the reaction rate evaluation by use of the E-vs-I curve. The following example illustrates the use of an E-vs-I corrosion curve in evaluating corrosion stability.

Figure 33(a) shows the E-vs-I curve recorded for an S-gun-aluminized test electrode in 0.1M sodium acetate solution at pH 7.8. This curve is compared with the one in Fig. 33(b), where the same test electrode was used, but with addition to the electrolyte of a 0.001M sodium chloride contaminant. The curves are similar except that the latter exhibits larger currents at a given potential than does the former. We conclude that the presence of a chloride contaminant (∿30-40 ppm) decreases the corrosion stability of the test electrode.

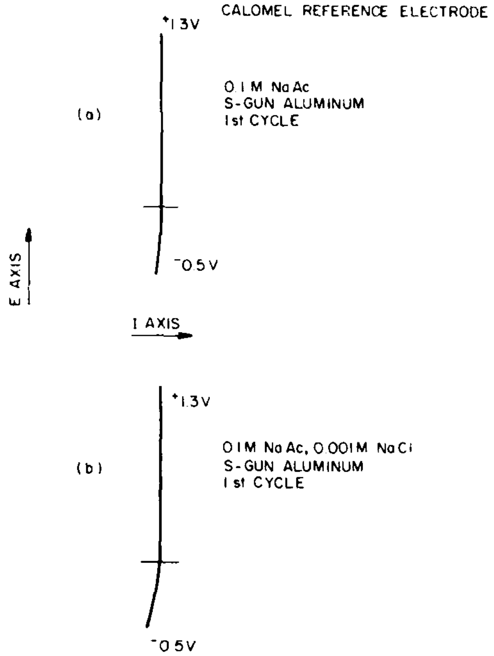

Figure 33. E-vs-I curves on aluminum-metallized substrate.
(a) Without and (b) with NaCl.

Similar types of measurements follow in subsequent subsections. We believe that these electrochemical techniques can be used to establish metallization and environmental conditions that enhance the corrosion stability of metallized substrates.

2. Effects of Contaminants on the Corrosion Processes of Aluminized Substrates

Fluoride, chloride, and bromide electrolyte contaminants have been investigated in the pH range of 4-9. The electrolyte used was either a 0.5M Na_2SO_4 (its pH adjusted with NaOH or H_2SO_4), or 0.5M $Na(CH_3COO)/CH_3COOH$ buffers. Halide contamination levels studied were 0.005M and 0.0005M. The typical corrosion reaction observed for most samples was cathodic (i.e., a current flow was detected in the sample when a negative potential was applied to it). The pH, contaminant concentration, and integrity of the Al_2O_3 passivation layer all influence the magnitude of this current flow. Previous investigators have related these cathodic reactions to the dissolution of $Al(OH)_3$, as shown below [120,167]:

$$Al^{3+} + 3\ H_2O \rightarrow Al(OH)_3 + 3/2\ H_2 \uparrow$$

Our observation of reductions in current flow as the pH is increased from 4 to 8 is consistent with this type of reaction. The presence of halide contaminants tends to increase the rate of this type of corrosion reaction. Among the more significant variations in the corrosion stability of test electrodes that have been observed in these studies for halide contaminations are the following:

1. Spontaneous corrosion reaction in the absence of externally applied electrochemical bias.
2. Greatly accelerated corrosion reaction rates.
3. Indications of different and unique corrosion mechanisms.

These aspects of corrosion stability in the presence of a halide contaminant are discussed in turn for bromide, chloride, and fluoride.

Sodium bromide was introduced at the 0.005M concentration level in sodium acetate/acetic acid electrolyte covering the pH range of 4.5-7.8. Figure 34 shows a typical baseline corrosion curve in the absence of halide contamination and the effect of the bromide contaminant at the same pH. The bromide contaminant does not appear to change the general appearance of the E-vs-I curve, but corrosion currents are enhanced when this contaminant is present.

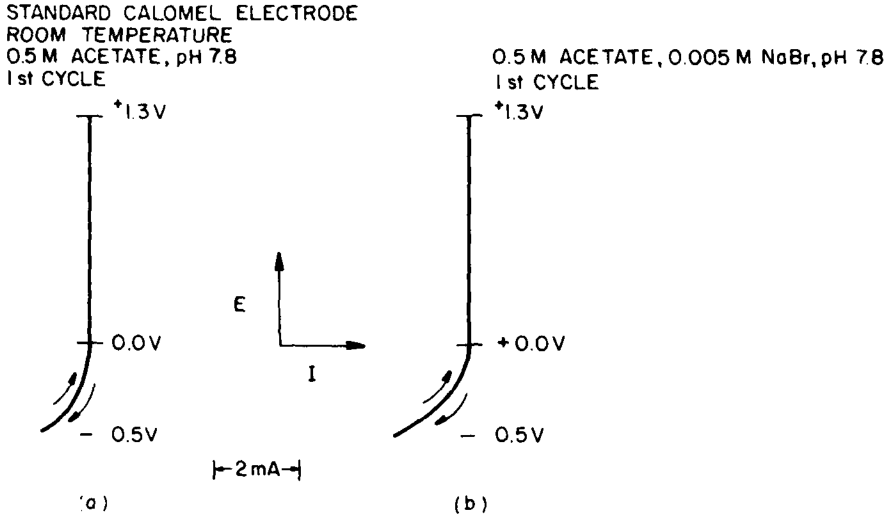

Figure 34. E-vs-I curves for bromide contamination.

Several experiments were carried out in the presence of a chloride contaminant. Figure 35(a) displays the E-vs-I curve for a 0.005M chloride ion contamination level in an acetate buffer solution with a pH of 4.5. Note that a substantial current is present over a wide range of potential. Our coulomb counter also indicated substantial current flow in the absence of an applied electrochemical bias. A positive bias potential of +0.75 V (SCE) is required to inhibit the cathodic reaction. Inspection of the corroded test electrode [see Fig. 35(b)] shows extensive pitting of the sample, although surrounding portions exhibit more limited corrosive attack. Rough portions of some of the E-vs-I curves probably reflect the observed pitting of the sample, as the pitting potential depends on size, depth, and concentration gradients [3,77] (i.e., corrosion within different pits can occur at different potentials, depending on the aforementioned variables). The reduction in corrosion currents upon each successive corrosion cycle probably reflects the passivation of corrosion sites by reaction products. The cathodic corrosion current for each corrosion cycle

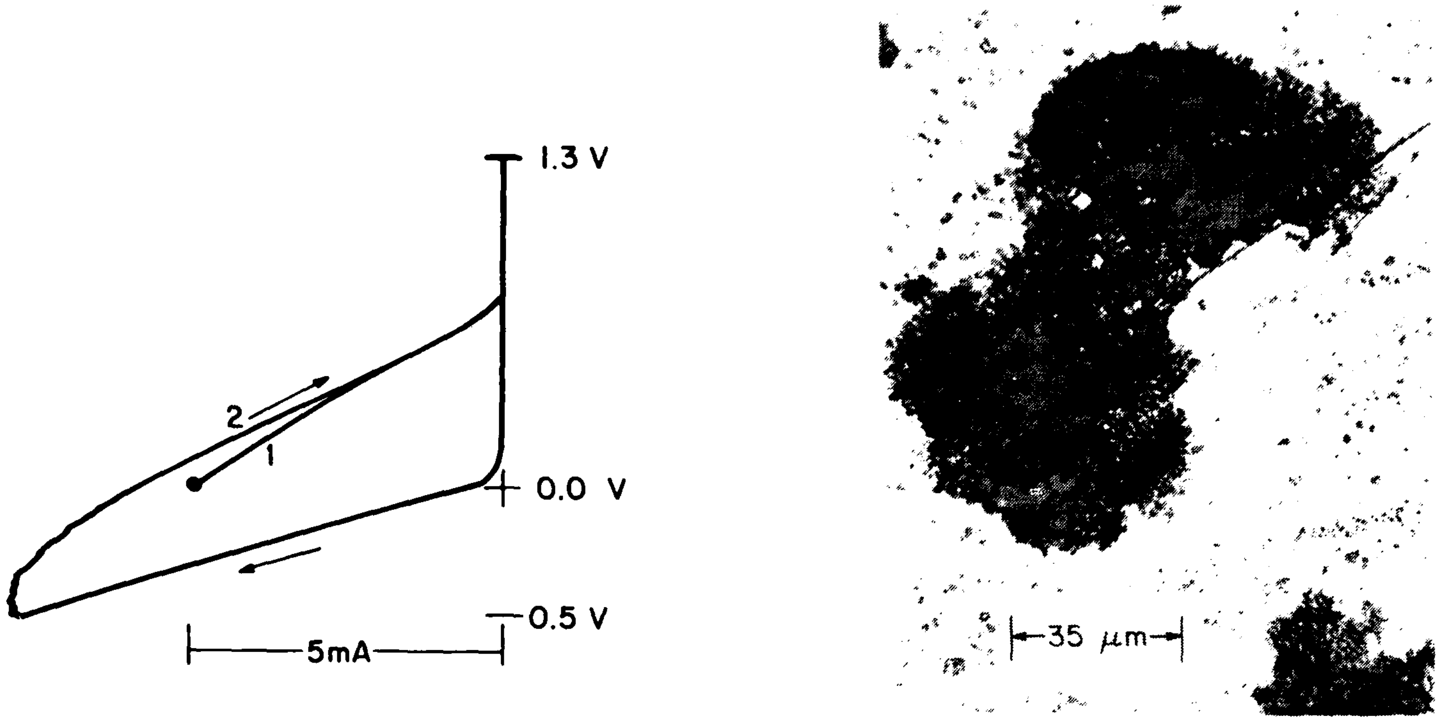

(a)

(b)

Figure 35. E-vs-I curve for chloride-contaminated corrosion and photograph of chloride-induced pitting. (a) E-vs-I curve, pH 4.5, acetate buffer, 0.005M NaCl. (b) Photograph of pitting; same conditions as in (a).

has increased by a factor of approximately 1000; but, more significantly, the open-circuit corrosion current was ~10 mA/cm^2. At the 0.0005M chloride concentration level, neither pitting nor spontaneous corrosion was observed. The E-vs-I curve resembled that of the baseline in the absence of contaminants. At pH values exceeding 5.8 and at 0.005M concentrations, pitting or spontaneous corrosion again failed to be observed, although the cathodic current flows tend to be enhanced over the baseline curves.

Fluoride contamination of the electrolyte produces spontaneous corrosion of aluminized substrates over a wide range of conditions. Fluoride initiates this corrosion much faster than do the chloride and bromide contaminants mentioned above. For instance, under chloride contamination conditions identical with those shown in Fig. 35(a), a replacement of the chloride with 0.005M fluoride and standing for 24 hours at room temperature can completely corrode the exposed aluminum on the silicon substrate. Although at higher pH values this attack does not begin or proceed so rapidly, the spontaneous corrosion (without external bias) [illegible] observed over the entire pH range (4-9) and at concentrations of sodium fluoride as low as 0.0005M (~10 ppm). A typical E-vs-I curve for a 0.005M NaF contamination level is displayed in Fig. 36. Note the large current over a wide range of external potential and the unique characteristic of the cyclic current response. The cathodic current cycle is the opposite of that observed previously for chloride and baseline curves: After application of the maximum negative potential, the cathodic current flow is reduced; chloride and baseline E-vs-I curves, however, show increased current flow. This unique effect of fluoride contamination on E-vs-I curves suggests a different reaction or rate-controlling mechanism for the observed cathodic current. Inspection of fluoride-corroded test electrodes indicates attack and deterioration of the entire exposed surface of the test electrode. Close inspection of the E-vs-I curves obtained from the later corrosion cycles indicates two loops in the curves, suggesting the presence of two corrosion processes (i.e., possibly, the fluoride curve and baseline curve may be superimposed) (see Fig. 36). This evidence indicates that two cathodic corrosion processes may be operational in the presence of fluoride contaminants.

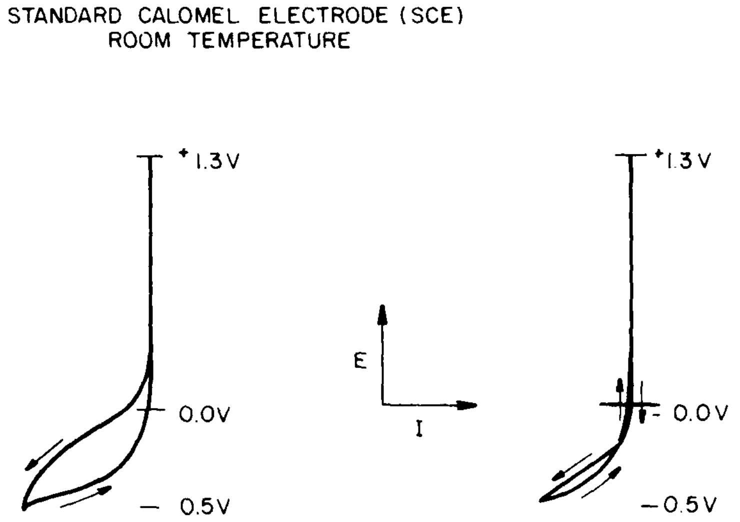

1st CYCLE

(a)

5th CYCLE

(b)

Figure 36. E-vs-I curves for fluoride-contaminated corrosion.

Pitting of some fluoride-corroded test electrodes has been observed in addition to the general surface attack. Figure 37 shows fluoride contaminant pitting. The pits are almost perfect circles, although of varying diameter. Each appears to have a central nucleation site, probably from a spurious contaminant, as shown in Fig. 37(b). Evidently, the corrosion begins at the center of the pit and proceeds uniformly from that point. In this case, the pitting is believed to have a minimal effect on the E-vs-I curve, since the curve differs very little from fluoride-corroded samples that did not show any pitting. This observation is in contrast to the pitting observed for chloride-contaminated test electrodes; in their case the E-vs-I curve differed substantially from that of the unpitted samples.

3. Effects of Alloying on the Corrosion Stability of Aluminized Substrates

The relative corrosion stability of alloyed and unalloyed aluminized substrates was evaluated in the presence of a chloride contaminant. Filament-evaporated aluminum (five 9s pure) was deposited on polished (100)

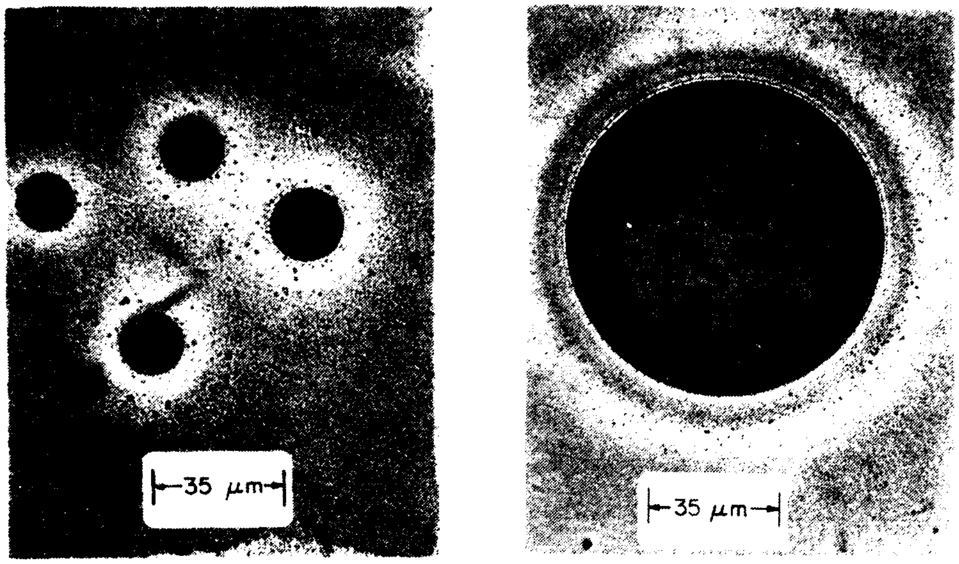

(a) (b)

Figure 27. Photographs of fluoride-induced pitting; 0.5M Na_2SO_4, 0.005M NaF. (a) pH $\sim$ 8.0. (b) pH $\sim$ 7.0.

silicon wafers to a thickness of 1 μm. During the same evaporator run, aluminum films were also deposited on silicon wafers that were covered with a 1-μm-thick layer of thermally grown SiO_2. Selected samples of both types of aluminized wafers were alloyed at 450°C in forming gas. The relative corrosion stability was evaluated in $Na(CH_3COO)/CH_3COOH$ electrolyte (pH 4.3-4.6) with 0.005M chloride contaminant. After the test samples were allowed to stand overnight (22-24 h) in electrolyte solution, the open-circuit corrosion current was measured, and the E-vs-I curve for each was recorded over the potential range of +1.3 to -0.5 V (SCE). Inspection of the samples visually and under a low-power microscope also yielded corrosion stability measurements that correlated well with electrochemical techniques. The extent of localized pitting corrosion can easily be determined, since breakthroughs in the aluminum film to the underlying silicon and silicon oxide layers are readily seen. Comparisons of the number and size of the corrosion pits can be used to determine corrosion stability. Actually, small pH adjustments produced by changes in the acetate/acetic acid ratio make many of these tests for relative corrosion stability more definitive. Open-circuit corrosion currents and their corresponding corrosion pits could be observed for some samples, but not for others.

These studies showed no difference in the relative corrosion stability of the alloyed, filament-evaporated aluminum layers on silicon or silicon dioxide. There were, however, detectable differences in corrosion stability between alloyed and unalloyed samples. Alloyed samples exhibited better corrosion stability than unalloyed samples.

Similar investigations were done also with E-beam-aluminized substrates. Samples of unalloyed E-beam-aluminized (100) silicon wafers were compared with similar E-beam wafers that had been alloyed at 450°C in forming gas (90% N_2 and 10% H_2) for 20 minutes. At a 0.005M chloride contamination level in acetic acid/sodium acetate buffers in the pH range of 4.3-4.6, the unalloyed aluminized wafers produced corrosion pits that were more numerous and had a larger diameter than the alloyed aluminum substrate. In one case the alloyed aluminum did not pit, while the unalloyed aluminum did. The alloyed E-beam-aluminized substrate exhibited improved corrosion stability over an unalloyed aluminized substrate. Alloyed S-gun-aluminized substrates exhibited a similar corrosion stability behavior.

The analytical characterization of these thin films, discussed in the next section (IV.F), may offer a possible explanation for the improved corrosion stability of alloyed aluminum substrates. The most striking change in film properties that occurs after the postheat treatment is the increased grain size of the film. Typically, the as-deposited grain size was nominally 1000 Å; a postheat treatment results in grain sizes of 10,000 Å or greater. Larger grain size means that grain boundaries make up a smaller fraction of the film, and this diminished fraction may account for the increase in corrosion stability. Corrosion attack of Al has been observed to begin at the grain boundaries [29]. Corrosion potentials at the grain boundary have been measured and were found to differ significantly from those measured within the grains [29]. However, other changes in film properties, such as the redistribution of impurities within the film during heating, incorporation of the ambient gases into the film, or changes in crystalline habit of the film may also affect corrosion stability. Although all of these factors could have an influence, grain size appears to be particularly significant.

Experiments were also done to evaluate the effect of the alloying ambient upon the corrosion stability of the sample. Pure (five 9s) aluminum films were deposited by E-beam evaporation and subsequently alloyed in forming gas or nitrogen at 450°C for 20 minutes. Electrochemical bias techniques were used to determine the relative corrosion stabilities of several samples. In this case, no pitting was observed in any of the samples, but significant differences in their E-vs-I curves were noted. The aluminum samples were allowed to stand at room temperature for 24 hours in acetic acid/acetate buffer (pH 4.5) with 0.010M chloride contaminant. The initial bias was applied at +1.3 V, and the potential scan for three cycles was recorded. The effect of H_2 in inhibiting intermetallic formation has been reported [64].

Figures 38(a) and 38(b) show the E-vs-I curves for E-beam aluminum films alloyed in forming gas and nitrogen gas, respectively. The cathodic corrosion currents for the samples alloyed in forming gas are smaller than those for the samples alloyed in nitrogen gas. The shape of the forming-gas curve is different as well. A break in the cathodic current (decreasing voltage scan) is observed at approximately 0.15 to 0.10 V (SCE). Some difference in the properties or composition of the aluminum film seems to diminish the cathodic corrosion currents. The incorporation of H_2 gas into the Al film or the formation of some related product could explain the increased corrosion stability of the H_2-alloyed film. A hydrogen-rich passivating film could have altered the breakdown potential, increasing the corrosion stability of the film. The actual reason for this increased stability of H_2-alloyed aluminum films may be much more complex, or due to entirely different considerations. In any case, our evaluation of the relative corrosion stability of these films shows that hydrogen gas in the ambient improves corrosion stability.

This improved corrosion stability, however, may not be as significant as that observed for alloyed compared with unalloyed aluminum. Whereas

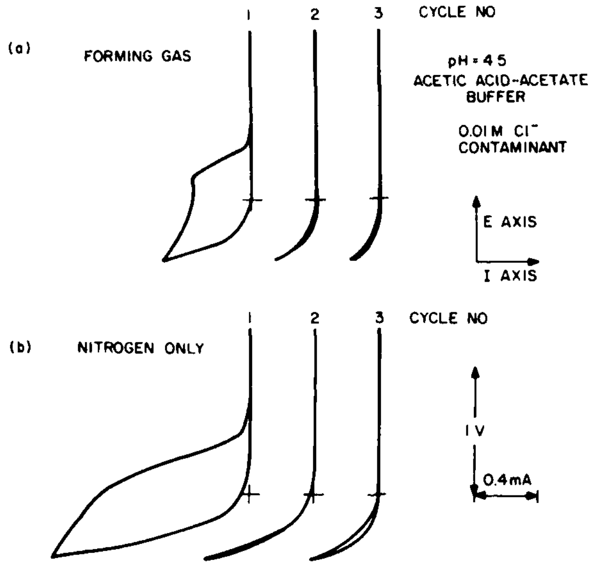

Figure 38. E-vs-I curves for alloyed aluminum films.

aluminum films produced from either of the two alloying ambients were resistant to pitting attack, unalloyed samples exhibited substantial pitting under similar conditions.

4. Corrosion Processes on Gold Substrates

Electrochemical bias techniques were used to analyze possible corrosion processes on a gold-trimetal film. Silicon wafers were processed to produce a gold-trimetal film of platinum-titanium-gold in which the gold is deposited by electroplating. E-vs-I curves were recorded by electrochemical bias techniques. Initial experiments were done on gold foil, and later experiments on the trimetal film. E-vs-I curves over the potential range of +1.3 to -0.5 V were obtained in various electrolytes and in the presence of chloride contaminant. The gold-plated layer behaved similarly to the gold foil in our studies.

Figure 39 displays a typical E-vs-I plot for gold-trimetal or gold foil test samples. Corrosion currents were observed only when the samples had an applied electrochemical bias. Several breaks in the positive (anodic) portion of the curve are evident. These changes in corrosion current reflect the complex oxidation processes that occur on the gold surface. Au^+

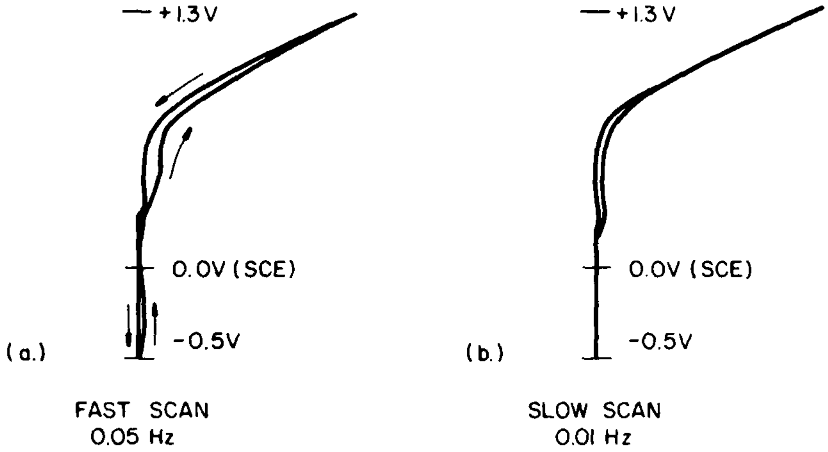

Figure 39. E-vs-I curves for gold-trimetal substrate.

and Au^{3+} oxidation states are possible, along with various hydroxide and hydronium ion species. Inasmuch as slower scan rates produce nearly identical curves on the forward and reverse portions of the cycle, these processes appear to be highly reversible. The small current observed for the cathodic portion of the curves reflects, we believe, the reduction of the oxide products formed during the positive (anodic) portion of the scan. Slower scan rates produce hardly any currents during the cathodic portion of the scan.

Chloride contaminants (up to 0.5M concentration) produce curves that are similar but not identical to the curves described for Fig. 39. The oxide formation processes still appear dominant under anodic bias. Chloride ion complexes appear to produce only small perturbations in the shape of the curves.

Visual examination of the gold film revealed no change in appearance for the exposed portion of the test sample. Although appreciable corrosion currents are observed under electrochemical bias, little or no gold material appears to be displaced from the test sample. The oxidation processes do not appear to produce readily soluble products, and are highly reversible.

5. Evaluation of Film Stress Effects on Corrosion Stability

Aluminum films (rf-sputtered) were deposited on Corning* Code 0211 thin-glass microsheets. The stress in the films was varied by controlling the target potential. The degree of curvature of the microsheet was used to determine the stress in the deposited films. Subsequently these films were tested for their relative corrosion stability by electrochemical bias and open-circuit corrosion current techniques. Acetic acid/acetate buffers, at pH 4.3-4.6, with 0.01M NaCl contaminant, were the electrolytes employed. The three criteria used for determining the relative corrosion stability for these samples were (i): average corrosion current at -0.375 V (SCE) during the E-vs-I cycle; (ii) the open-circuit corrosion current with no bias scan [i.e., at 0.0 V (SCE)]; and (iii) the number of corrosion pits observed on the samples. In Table 9, these results are summarized for several experiments.

The samples are ranked in the order of their relative corrosion stability, determined by their open-circuit corrosion current and extent of pitting: 50-V > 200-V > 0-V bias. However, the E-vs-I cycle currents from some experiments suggest that film under compressive stress behaves somewhat differently under corrosive environments than does film under tensile stress. Samples under compressive stress (50-V bias) showed no pits, although the magnitude of the current observed during the E-vs-I cycle on some occasions was similar to that of samples which had pitted. The corrosion processes affecting compressive films may be more uniform than those that affect films under tensile stress. Thus, compressive forces may tend to close cracks or potential pitting sites, while tensile stresses may tend to open and expose them. Increasing the magnitude of tensile stress did not appear to decrease the corrosion stability; in fact, we observed the opposite behavior.

These results, however, must be considered inconclusive. Other factors may be more important in determining the corrosion stability of these samples. For example, the contaminant level (particularly of sodium) measured for the 0-V-bias-deposited film (low tensile) was greater than

---

*Corning Glass Co., Corning, NY.

TABLE 9. CORROSION STABILITY MEASUREMENTS ON FILMS OF KNOWN STRESS

Sample Identification					
Bias (V)	Stress (1×10^7) (dyn/cm^2)	Open-Circuit* Corrosion Current (mA)	Current (mA) at* -0.375 V (SCE)	Number of Pits*	Additional Comments
200	10.0 tensile	0.2	0.3	13	Small pits
0	2.6 tensile	0.6	0.5	16	Pits larger than in previous sample
50	5.6 compressive	0.15	0.52	None	
200	10.0 tensile	0.26	0.40	6	
0	2.6 tensile	0.64	0.73	22	
50	5.6 compressive	0.17	0.75	None	Uniform corrosion
200	10.0 tensile	0.15	0.80	1	
0	2.6 tensile	0.20	1.00	6	
50	5.6 compressive	0.12	0.53	4	Pits initiated by cracked samples

---

*Sample area is 0.49 cm^2.

that measured for other samples. Grain size and the distribution of contaminants may also affect the corrosion stability of the films.

6. Discussion of Electrochemical Evaluations

The initial portion of this discussion is devoted to examining some of the complexities of corrosion processes on aluminum-metallized IC devices. Some traditional methods of studying corrosion processes are presented in terms of their applicability to characterizing IC device corrosion processes.

Figure 40 displays the Pourbaix diagrams for the aluminum-water system [175]. This diagram is based on thermodynamic data and shows the possible reaction products under various conditions of pH and electrochemical potential bias. As indicated by the passivity region between the pH values of 4-9, aluminum corrosion resistance is assocated with the protective qualities of the alumina (Al_2O_3) layer. This diagram, however, only gives information on the thermodynamic possibility of electrode reactions; it does not permit one to draw conclusions as to whether slow kinetic steps inhibit corrosion or whether passivity will occur because the protective surface film fails to dissolve. These issues are particularly relevant for aluminum in the presence of halide contaminants, since the halides may attack the Al_2O_3 passivating layer at rates exceeding formation rates.

Although a separate Pourbaix diagram can be constructed for every level of contaminant concentration, it should be emphasized that corrosion is a dynamic process. When we used fluorescent pH indicators (see Section IV.G) to observe the cathodic corrosion sites on IC devices, we found that the boundaries of the sites were not static, and that the intensity of the fluorescence changed considerably. In addition, contaminant ions or ionic corrosion products on an IC device under external bias tend to migrate under appropriate anodic or cathodic bias, creating a dynamic material balance. Thus, the usefulness of these diagrams is quite limited.

Tafel kinetics represents a traditional method of characterizing electrochemical reaction rates as a function of the overpotential for the

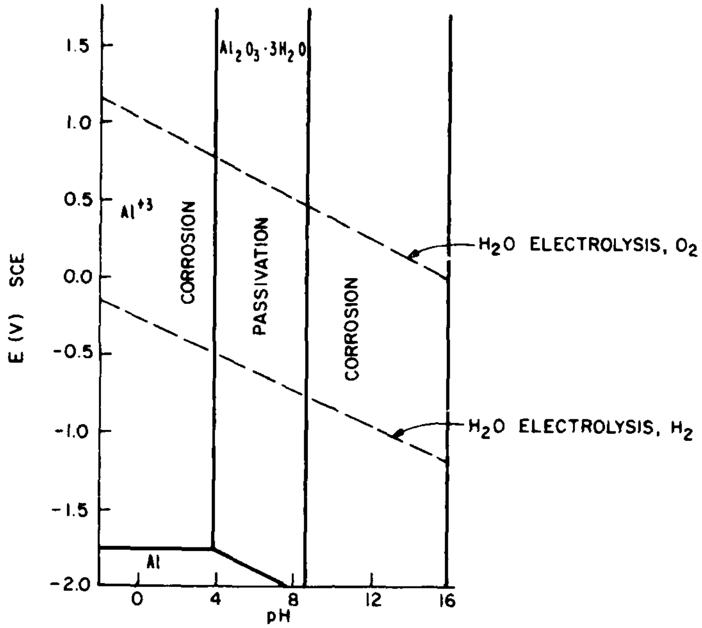

Figure 40. Potential-pH equilibrium diagram of the aluminum-water system.

reaction. Essentially, a plot of the electrochemical potential versus the measured current density follows the relationship:

$$E = b \cdot \log(i) + a$$

where b is the Tafel slope characterizing the reaction rate as a function of the overpotential, i the current density, and E the applied potential. Because many corrosion reactions may occur at a common potential, the determination of Tafel slope b for desired reactions can be complicated by competing reactions. Should some reactions dominate in one potential range and be insignificant in another, a single sample may yield several Tafel slopes.

Cyclic voltammetric methods can add an additional complication because the fast scan time may not provide for the diffusion of constituents for the electrochemical process. However, the cathodic processes observed on our Al test electrodes during tests with slower scan times showed little or no change in the E-vs-I curves, suggesting that diffusion terms for these processes may be small.

Figure 41 plots the potential E (SCE) vs log(i) for a typical cathodic reaction on an Al test electrode (in the absence of pitting corrosion). Only

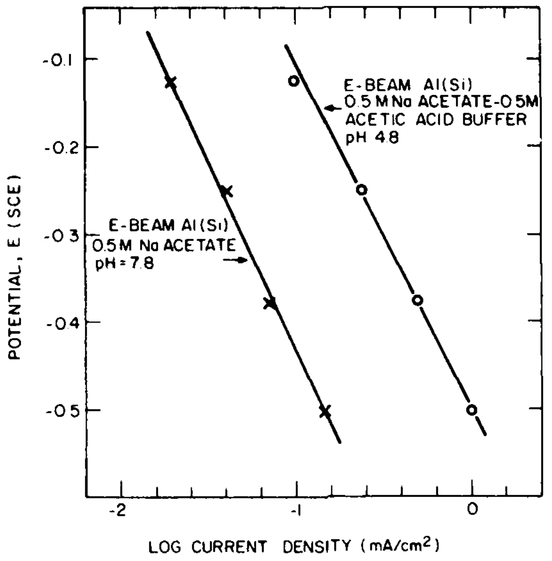

Figure 41. Tafel plot for cathodic process on aluminum test electrodes.

two cases are shown on this graph, but data from other test Al electrodes show similar behavior. The Tafel slopes are similar in spite of different current densities for the cathodic process. This observation suggests that the potential at which the cathodic process is initiated determines the rate of the reaction as a function of the electrochemical potential. A number of investigators have reported the pitting potential (i.e., the potential at which pitting is initiated) to be sensitive to a number of variables, including electrolyte composition, contact time, and the electrochemical history of the sample.

The exchange current is determined from the Tafel plot at the initiation potential. However, this potential is sensitive to external variables, making the determination difficult. For Al metallizations, the initiation potential can change dramatically with conditions so that erroneous exchange currents are obtained at the specified initiation potentials.

Although Tafel kinetics may be useful for characterizing electrochemical reactions in contact with aqueous solution, the corrosion rates on metallized ICs may be determined more by current and chemical transport paths than by the overpotential of the reaction. Diffusion and transport terms may indeed be large for metallized ICs where corrosion sites are not in contact with electrolytes. Localized corrosion processes do not require long transport paths, but it is not clear what transport mechanisms are present at the localized corrosion sites.

The corrosion stability measurements taken by cyclic voltammetric methods are largely qualitative. Even if they could be made more quantitative, their relevance in determining corrosion rates on metallized IC devices is limited. As pointed out in Section IV.C, current and mass transport paths may be limiting in determining the corrosion rate. This corrosion rate of metallization in contact with a strong electrolyte in aqueous solution may not be applicable to IC device environmental conditions. A measure of relative corrosion stability, however, may provide a method of optimizing material and environmental conditions for metallization of IC devices. We hope that these electrochemical evaluations can be applied to IC metallizations. The cyclic voltammetry method quickly evaluates corrosion stability over a range of electrochemical bias conditions. For corrosion to occur, similar electrochemical bias conditions must exist at localized sites on the IC metallizatons.

During these studies, several conclusions concerning relative corrosion stability, were reached:

o Fluoride or chloride contaminant on aluminized substrates greatly decreases corrosion stability. Under some circumstances fluoride may decrease corrosion stability more than chloride.

o Alloying the aluminum increases corrosion stability. Hydrogen gas in the heat treatment ambient further increases it.

o Chloride contaminant on a gold-trimetal layer does not appreciably alter the corrosion process.

o Stress in the aluminum films does not correlate well with the corrosion stability. However, films under compression may exhibit improved corrosion stability.

We have demonstrated that electrochemical bias techniques can provide valuable information about methods and materials suitable for optimizing corrosion stability. Only a few variables that affect this stability have been studied here. The reasons and the mechanisms for the observed improvement in the corrosion stabilities are not well understood. Extensive and more detailed studies are therefore required.

7. Suggestions for Further Study

The most important factor in determining the corrosion stability of aluminum is the nature of the passivating oxide layer. Among the several types of aluminum corrosion, the most commonly encountered is pitting. Apparently its highly localized nature also makes this the most likely and most damaging type of corrosion for aluminized substrates and devices. The mechanisms associated with pitting may also be important in other types of corrosion processes, such as intergranular corrosion [78]. The literature on pitting corrosion of aluminum alloys and metals is extensive, yet inconclusive [49,160]. There is hardly any literature information available on the corrosion stability of thin films of aluminum used for electronic devices. Several studies have examined spurious contaminants that induce pitting in aluminized alloys and metal, the most notable and effective one being chloride ion. However, the reason for its being more reactive than other corrosion contaminants is not well understood. Numerous models have been proposed to characterize the corrosion cell within pits [3,77]. Apparently the initiation of pitting corrosion appears to be particularly sensitive to contaminants and external agents [49,175,176]. If chloride contaminants are present, pitting potentials (i.e., electrochemical potential required to induce pitting) can be shifted significantly by the presence of other contaminants. Our corrosion studies have encountered similar behavior. The pH, chloride contaminant level, and inert electrolyte composition and concentration all influence the pitting process. Pitting can be either accelerated or delayed, and is sometimes inhibited altogether.

There are two main reasons why these literature reports and our own observations have significance for encapsulated devices. First, the environment within plastic-encapsulated devices is not well characterized. The corrosion stability of aluminum can be easily influenced (both enhanced or diminished) by the presence of other agents that are not corrosive by themselves. Materials associated with plastic encapsulants and passivating layers can greatly affect corrosive processes. The effects of these contaminants on corrosion, both by themselves and in concert with common contaminants (chloride), need to be characterized to determine the optimum materials for reducing the likelihood of device reliability problems from corrosion.

Second, these observations also suggest improvements in the corrosion stability of aluminized substrates through special process modifications or treatments. The presence of various organic compounds in salt (NaCl) solutions has been observed to reduce corrosion processes [2]. Chromate treatments of aluminum metal have also been observed to delay or inhibit the initiation of pitting corrosion [15,122]. Similar treatments might also improve the corrosion stability of aluminized substrates in plastic-encapsulated devices. Potential corrosion inhibitors need to be evaluated in electronic devices to determine their effectiveness, along with their compatibility with semiconductor processing and performance. Corrosion inhibitors could greatly increase the reliability of aluminized devices under normal operating conditions as well as in the presence of harsh environmental factors.

F. ANALYSIS OF MATERIALS AND FILMS

In this section, electrical, chemical, and physical analyses of the materials comprising the test device structures are reviewed. These analyses include dielectric and metal layers and their electrical properties. Grain-size measurements and impurity distributions are discussed as well. The determination of dielectric film thickness and phosphorus content is discussed in Section III.B.2.

1. Electrical Properties of Passivation Layers

Electrical properties of the bulk and surface of CVD SiO_2 and PSG films and the effects of moisture on these properties have been reported [45,118,196,213]. Similar electrical properties of SINCAP were also investigated [46]. During the measurement of potential profiles (see Section IV.C.4) the question of SINCAP bulk resistivity arose. A series of samples was prepared to determine this parameter as a function of SINCAP deposition conditions.

A series of SINCAP depositions was carried out with varying SiH_4/NH_3 flow-rate ratios and with N_2 as the carrier gas. These flow variations produced huge changes in the SINCAP bulk resistivity, as shown in Table 10. The resistivity measurements were done by evaporating 1-mm dots of aluminum on the SINCAP and measuring the current at an electric field of 1×10^6 V/cm in the SINCAP.

TABLE 10. RESISTIVITY OF SINCAP vs SiH_4/NH_3 FLOW-RATE RATIO IN NITROGEN CARRIER GAS

SiH_4/NH_3	Resistivity* ($\Omega \cdot$cm)
1:40	10^{17}
1:10	10^{17}
1:2	10^{15}
1:1	10^{13}
1:0.5	10^{11}
1:0	10^{7}

---

*Order-of-magnitude values.

To achieve suitable deposition rates, most production processes are based on a SiH_4/NH_3 ratio of about 1:1 so that the SINCAP layers used on ICs in general are fairly conducting compared with PSG films. Thus, the failure of the potential-profile electrode measurement for the SINCAP sample is understandable.

2. Purity of Aluminum Films Deposited by Various Methods

Trace contaminants in metal films can affect the structural, physical, and chemical properties of thin-metal films, and could therefore influence susceptibility to corrosion. The determination of types and quantity ranges of contaminants is thus of considerable importance.

Samples of aluminum films of the types used for various tests in our corrosion studies were analyzed for solid impurities by emission spectrographic analysis with a 3.4-m Jarrel-Ash Ebert spectrograph. The films,

AD-A090 028 RCA LABS PRINCETON NJ F/G 11/6
CORROSION OF METAL FILMS WITH DEFECTIVE SURFACE PROTECTION LAYE--ETC(U)
JUL 80 R B COMIZZOLI, L K WHITE, W KERN F30602-78-C-0276
UNCLASSIFIED PRRL-79-CR-42 RADC-TR-80-236 NL

2 OF 2
AD A
090028

END
DATE
FILMED
11-80
DTIC

typically of 1-μm thickness, were deposited on polished single-crystal silicon with or without a thermally grown SiO_2 layer, and on thin Corning Code 0211 microscope cover glass discs (used for intrinsic-stress measurements). The source aluminum or Al-Si alloy were in all cases better than five 9s pure. Methods of film deposition, employed under the usual operating conditions, were E-beam evaporation, S-gun dc sputtering, filament evaporation, and rf sputtering at bias voltages of 0 to -200 V. Pertinent deposition conditions are listed in Table 11. No alloying or other heat treatments were performed on these samples. The E-beam-evaporated and S-gun-sputtered films exhibited clean and specular surfaces. The films obtained from the filament evaporation were hazy, and the rf-sputtered samples had a dark-gray and matte appearance due to a microscopically granular surface structure. For analysis, all films were dissolved in a small volume of concentrated hydrochloric acid and taken up in spectrographic-grade graphite powder. We observed that the silicon-containing Al films dissolved much more readily in HCl than did the films without added silicon. The results are presented in Table 12. The elements C, P, S, Cl, and O were not present or are not readily detectable by emission spectrographic analysis.

The impurity element of highest concentration is silicon. It occurred in films where no silicon was added to the aluminum. The film that was deposited by rf sputtering at -50-V bias (sample #7) showed a particularly high Si concentration of 120-1200 ppm. Other impurities, in the various samples, extended over the following ranges: Calcium from 0 to 300 ppm, magnesium from 1 to 50 ppm, iron from 0 to 20 ppm, and copper from 0.1-50 ppm. Boron was present only in some samples at 6-60 ppm, and sodium occurred in only one film at a concentration of 60-600 ppm. Aluminum deposition by S-gun sputtering introduced a high level (5-50 ppm) of copper. Deposition by rf sputtering, particularly at bias voltages of zero and -50 V, tended to lead to relatively large concentrations of impurities. Sample #7 exhibited the highest detectable impurity level; this corresponded to an aluminum purity in the range of 99.86 to 99.986%. Sample #3, obtained by filament vacuum evaporation, was the purest: 99.979 to 99.998% by wt of Al.

TABLE 11. TYPICAL CONDITIONS FOR DEPOSITING ALUMINUM FILMS

Method of Film Deposition	System Pressure		Condition			
	(Torr)	(Pa)	Substrate Temperature (°C)	Source to Substrate Distance (cm)	Other Key Parameters	Deposition Rate (Å/s)
Vacuum evaporation - electron beam	$1.2\text{x}10^{-6}$ (Ar)	$1.6\text{x}10^{-4}$ (Ar)	35-50	25-30	-	100-150
Vacuum evaporation - filament	$1.2\text{x}10^{-5}$	$1.6\text{x}10^{-3}$	40-50	22.5	Tungsten filament	30-40
Sputtering - rf mode	$3.0\text{x}10^{-5}$ (Ar)	$4.0\text{x}10^{-3}$ (Ar)	50-125	5.2	Target potential 1500 V	0.67
Magnetron sputtering - dc mode, S-gun	$2.5\text{x}10^{-6}$ (Ar)	$3.3\text{x}10^{-3}$ (Ar)	25-35	48 (rotating)	500 V, 4.5 A	150-200

TABLE 12. EMISSION SPECTROGRAPHIC ANALYSIS OF IMPURITIES IN DEPOSITED ALUMINUM FILMS

Sample and Method of Deposition	Impurity (ppm by wt)						
	Si	Ca	Mg	Fe	B	Cu	Na
Al on Si E-beam evaporation	20-200	20-200	3-30	0.6-6	-	0.15-1.5	-
Al on Si S-gun sputtering	20-200	15-150	2-20	0.6-6	-	5-50	-
Al on SiO_2 Filament evaporation	20-200	-	1-10	-	-	0.1-1	-
Al(Si) on Si S-gun sputtering	1% nominal	10-100	1-10	2-20	6-60	5-50	-
Al(Si) on Si E-beam evaporation	1% nominal	10-100	1-10	0.6-6	-	0.15-1.5	
Al on glass Sputtered, 0 bias	30-300	30-300	5-50	2-20	-	1-10	60-600
Al on glass Sputtered, -50-V bias	120-1200	10-100	2-20	2-20	6-60	0.6-6	-
Al on glass Sputtered, -100-V bias	20-200	20-200	3-30	2-20	6-60	0.6-6	-
Al on glass Sputtered, -200-V bias	20-200	10-100	2-20	0.6-6	6-60	1-10	-

Of the contaminants not readily detectable by emission spectrographic analysis, only the halides, oxygen, and water vapor (residual in the deposition chamber) might be expected to affect corrosion if present in the aluminum films at substantial concentrations.

3. Metal Grain Size

Among the important factors that have major effects on corrosion processes are the surface and internal microstructures of the metal film. Analyses were therefore undertaken to determine the orientation and size of the microscopic grains in the aluminum films used in these studies.

Attempts to delineate the grains by chemical etching combined with microscopic examination techniques were not successful, even though a large variety of etchants and techniques were tested. Therefore, x-ray techniques were used to classify aluminum films according to size of crystallites (grains and preferred crystal orientation). Films representative of those used for the present corrosion study project were selected. The films were approximately 1-μm thick and consisted of pure (five 9s) Al or of 1-2% Si in Al. They were deposited by E-beam evaporation, S-gun sputtering, filament evaporation, and rf sputtering, under the conditions specified in Table 11 of Section IV.E.2. The substrates were slices of polished (100) Si, thermally oxidized Si (0.5-μm SiO_2), and Corning Code 0211 soda lime glass. Some of the samples were heated for 20 minutes at 450°C in forming gas to alloy or to simulate alloying.

X-ray diffractometry (line broadening) studies could not be used to determine the crystallite size of all samples, as this method is sensitive only in the 1000-Å range or below. The crystallite size of many samples was found to be greater by approximately an order of magnitude or more. The Laue method was therefore employed to assist in the overall ranking of samples by crystallite size. For samples having the largest crystallite size (approx. 1 μm or greater), the relative spottiness of a diffraction ring recorded on the Laue pattern served as a means of ranking.

The results of the x-ray study are summarized in Table 13. The pure-Al film on SiO_2 of sample #10, although its exact numerical value cannot be assigned, had the largest crystallite size (several micrometers). This film

TABLE 13. SUMMARY OF X-RAY ANALYSES OF ALUMINUM FILMS

Preparation of Films		Analysis			
		100% Al on			
Method of Deposition*	Postheat Treatment	Si	SiO_2	Glass	1-2% Si in Al on Si
E-beam evaporation	None	#1: 900 Å (D); random orientation			
	450°C 20 min H_2-N_2 **	#1A: ~1 μm; strong (111) orientation; (L)			#2: 800 Å (D); slight (100) orientation
S-gun sputtering	None		#5: 1200 Å (D); random orientation		#7: 1000 Å (D); random orientation
	450°C	#6: ~1 μm; strong (111) orientation; (L)	#10: several μm; random orientation; (L)		#8: 1000 Å (D) random orientation
Filament evaporation	None				
	450°C 20 min H_2-N_2	#4: ~1 μm; strong (111) orientation; (L)	#3: 1 μm; strong (111) orientation; (L)		
rf sputtering (-100-V bias)	None			#9: 450 Å (D); random orientation	

---

*See Table 11 in Section IV.F.2 for conditions.

**Forming gas.

LEGEND: (D) By diffractometry.
(L) From Laue photographs.

was deposited by S-gun sputtering followed by heating at 450°C. Samples #1A, 3, 4, and 6 had the next-largest size (~1 μm), followed by #1, 2, 5, 7, and 8, which had a crystallite size of approximately 0.1 μm. The smallest crystallite size, obtained for sample #9 (Al/glass), was 450 Å. Large differences in the texture of these films were also observed. The fact that only (111) and (222) reflections were observed on a normal diffractometry trace proved that samples #1A, 3, 4, and 6 were of strong (111) preferential orientation. The remaining samples were much more randomly oriented.

An indication of the range of crystallite sizes encountered can be appreciated by comparing Figs. 42 and 43. Figure 42 is typical of the Al (111) reflection observed for those samples having the larger crystalline size (~1 μm or greater). It is identical to that of the Au (111) reflection standard shown in Fig. 44. For the Au standard, no broadening due to strain and/or crystallite size was observed for Au (111), (200), (220), (311), and (222) reflections. The Au standard thus served as a means of measuring instrumental broadening. The Al (111) reflection of sample #9 (Al/glass) shown in Fig. 43 is obviously broadened. Crystallite sizes calculated for (111) and (200) reflections of sample #9 were 425 and 451 Å, respectively. Thus the range of crystallite sizes encountered in this series differed by more than an order of magnitude.

G. SURFACE pH MEASUREMENTS

The use of ultraviolet fluorescent acid/base indicators was examined as a possible technique for determining localized changes in the pH at very small thin-film electrodes. A number of these pH-sensitive, fluorescent organic compounds were tested on Al- and Au-metallized substrates and IC devices. Table 14 lists the indicators tested, their pH range sensitivity in aqueous solution, and the expected color change. In some cases, the color of the emitted light changes with variations in pH; in other cases the fluorescence of the compound changes from colorless to a visible color at a certain pH.

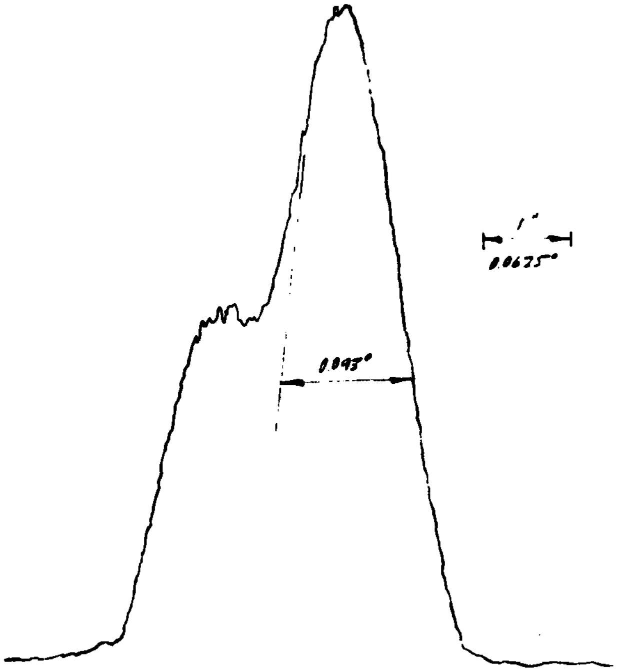

Figure 42. Diffractometer trace of (111) Cu $K_{\alpha_1-\alpha_2}$ reflection; sample #3. [Intensity (ordinate) vs angle (abscissa).]

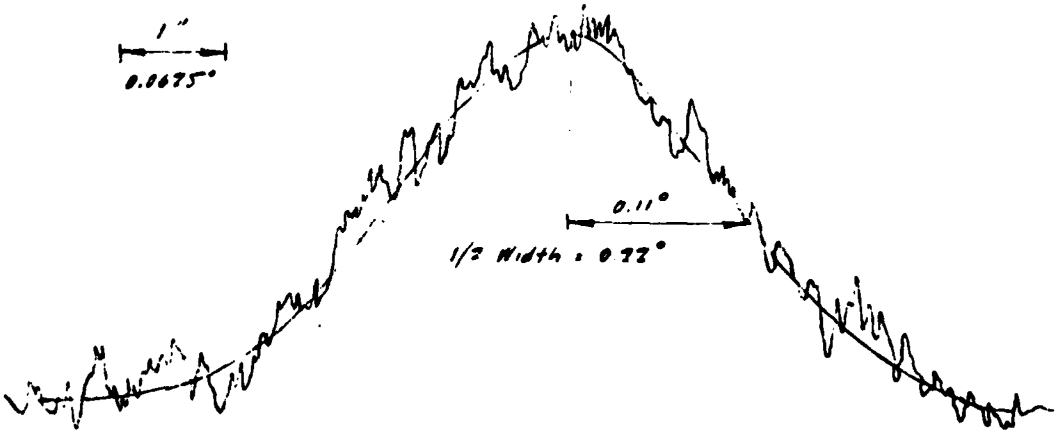

Figure 43. Diffractometer trace of (111) Cu $K_{\alpha_1-\alpha_2}$ reflection; sample #9. [Intensity (ordinate) vs angle (abscissa).]

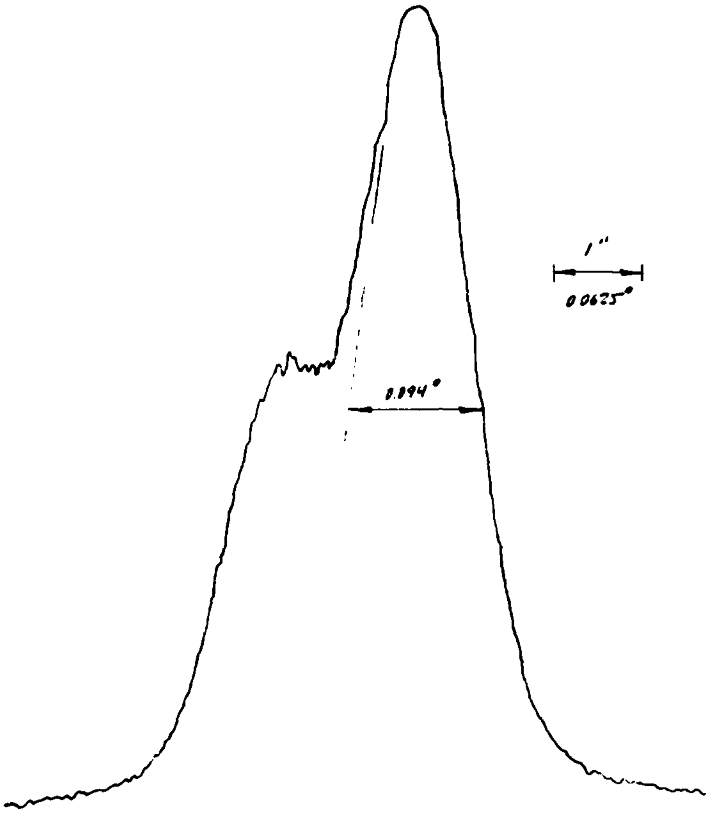

Figure 44. Diffractometer trace of (111) Cu $K_{\alpha_1-\alpha_2}$ reflection; Au-standard.

These fluorescent pH indicators, in ethanol-glycerol-FC-93* surfactant solutions were applied to the kinds of films encountered in IC manufacture. The films included aluminum- and gold-metallized substrates, thermal SiO_2, and phosphosilicate glasses. Humid ambients of air, HCl, and ammonia were tested to determine the sensitivity of the indicators to external environmental factors. A long-wavelength UV source was used to activate the compounds. The decorating performance of the indicators was evaluated by visual examination and optical microscopy.

The following indicators fluoresced after application to thermal SiO_2, aluminum, and gold surfaces: fluorescein, dichlorofluorescein, β-methylesculetin, and β-methylumbelliferone. The β-naphthol composition fluoresced

---

*3M Company, St. Paul, MN.

TABLE 14. EFFECTS OF CHANGING pH ON COLOR AND FLUORESCENCE OF ACID/BASE INDICATORS IN AQUEOUS SOLUTION*

	From		To	
Indicator	pH	Appearance	pH	Appearance
Eosine YS	0	Yellow	3.0	Yellow
Erythrosine	0	Yellow	3.6	Yellow
Esculin	1.5	Colorless	2.0	Blue
Chromotropic acid	3.5	Colorless	4.5	Blue
Fluorescein	4.0	Colorless	4.5	Green
Salicylic acid	2.5	Colorless	3.5	Blue
Dichlorofluorescein	4.0	Colorless	5.0	Green
β-Methylesculetin	4.0	Colorless	6.2	Blue
Quinine	5.0	Blue	6.1	Violet
β-Methylumbelliferone	7.0	Colorless	7.5	Blue
1-Naphthol-4-sulfonic acid	6.0	Colorless	6.5	Blue
Acridine Orange	8.4	Orange	10.4	Green
β-Naphthol	8.6	Colorless	10.0	Blue
Coumarin	9.8	Deep green	12.0	Light green

---

*J. DeMent, "Fluorescent Indicators," in R. C. Weast, ed., *CRC Handbook of Chemistry and Physics*, 58th ed., CRC Press, Cleveland, Ohio, 1977, pp. D-138 to D-139.

**Underscoring of a color designates fluorescence.

slightly on the Al film, but did not fluoresce on the Au film. The 1-naphthol-4-sulfonic acid indicator was observed to fluoresce in NH_3 ambient on SiO_2. All of the indicators ceased to fluoresce when HCl was added to the ambient. This lack of fluorescence is consistent with the expected drop in pH of the ambient. The addition of ammonia to the ambient re-activated some of the fluorescence.

With a few minor exceptions, the indicators exhibit the same fluorescent properties on different substrate surfaces. This observation suggests that they are more sensitive to the ambient than to the surface states in the absence of any applied external bias. Surface pH differences, however, might be small under these conditions. Pretreating the SiO_2 substrate with HCl and NH_4OH to change surface pH prior to application of the fluorescent indicator produced no change in fluorescent behavior compared with an un-pretreated sample. In addition, fluorescent indicators on 3% PSG glasses exhibited a behavior similar to that observed on CVD SiO_2 substrates. In spite of this apparent lack of sensitivity to the substrate, our initial experiments identified the fluorescent pH indicators that are the most sensitive to environmental factors. Once identified, these indicators were used to decorate test devices under an applied external bias. Figures 45 and 46 display aluminized IC devices decorated with fluorescent indicators in the presence of external bias (20 V) in a moist ambient. The indicators shown are β-methylumbelliferone and β-naphthol. In some cases the localized fluorescence was observed at defects that could be seen under visible light, although not all defects exhibited fluorescence. Also, localized fluorescence was observed at sites where no apparent defect was present in visible light. The fluorescence observed here was activated immediately when the bias was applied, and tended to spread out from a central point as the bias was kept on. When the bias was turned off, the localized fluorescence faded much more slowly than it had taken to be activated. In addition, gas bubbles were observed to emanate from sites where localized fluorescence had occurred. Apparently, the surface tension of the moist substrate surface tended to trap the bubbles.

These observations can be interpreted as follows: The fluorescent indicators are decorating corrosion sites. More specifically, they are

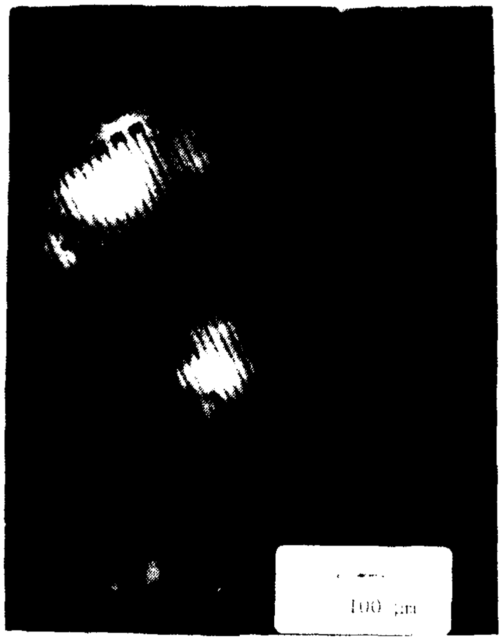

Figure 45. β-Naphthol decoration, long-wave UV source with 20-V bias. Humid ambient, room temperature.

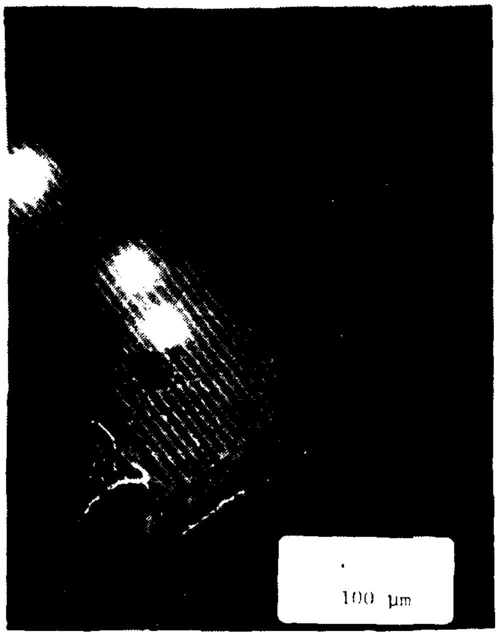

Figure 46. β-Methylumbelliferone decoration, long-wave UV source with 20-V bias. Humid ambient, room temperature.

decorating the sites of the cathodic reactions. Hydrogen production at these sites ($2 H^+ + 2 e^- \rightarrow H_2$) reduces the concentration of H^+, thus activating the pH indicator (β-naphthol is activated in aqueous solution at a pH above 8.6; β-methylumbelliferone, at a pH above 7.5). The cathodic corrosion sites occur at defects in the passivating layer, but not all defects destroy the passivating properties of the Al_2O_3 film on Al. Evidently, the change in pH of the cathodic reaction site spreads out rapidly from the central defect, producing the initial reaction site.

The slow deactivation of the fluorescent indicator after the bias was turned off indicates that the pH at the cathodic reaction site takes time to revert to its original state. Either the corrosion reaction has some inertia after the applied bias is turned off and slows down gradually, and/or diffusion of H^+ into the reaction region or of OH^- out of the region is slow.

In similar experiments with fluorescein dye and gold metal, the fluorescence was quenched at the anode, indicating that the pH at the anode was 4.0 or less.

For this IC decorating technique, the importance of the moist ambient required to observe fluorescence should be emphasized. Presumably, the moisture present on the device surface is needed to activate certain indicators. The indicators considered here are activated by loss of a proton from the molecule. The transfer mechanism may require water on the surface of the IC. Even under conditions of high humidity, however, only a few indicators perform well. Fluorescein, although exhibiting a bright green fluorescence when applied to a device (i.e., before the ethanol solvent evaporates), cannot be used effectively. Its fluorescent intensity is quite sensitive to the amount of solvent present and diminishes drastically with solvent evaporation. But for a short period of time, as the solvent is evaporating, localized fluorescence can be activated for the fluorescein indicator by external bias; β-methylumbelliferone and β-naphthol are preferable. They exhibit better drying properties, and localized fluorescence can be observed for long periods of time after their application to the substrate.

The application solvent for decorating the IC with the indicator is important. Although we have been able to observe fluorescence for the β-methylumbelliferone with an application solution consisting of pure ethanol, the performance of the indicator can be improved by the use of wetting agents. A glycerol-FC-93 surfactant mixture in the application solvent (1 part of mixture to 100 parts ethanol) produced good results, including stronger fluorescent intensity. This made it possible to detect smaller localized corrosion sites with less difficulty.

Fluorescent pH indicators provide a useful method of decorating localized corrosion sites on IC devices, but not one that should be considered a method for determining the exact pH of an IC surface. Although in aqueous solution a pH range can be assigned to a change in fluorescence, a similar change on a metallized and insulated IC surface may not correspond to that same pH range; yet a change in pH definitely occurred. To produce fluorescence, the indicator must lose a proton. This loss, and the molecule's subsequent fluorescent behavior, appear to offer a means of detecting a cathodic corrosion site ($2\ H^+ + 2\ e^- \rightarrow H_2\uparrow$) on the IC. Our observations have shown the fluorescent pH indicator capable of detecting corrosion sites that were not apparent upon normal visual observation. The same technique can identify the specific defects that produce corrosion sites on an IC.

H. OTHER MEASUREMENTS

In this section, various other tests and exploratory measurements are discussed. These include effects of surface treatment on surface conduction, hygroscopic effects, gravimetric measurements of metal conversion by corrosion, and long-term exposure to low levels of moisture.

1. Surface Treatment Effects On Surface Conduction

Various surface treatments strongly affect the surface conduction of oxides and glasses. These treatments include etching, heating, and reactions with surface coupling agents such as hexamethyldisilazane (HMDS). Relevant experiments were all done with aluminum comb devices passivated with 8000-Å-thick PSG containing 4% by wt of phosphorus.

a. Etching and Heat Treatment

Electrical measurements were taken at room temperature at a relative humidity of 85% with 100 V applied. Measurements of B and D combs were done after various sample treatments. The results are presented in Table 15.

TABLE 15. SURFACE CONDUCTION AFTER ETCHING AND BAKING

Treatment	Current Comb B	 Comb D
Room Storage	3×10^{-11}	2×10^{-9}
Water Clean + 125°C Bake*	6×10^{-14}	3×10^{-10}
15 s in Buffer HF, Rinse, 125°C Bake*	1×10^{-13}	1×10^{-8}
15 s in Buffer HF, Rinse, 250°C Bake*	6×10^{-13}	8×10^{-13}

---

*Similar results were obtained for bake times of 15 and 30 minutes.

These results emphasize the highly conducting nature of freshly etched surfaces in humid ambient, and the necessity of heating above 200°C to remove adsorbed water.

b. Hexamethyldisilazane (HMDS) Treatment

In these measurements, aluminum comb patterns were used to illustrate effects of HMDS treatment on surface current. We had done similar measurements prior to this contract, and were able to demonstrate moisture reliability improvement on a particular device.

The HMDS treatment is done by immersing the sample in HMDS for 30 minutes, air drying, and baking at 80°C for one hour in room air. Current measurements were done at 23°C and 85% rh on B and D combs of aluminum with 4% PSG passivation of 8000-Å thickness. A potential of 100 V was applied. The effects of 200°C baking and HMDS treatment were investigated. Typical results are shown in Table 16.

TABLE 16. SEQUENTIAL TEST OF HMDS SURFACE TREATMENT

Treatment*	Current Comb B	Current Comb D
After Storage	4×10^{-9}	1×10^{-7}
200°C Bake, 1 h	6×10^{-12}	6×10^{-11}
Overnight Storage	8×10^{-11}	2×10^{-7}
200°C Bake (1 h) and HMDS	8×10^{-13}	7×10^{-11}
Overnight Storage	1×10^{-12}	1×10^{-10}

The most important observation is the much smaller increase in surface current observed after overnight storage following HMDS treatment, compared to overnight storage without HMDS treatment.

2. Hygroscopic Effects

At high relative humidities, 85% ≤ rh ≤ 95%, water droplets sometimes formed at positive bond pads, as observed in the probe station. When this occurred, the normally steady current became quite noisy, with frequent, large spikes of current. With two sodium-contaminated comb patterns, this spiking occurred without any water droplet formation evident at the bond pads. This suggested that liquid water was being formed at sites within the comb pattern, possibly at the intentional passivation defects. However, no water was found by optical microscopy. To further explore the possibility of localized droplet formation, the stylus of a hardness testing apparatus was used to make scratches and cracks in PSG passivation over aluminum combs. With practice, scratches and cracks of reproducible dimensions could be formed. Then the currents obtained on the scratched devices were compared with those on the unscratched devices. No differences in current magnitude could be detected, and no droplet formation was observed.

A brass sample cell was constructed which permitted observation at 385X of a sample in a controlled humidity ambient. A bipolar device with a large aluminum capacitor, over which PSG cracks had been induced by prior heating, was used in attempts to observe the formation of liquid water in these cracks while cycling from low to high humidity. No observable changes occurred.

3. Gravimetric Measurements

The feasibility of a gravimetric determination of corrosion rate was examined by depositing aluminum on a quartz crystal oscillating at about 6 MHz. Aluminum was sputtered onto the crystal to a thickness of 527 Å. Exposure to an oxygen partial pressure of about 0.1 Torr for nine minutes, followed by exposure to room air for about two minutes, generated a mass change corresponding to a total oxide thickness of about 25 Å. These thickness values were calculated, after correction for temperature changes, from the mass changes reflected in the resonant frequency shift.

The instrument used in these determinations exhibits a stability of ±1 Hz. Formation of Al_2O_3 in the tens-of-Angstrom thickness range corresponds to a frequency shift of tens of Hz. Thus, this method could be used to monitor with high sensitivity the corrosion of aluminum as deposited by various methods. However, any in situ measurement would be complicated by the processes of water absorption, adsorption, and desorption, as these would produce corresponding mass changes.

4. Exposure of Aluminum to Low Levels of Moisture

In hermetic packages that have good seals, it is still possible to have some low moisture content in the cavity due to water in the sealing ambient, adsorption on the cavity surfaces, or outgassing from materials. To investigate possible long-term corrosion due to these low moisture levels, aluminum test devices were sealed in stainless-steel bombs in air with 1000 ppm H_2O.

Three aluminized test devices were placed in each of five pressure vessels containing room air with 1000 ppm H_2O. These were stored for 800 hours at temperatures of 125°C (two vessels), 155°C, 200°C, and 250°C.

Microscopic examination revealed no aluminum attack. This indicates that storage of hermetic devices above the dew point with up to 1000 ppm moisture will probably not induce corrosion in the absence of galvanic corrosion, which was not evaluated in this test. However, for packaged devices, the presence of metals other than aluminum, such as gold on package posts, could lead to long-term galvanic corrosion of the aluminum bond wires [17].

SECTION V

CONCLUSIONS AND RECOMMENDATIONS

This work has shown for the first time that measurements of corrosion current between passivated, thin-film metal electrodes can be carried out on test devices produced by standard IC processing. Procedures established for measuring both corrosion current and corrosion rate as functions of relative humidity and temperature yielded new insights into the corrosion process. As a result, knowledge obtained in earlier studies, about unpassivated metal corrosion, could be applied to passivated systems. Cathodic corrosion was found to be much more likely than anodic corrosion. There was found to be close agreement between the dependence of current on relative humidity and the dependence of the quantity of adsorbed water on relative humidity, suggesting that current transport in the film is the rate-limiting factor. Surface treatments can lower the surface current dramatically, and presumably lower the corrosion rate as well. The presence of large anodes increases the probability of cathodic corrosion. Current efficiencies for corrosion were quite small, ranging from ~0.003 for SINCAP passivation up to 0.08 for PSG passivation. Because currents are too small for any appreciable corrosion by ionic transport at the interface between thermal oxide and PSG, this possibility was ruled out.

Measurements of corrosion rate by line resistance change and of corrosion current by electrochemical cell voltammetry yielded valuable conclusions about the effects of processing on corrosion stability. Alloying, a normal production process for aluminum thin films, enhances their corrosion stability. The presence of hydrogen in the alloying ambient further increases the stability of these films. Corrosion of aluminum with SINCAP passivation proceeds much more slowly than with PSG passivation.

Sputtered (S-gun) aluminum corrodes much more slowly than does filament-evaporated aluminum, probably because the grain size of S-gun aluminum is large. This is a finding of considerable technical significance to solid-state device processing.

The presence of sodium below the passivation glass markedly increases the corrosion rate for aluminum at the cathode, but does not change the rate at the anode. Gold migration was not detected, but there was some gold corrosion at the anode. In the electrochemical cell, only small differences in gold corrosion processes were found when chloride ion was added. Aluminum corrosion processes, however, are very much affected by chloride ion, and even more so by fluoride ion. Surface conduction, on the other hand, is enhanced much more by the presence of NaCl than of NaF. Thus, fluoride ion may be a smaller factor in IC corrosion than chloride ion. Aluminum films under compressive stress are more corrosion resistant than films under tensile stress. There was no correlation, however, between the level of tensile stress and corrosion.

Fluorescent dye application can indicate the location of a corrosion site that is otherwise not visible. Further, the dye can indicate whether the corrosion site is at a high or low pH compared with the rest of the sample. Whereas the cathodic reaction increased the local pH, the anodic reaction decreased it. After the bias was removed, the dye fluorescence indicated that the corrosion mechanism might continue for some time. However, there was no evidence of purely chemical corrosion in the humidity tests with unbiased thin films.

Additional work should yield interesting data and useful conclusions. We especially recommend the following areas of investigation:

- For a single metal plus passivation system, use identical or similar test patterns and procedures to investigate in greater detail the corrosion rate and current dependence on such factors as voltage, time, temperature, and relative humidity.
- For plastic-encapsulated devices, use the test patterns to investigate corrosion rate and corrosion current.
- Study the effect of sodium or other contaminants on different passivation systems, including PSG, SINCAP, organic layers, or combinations of these.
- Investigate the effects of various metal treatments on corrosion processes and rates. Give special consideration to the use of corrosion inhibition in plastic packages.

- Investigate the use of insulator treatments such as HMDS application to enhance reliability.
- Develop and use an appropriate test pattern to study the effects of stress cracks in passivation on metal corrosion.
- Use the fluorescent dye method first to identify corrosion sites and then to monitor corrosion at these sites as a function of various conditions, such as time, humidity, and temperature.
- Investigate further the corrosion of aluminum with SINCAP passivation in the presence of chloride ion.

REFERENCES

1. W. H. Abbott, "Air Pollution and Failure Mechanisms of Electronic Interfaces," Electrochem. Soc. Ext. Abstr. 78-2, 657-658 (Oct. 1978).

2. M. F. Abd Rabbo, J. A. Richardson and G. C. Wood, "A Study of the Effects of Inhibitive and Aggressive Ions on Oxide-Coated Aluminum Using Secondary Ion Mass Spectrometry," Corrosion Sci. 16, 677-687 (1976).

3. R. Alkire and D. Siitari, "The Location of Cathodic Reaction During Localized Corrosion," J. Electrochem. Soc. 126, 15-22 (1979).

4. R. S. Alwitt, "The Aluminum-Water System," in J. W. Diggle and A. K. Vijh, eds,. Oxides and Oxide Films, Vol. 4, Marcel Dekker, Inc., New York, 1976, pp. 169-254.

5. L. K. Anderson, "Some Package Reliability Implications of Current Trends in Large Scale Silicon Integrated Circuits," 16th Ann. Proc. Reliab. Phys., pp. 121-123 (1978).

6. S. Anderson and D. D. Kempton, "Some Phenomena Related to the Hydrophobicity of Silicate Glasses and Adsorbed Oxygen," J. Amer. Ceram. Soc. 43, 484-488 (1960).

7. P. A. Arutyunov and K. A. Keidzhyan, "The Use of Test Structures in Assessing the Quality and Reliability of LSI Circuits," Sov. Microelectron. 6(6), 390-397 (Nov./Dec. 1977).

8. Y. Awakuni and J. H. Calderwood, "Water Vapour Adsorption and Surface Conductivity in Solids," J. Phys. D: Appl. Phys. 5, 1035-1045 (1972).

9. C. M. Bailey, "Effects of Burn-in and Temperature Cycling on the Corrosion Resistance of Plastic Encapsulated Integrated Circuits," 15th Ann. Proc. Reliab. Phys., pp. 120-124 (1977).

10. C. M. Bailey, Jr., "Reliability of Plastic Encapsulated Integrated Circuits," Proc. Symp. Plastic Encapsulated/Polymer Sealed Semiconductor Devices for Army Equipment (US Army ERADCOM, Fort Monmouth, NJ), pp. 97-107 (1978).

11. C. M. Bailey, Jr., "Reliability of Plastic Encapsulated Integrated Circuits," Proc. Tech. Program Int. Microelectron. Conf. (Anaheim, CA/New York, NY), pp. 246-252 (1978).

12. C. M. Bailey, "Plastic Encapsulated ICs: A Reliability Evaluation," Electron. Pkg. Prod. 18(6), 129-134 (June 1978).

13. M. K. Balazs, "The Identification of Contaminants and Their Sources in the Processing of Semiconductor Integrated Circuits," Proc. ATFA-77, pp. 42-47 (Sept. 1977).

REFERENCES (Continued)

14. C. B. Bargeron and R. B. Givens, "Localized Corrosion of Aluminum: Blister Formation as a Precursor of Pitting," J. Electrochem. Soc. 124, 1845-1848 (Dec. 1977).

15. J. J. Bart, "Analysis of Deposited Glass Layer Defects," 13th Ann. Proc. Reliab. Phys., pp. 128-135 (1975).

16. J. J. Bart, "Scanning Electron Microscopy for Complex Microcircuit Analysis," 16th Ann. Proc. Reliab. Phys., pp. 108-111 (1978).

17. J. J. Bart and E. A. Doyle, Jr., "An Avionic System Long-Term Microcircuit Corrosion Problem," GOMAC (Government Microcircuits Applications Conference) Proc., pp. 80-83 (Nov. 1976).

18. R. G. Bates, Determination of pH-Theory and Practice, 2nd ed., John Wiley & Sons, Inc., New York, 1973.

19. C. Beck, "Phosphorus Concentration in Low Temperature Vapor Deposited Oxide," Solid State Technol. 20(12), 58-60 (Dec. 1977).

20. H. M. Berg and W. M. Paulson, "The Factors Affecting Aluminum Corrosion in Plastic Semiconductor Packages," Electrochem. Soc. Ext. Abstr. 77-1, 33-34 (May 1977).

21. H. M. Berg and W. M. Paulson, "Aluminum Corrosion in Plastic-Encapsulated Devices," Proc. Symp. Plastic Encapsulated/Polymer Sealed Semiconductor Devices for Army Equipment (US Army ERADCOM, Fort Monmouth, NJ), pp. 197-212 (1978).

22. R. G. Berger, K. M. Gardiner, and N. A. Sinclair, "Manufacturing Handling and Semiconductor Reliability," Proc. Tech. Program Int. Microelectron. Conf. (West/East), pp. 173-182 (1976).

23. R. G. Berger, Jr., and A. J. Gregoritsch, "Induced Passivation Defect Study," 13th Ann. Proc. Reliab. Phys., pp. 121-127 (1975).

24. U. Bertocci and R. W. Shideler, "Detection and Analysis of Electrochemical Noise for Corrosion Studies," Electrochem. Soc. Ext. Abstr. 78-2, 336-337 (Oct. 1978).

25. A. Berzins, R. T. Lawson, and K. J. Mirams, "Aluminum Corrosion Studies III: Chloride Adsorption Isotherms on Corroding Aluminum," Austral. J. Chem. 30, 1891-1903 (1977).

26. W. W. Binger, E. H. Hollingsworth, and D. O. Sprowls, "Resistance to Corrosion and Stress Corrosion," in Aluminum, Vol. 1, K. R. Van Horn, ed., Properties, Physical Metallurgy and Phase Diagrams, American Society for Metals, Metals Park, OH, 1967, pp. 209-254.

REFERENCES (Continued)

27. F. D. Bogar and R. T. Foley, "The Influence of Chloride Ion on the Pitting of Aluminum," J. Electrochem. Soc. 119, 462-464 (April 1972).

28. H. Bohni and H. H. Uhlig, "Environmental Factors Affecting the Critical Pitting Potential of Aluminum," J. Electrochem. Soc. 116, 906-910 (July 1969).

29. A. P. Bond, G. F. Bolling, H. A. Domian, and H. Biloni, "Microsegregation and Tendency for Pitting Corrosion in High Purity Aluminum," J. Electrochem. Soc. 113, 773-778 (Aug. 1966).

30. G. W. Brassell and D. R. Fancher, "Electrically Insulative Adhesives for Hybrid Microelectronic Fabrication," IEEE Trans. Components Hybr. Mfg. Technol. CHMT-1, 192-197 (June 1978).

31. B. F. Brown, C. T. Fujii, and E. P. Dahlberg, "Methods for Studying the Solution Chemistry Within Stress Corrosion Cracks," J. Electrochem. Soc. 116, 218-219 (Feb. 1969).

32. G. A. Brown, K. Lovelace, and C. Hutchins, "A Process Control Test for Lateral Charge Spreading Susceptibility," 11th Ann. Proc. Reliab. Phys., pp. 203-207 (1973).

33. U. C. Brown and J. R. Sim, "Failure Mechanisms in Beam Lead Semiconductors," Proc. 27th Electronic Comp. Conf., pp. 188-192 (May 1977); IEEE Trans. Parts Hybr. Pkg. PHP-13, 225-229 (Sept. 1977).

34. G. F. Cerofolini and C. Rovere, "The Role of Water Vapour in the Corrosion of Microelectronic Circuits," Thin Solid Films 47, 83-94 (1977).

35. C. C. Chang, D. B. Fraser, M. J. Grieco, T. T. Sheng, S. E. Haszko, R. E. Kerwin, R. B. Marcus, and A. K. Sinha, "Aluminum Oxidation in Water," J. Electrochem. Soc. 125, 787-792 (May 1978).

36. C. C. Chang, T. T. Sheng, D. V. Speeney, and D. B. Fraser, "Si Depth Profile and Contaminants in Si-Doped Al Film," J. Appl. Phys. 47, 1790-1794 (May 1976).

37. N. J. Chaplin and A. J. Masessa, "Reliability of Epoxy and Silicone Molded Tape-Carrier Silicon Integrated Circuits With Various Chip-Protective Coatings," 16th Ann. Proc. Reliab. Phys., pp. 187-193 (1978).

38. G. T. Cheney et al., "Special Issue on Device Reliability," IEEE Trans. Electron Devices ED-26, 1-108 (Jan. 1979).

39. K. Chow and L. G. Garrison, "Phosphorus Concentration of Chemical Vapor Deposited Phosphosilicate Glass," J. Electrochem. Soc. 124, 1133-1136 (July 1977).

REFERENCES (Continued)

40. A. Christou, "Assessment of Silicone Encapsulants for Hybrid Integrated Circuits (HIC)," IEEE Trans. Parts Hybr. Pkg. PHP-13, 298-304 (Sept. 1977).

41. A. Christou, "Reliability Aspects of Moisture and Ionic Contamination Diffusion Through Hybrid Encapsulants," Proc. Tech. Progr. Int. Microelectron. Conf. (Anaheim, CA/New York, NY), pp. 237-245 (1978).

42. A. Christou, "Moisture Diffusion Through Hybrid-Circuit Encapsulants," Electronic Pkg. Prod. 19(4), 91-96, 98, 100 (April 1979).

43. A. Christou, J. R. Griffith and W. Wilkins, "Reliability Testing of Fluorinated Polymeric Materials (FNP) for Hybrid Encapsulation," 16th Ann. Proc. Reliab. Phys., pp. 194-199 (1978).

44. A. Christou and W. Wilkins, "Assessment of Silicone Encapsulation Materials: Screening Techniques," 15th Ann. Proc. Reliab. Phys., pp. 112-119 (1977).

45. R. B. Comizzoli, "Bulk and Surface Conduction in CVD SiO_2 and PSG Passivation Layers," J. Electrochem. Soc. 123, 386-391 (March 1976).

46. R. B. Comizzoli, "Surface and Bulk Electrical Conduction in Low-Deposition-Temperature Si_3N_4 and Al_2O_3 Films for Silicon Devices," RCA Rev. 37, 473-482 (Dec. 1976).

47. R. B. Comizzoli, "Aluminum Corrosion in the Presence of Phosphosilicate Glass and Moisture," RCA Rev. 37, 483-490 (Dec. 1976).

48. R. B. Comizzoli, "Nondestructive, Reverse Decoration of Defects in IC Passivation Overcoats," J. Electrochem. Soc. 124, 1087-1095 (July 1977).

49. S. M. de DeMicheli, "The Electrochemical Study of Pitting Corrosion of Aluminum in Chloride Solutions," Corrosion Sci. 18, 605-616 (1978).

50. N. F. De Rooij, R. J. S. Sieberdink, and R. M. Tromp, "An Investigation of the Hydration Properties of Chemically Vapour-Deposited Silicon Dioxide Films By Means of Ellipsometry," Thin Solid Films 47, 211-218 (1977).

51. G. A. DiBari and H. J. Read, "Electrochemical Behavior of High Purity Aluminum in Chloride Containing Solutions," Corrosion-NACE 27, 483-493 (Nov. 1971).

REFERENCES (Continued)

52. H. K. Dicken, "Cost and Reliability Trends of Plastic Encapsulated Integrated Circuits," Proc. Symp. Plastic Encapsulated/ Polymer Sealed Semiconductor Devices for Army Equipment (US Army ERADCOM, Fort Monmouth, NJ), pp. 130-142 (1978).

53. B. S. Duncan and R. P. Frankenthal, "Effect of pH on the Rate of Corrosion of Gold in Acid Sulfate Solutions," J. Electrochem. Soc. 126, 95-97 (Jan. 1979).

54. G. H. Ebel, "Failure Analysis Techniques Applied in Resolving Hybrid Microcircuit Reliability Problems," 15th Ann. Proc. Reliab. Phys., pp. 70-81 (1977).

55. M. Edwards, "Effects of Fillers on Electrical Performance of Semiconductor Grade Liquid Epoxy Systems," Proc. Tech. Program Int. Microelectron. Conf. (Anaheim, CA/New York, NY), pp. 232-236 (1978).

56. A. Ertel and H. J. Perlstein, "The Hermeticity Hoax," Proc. 1978 Ann. Reliab. Maint. Symp., pp. 448-453 (Jan. 1978).

57. C. A. Evans, Jr., and R. J. Blattner, "Modern Experimental Methods for Surface and Thin-Film Chemical Analysis," Ann. Rev. Mater. Sci. 8, 181-214 (1978).

58. U. R. Evans, The Corrosion and Oxidation of Metals, Edward Arnold Publishers, Ltd., London, England, 1960.

59. U. R. Evans, The Corrosion and Oxidation of Metals, 2nd Suppl. Vol., Edward Arnold Publishers, Ltd., London, England, 1976.

60. D. R. Fancher and R. G. Horner, "Hybrid Package Hermeticity and Moisture Level Monitoring," Proc. 1978 Int. Microelectron. Symp., pp. 114-120, ISHM (Sept. 1978).

61. L. G. Feinstein, "Failure Mechanism in Molded Microelectronics Packages," NEPCON/West - NEPCON/East, 1979 (preprint).

62. A. V. Ferris-Prabhu, "Contaminant Induced Aging in Integrated Circuit Packages," Proc. 28th Electronic Comp. Co[illegible], pp. 1-6 (Apr. 1978).

63. J. A. Ferro, "An Accelerated Method for Effective Process Control of Plastic Encapsulated Nichrome PROMS," 15th Ann. Proc. Reliab. Phys., pp. 125-127 (1977).

64. P. J. Ficalora and D. Y. Shih, "The Effect of Hydrogen on Rate of Formation of Intermetallics in the Cu-Sn, Ag-Sn, and Ni-Sn Systems," 17th Ann. Proc. Reliab. Phys., pp. 87-90 (1979).

65. M. J. Fox, "A Comparison of the Performance of Plastic and Ceramic Encapsulations Based on Evaluation of CMOS Integrated Circuits," Microelectron. Reliab. 16(3), 251-254 (1977).

REFERENCES (Continued)

66. J. P. Franey, "Trace Gas Flow Control Using Polymer Permeation," Electrochem. Soc. Ext. Abstr. 78-2, 659-660 (Oct. 1978).

67. R. P. Frankenthal, "Corrosion in Electronic Applications," in R. Sard, H. Leidheiser, Jr., and F. Ogburn, eds., Properties of Electrodeposits - Their Measurement and Significance, The Electrochemical Society, Princeton, NJ, 1975, pp. 142-169.

68. R. P. Frankenthal and W. H. Becker, "Corrosion Failure Mechanisms for Gold Metallizations," Electrochem. Soc. Ext. Abstr. 78-2, 661-662 (Oct. 1978).

69. R. P. Frankenthal and D. E. Thompson, "Electrochemical Behavior of Electronic Materials," pp. 90-92 in R. Baboian, ed., Electrochemical Techniques for Corrosion, Natl. Assoc. Corrosion Engineers, 1977.

70. F. N. Fuss and C. T. Hartwig, "Corrosion of Solder-Coated Ti-Pd-Au Thin-Film Conductors in a Moist Chlorine Atmosphere," Proc. 27th Electronic Components Conf., pp. 72-83 (May 1977).

71. T. R. Gagnier and E. M. Kimball, "Storage Reliability Verification Testing Program for Plastic Encapsulated Integrated Circuits," Proc. Symp. Plastic Encapsulated/Polymer Sealed Semiconductor Devices for Army Equipment (US Army ERADCOM, Fort Monmouth, NJ), pp. 108-119 (1978).

72. L. J. Gallace, "Reliable Plastic-Packaged IC's and Power Transistors," Proc. Symp. Plastic Encapsulated/Polymer Sealed Semiconductor Devices for Army Equipment: (US Army ERADCOM, Fort Monmouth, NJ), pp. 168-183 (1978).

73. L. J. Gallace, L. A. Jacobus, E. J. Pfiffner, and C. A. West, "Accelerated Reliability Evaluation of Trimetal Integrated Circuit Chips in Plastic Packages," IEEE Trans. Components Hybr. Mfg. Technol. CHMT-2, 172-179 (June 1979).

74. L. J. Gallace, H. J. Khajezadeh, and A. S. Rose, "Accelerated Reliability Evaluation of Trimetal Integrated Circuit Chips in Packages," 16th Ann. Proc. Reliab. Phys., pp. 224-228 (1978).

75. L. J. Gallace, H. Khajezadeh, and A. S. Rose, "High-Reliability Low-Cost Integrated Circuit Plastic Packages," GOMAC-78, Monterey, CA, Nov. 14, 1978, pp. 267-268.

76. L. J. Gallace, H. L. Pujol, and G. L. Schnable, "CMOS Reliability," Proc. 27th Electronic Components Conf., pp. 496-512 (May 1977); Microelectron. Reliab. 17(2), 287-304 (1978).

77. J. R. Galvele, "Transport Processes and the Mechanism of Pitting of Metals," J. Electrochem. Soc. 123, 464-474 (April 1976).

REFERENCES (Continued)

78. J. R. Galvele and S. M. de DeMicheli, "Mechanism of Intergranular Corrosion of Al-Cu Alloys," Corrosion Sci. 10, 795-807 (1970).

79. A. J. Gregoritsch, "Polyimide Passivation Reliability Study," 14th Ann. Proc. Reliab. Phys., pp. 228-233 (1976).

80. A. J. Gregoritsch, "Double Level Metallurgy Defect Study," 16th Ann. Proc. Reliab. Phys., pp. 28-32 (1978).

81. C. Grilletto, "An X-Ray Fluorescence Technique for the Rapid Determination of Phosphorus in PSG Film," Solid State Technol. 20(2), 27-30 (Feb. 1977).

82. F. J. Grunthaner, T. W. Griswold, and P. J. Clendening, "Migratory Gold Resistive Shorts: Chemical Aspects of a Failure Mechanism," 13th Ann. Proc. Reliab. Phys., pp. 99-106 (1975).

83. E. B. Hakim, "U.S. Army Panama Field Test of Plastic Encapsulated Devices," Microelectron. Reliab. 17(3), 387-392 (1978).

84. E. B. Hakim and B. Reich, eds., Proc. Symp. Plastic Encapsulated/Polymer Sealed Semiconductor Devices for Army Equipment (US Army ERADCOM, Fort Monmouth, NJ), pp. 1-249 (1978).

85. E. B. Hakim and H. A. Schauer, "Panama Field Test Results of Plastic Encapsulated Devices," Proc. Symp. Plastic Encapsulated/Polymer Sealed Semiconductor Devices for Army Equipment (US Army ERADCOM, Fort Monmouth, NJ), pp. 67-83 (1978).

86. E. B. Hakim and J. R. Shappirio, "Failure Mechanisms in Gold Metallized Sealed Junction Devices," Solid State Technol. 18(4), 66-68 (April 1975).

87. L. D. Hanley and J. H. Martin, "A Test of Parylene as a Protective System for Microcircuitry," 13th Ann. Proc. Reliab. Phys., pp. 53-57 (1975).

88. M. L. Harding, "Non-Hermetic Packaging for Commercial Hybrid Microcircuits," Proc. Symp. Plastic Encapsulated/Polymer Sealed Semiconductor Devices for Army Equipment (US Army ERADCOM, Fort Monmouth, NJ), pp. 225-239 (1978).

89. J. J. Harrahy, "Assessment of Plastic, Commercial Grade IC Failure Rates Achieved in Field Operation," Proc. Symp. Plastic Encapsulated/Polymer Sealed Semiconductor Devices for Army Equipment (US Army ERADCOM, Fort Monmouth, NJ), pp. 17-32 (1978).

90. R. W. Harriot, "Epoxy Testing for Hybrid Applications . . . How Reliable Is It?" Proc. 1978 Int. Microelectron. Symp., pp. 61-65, ISHM (Sept. 1978).

91. B. Harris and P. B. P. Phipps, "The Role of Adsorbed Water in Atmospheric Corrosion," Electrochem. Soc. Ext. Abstr. 79-2, 626-627 (Oct. 1979).

REFERENCES (Continued)

92. L. B. Harris, "Change in pH Near the Cathode During the Electrodeposition of a Bivalent Metal. Analysis," J. Electrochem. Soc. 120, 1034-1040 (Aug. 1973).

93. J. C. Harrison, "Control of the Encapsulation Material as an Aid to Long Term Reliability in Plastic Encapsulated Semiconductor Components (PEDs)," Microelectron. Reliab. 16(3), 233-244 (1977).

94. K. Heid, "Nichrome Passivation Coatings - Help or Hindrance?", Proc. 27th Electronic Components Conf., pp. 68-71 (May 1977).

95. T. P. Hoar, "On Corrosion Resistant Materials," J. Electrochem. Soc. 117, 17C-22C (Jan. 1970).

96. C. E. Holland, Jr., and C. A. West, "Navy High Reliability/Low Cost Integrated Circuit Program," Proc. Symp. Plastic Encapsulated/Polymer Sealed Semiconductor Devices for Army Equipment (US Army ERADCOM, Fort Monmouth, NJ), pp. 120-129 (1978).

97. L. Holland, The Properties of Glass Surfaces, John Wiley & Sons, Inc., New York, 1964, p. 228.

98. P. H. Holloway, "Analysis of Corrosion Products with Surface and Near-Surface Sensitive Analytical Techniques," Electrochem. Soc. Ext. Abstr. 78-2, 670-671 (Oct. 1978).

99. R. E. Honig, "Materials Characterization at RCA Laboratories," Solid State Technol. 13(3), 59-66 (March 1970).

100. R. E. Honig, "Characterization of Materials at RCA Laboratories," RCA Engineer 20(6), 62-69 (Apr./May 1975).

101. Von L. Horner and K. Meisel, "Corrosion Inhibitors 23: (1) Does There Exist a Structure-Efficiency Relation in the Organic Inhibitors of Aluminum Corrosion?", Werkstoffe u. Korrosion 29, 654-664 (1978).

102. A. T. Hubbard and E. C. Anson, "The Theory and Practice of Electrochemistry with Thin Layer Cells," in Vol. 4 of J. Bard, ed., Encyclopedia of Electrochemistry of the Elements, Marcel Dekker, Inc., New York, 1975, pp. 129-214 (see p. 135).

103. H. Inayoshi, K. Nishi, S. Okikawa, and Y. Wakashima, "Moisture-Induced Aluminum Corrosion and Stress on the Chip in Plastic-Encapsulated LSIs," 17th Ann. Proc. Reliab. Phys., pp. 113-117 (1979).

104. S. Iwata, A. Ishizaka, and H. Yamamoto, "Corrosion Test for Metallization for Plastic-Encapsulated IC's," J. Electrochem. Soc. 126, 110-114 (Jan. 1979).

REFERENCES (Continued)

105. R. O. Jones, "Developments Likely to Improve the Reliability of Plastic Encapsulated Devices," Microelectron. Reliab. 17, 273-278 (1978).

106. C. E. Jowett, "Failure Mechanisms and Analysis Procedures for Semiconductor Devices," Microelectron. J. 9(3), 5-13 (Jan./Feb. 1979).

107. V. S. Kale, "Interaction of Parylene and Moisture in Hermetically Sealed Hybrids," Proc. 28th Electronic Components Conf., pp. 344-349 (April 1978).

108. V. S. Kale and T. J. Riley, "A Production Parylene Coating Process for Hybrid Microcircuits," Proc. 27th Electronic Components Conf., pp. 245-251 (May 1977); IEEE Trans. Parts Hybr. Pkg. PHP-13, 273-279 (Sept. 1977).

109. W. Kern. "Characterization of Localized Structural Defects in Dielectric Films," RCA Rev. 34, 655-690 (Dec. 1973).

110. W. Kern and R. B. Comizzoli, "Techniques for Measuring the Integrity of Passivation Overcoats on Integrated Circuits," NBS Spec. Publ. 400-31, U.S. Dept. of Commerce, March 1977.

111. W. Kern, R. B. Comizzoli, A. W. Fisher and G. L. Schnable, "Improved CVD Techniques for Depositing Passivation Layers on ICs," Technical Report AFML-TR-75-160, Final Report for the period April 1974-June 1975, Air Force Materials Laboratory (LTE), Wright-Patterson AFB, Ohio 45433, Oct. 1975.

112. W. Kern and R. S. Rosler, "Advances in Deposition Processes for Passivation Films," J. Vac. Sci. Technol. 14, 1082-1099 (Sept.-Oct. 1977).

113. W. Kern and G. L. Schnable, "Low-Pressure Chemical Vapor Deposition for Very Large-Scale Integration Processing - A Review," IEEE Trans. Electron Devices ED-26, 647-657 (April 1979).

114. W. Kern, G. L. Schnable, and A. W. Fisher, "CVD Glass Films for Passivation of Silicon Devices: Preparation, Composition and Stress Properties," RCA Rev. 37, 3-54 (March 1976).

115. W. Kern, J. L. Vossen, and G. L. Schnable, "Improved Reliability of Electron Devices Through Optimized Coverage of Surface Topography," 11th Ann. Proc. Reliab. Phys., pp. 214-223 (1973).

116. H. Khajezadeh and A. S. Rose, "Reliability Evaluation of Hermetic Integrated Circuit Chips in Plastic Packages," 13th Ann. Proc. Reliab. Phys., pp. 87-92 (1975).

117. H. Khajezadeh and A. S. Rose, "Reliability Evaluation of Trimetal Integrated Circuits in Plastic Packages," 15th Ann. Proc. Reliab. Phys., pp. 244-249 (1977).

REFERENCES (Continued)

118. H. Koelmans, "Metallization Corrosion in Silicon Devices by Moisture-Induced Electrolysis," 12th Ann. Proc. Reliab. Phys., pp. 168-171 (1974).

119. H. Koelmans and H. J. Kretschman, "Water Droplet Formation During the Life Testing of IC's in a Humid Ambient," J. Electrochem. Soc. 125, 1715-1716 (Oct. 1978).

120. S. C. Kolesar, "Principles of Corrosion," 12th Ann. Proc. Reliab. Phys., pp. 155-167 (1974).

121. R. Kossowsky, "Analytical Techniques for Electronic Materials - A Comparative Evaluation," 16th Ann. Proc. Reliab. Phys., pp. 112-120 (1978).

122. M. Koudelkva, J. Augustynski, and H. Berthou, "On the Composition of the Passivating Films Formed on Aluminum in Chromate Solutions," J. Electrochem. Soc. 124, 1165-1168 (Aug. 1977).

123. J. Kruger, "New Approaches to the Study of Localized Corrosion," in R. Baboian, ed., Electrochemical Techniques for Corrosion, Natl. Assoc. Corrosion Engineers, 1977, pp. 35-41.

124. A. Kubovy and M. Janda, "The Influence of Residual Gas Pressure on the Stress in Aluminum Films," Thin Solid Films 42, 169-173 (1977).

125. D. J. Lando, J. P. Mitchell, and T. L. Welsher, "Conductive Anodic Filaments in Reinforced Polymeric Dielectrics: Formation and Prevention," 17th Ann. Proc. Reliab. Phys., pp. 51-63 (1979).

126. G. Landrum, "Moisture Related Failures in Epoxy Packages," Semiconductor Int. 2(5), 68-69 (June 1979).

127. M. H. Lee, J. M. Eldridge, G. Scherer, W.-Y. Lee, and C. H. Ting, "Electrochemical Studies of Processing Effects on Permalloy Thin Film Corrosion," Electrochem. Soc. Ext. Abstr. 78-2, 666-667 (Oct. 1978).

128. W.-Y. Lee and J. Eldridge, "Oxidation Studies of Permalloy Films by Quartz Crystal Microbalance, AES, and XPS," J. Electrochem. Soc. 124, 1747-1751 (Nov. 1977).

129. W.-Y. Lee, H. C. Siegmann, and J. M. Eldridge, "A Comparison of the Mass and Resistance Change Techniques for Investigating Thin Film Corrosion Kinetics," J. Electrochem. Soc. 124, 1744-1747 (Nov. 1977).

130. B. R. Livesay, "The Reliability of Electronic Devices in Storage Environments," Solid State Technol. 21(10), 63-68 (Oct. 1978).

REFERENCES (Continued)

131. R. K. Lowry, L. A. Miller, A. W. Jonas, and J. M. Bird, "Characteristics of a Surface Conductivity Moisture Monitor for Hermetic Integrated Circuit Packages," 17th Ann. Proc. Reliab. Phys., pp. 97-102 (1979).

132. R. K. Lowry, C. J. Van Leeuwen, B. L. Kennimer, and L. A. Miller, "A Reliable Dry Ceramic Dual In-Line Package," 16th Ann. Proc. Reliab. Phys., pp. 207-212 (1978).

133. N. Lycoudes, "Pressure Temperature Humidity Bias Method and System For Corrosion Studies of Plastic Encapsulated Integrated Circuits," Proc. Inst. Environmental Sci., pp. 213-221 (1977).

134. N. Lycoudes, "The Reliability of Plastic Microcircuits in Moist Environments," Solid State Technol. 21(10), 53-62, 68 (Oct. 1978).

135. I. A. Maier and J. R. Galvele, "Localized Corrosion on Slip Steps of Aluminum Straining," J. Electrochem. Soc. 125, 1594-1598 (Oct. 1978).

136. P. A. Malachesky, "Aluminum," in Vol. 6 of A. J. Bard, ed., Encyclopedia of Electrochemistry of the Elements, Marcel Dekker, Inc., New York, 1976, pp. 63-165.

137. J. E. Mann, W. E. Anderson, T. J. Raab, and J. S. Rollins, "Reliability of Deposited Glass," Technical Report RADC-TR-76-82, Final Report for the period March 1974-April 1975, for Rome Air Development Center by Rockwell International, March 1976, A024664.

138. F. Mansfield and J. V. Kenkel, "Laboratory Studies of Galvanic Corrosion of Aluminum Alloys," in Galvanic and Pitting Corrosion - Field and Laboratory Studies, ASTM STP 576, American Society for Testing and Materials, Philadelphia, PA, 1976, pp. 20-47.

139. A. D. Marderosian, "The Electrochemical Migration of Metals," Proc. 1978 Int. Microelectron. Conf., pp. 134-141, ISHM (Sept. 1978).

140. A. D. Marderosian and V. Gionet, "Water Vapor Penetration Rate into Enclosures with Known Air Leak Rates," 16th Ann. Proc. Reliab. Phys., pp. 179-186 (1978).

141. A. D. Marderosian and C. Murphy, "Humidity Threshold Variations for Dendrite Growth on Hybrid Substrates," 15th Ann. Proc. Reliab. Physics, pp. 92-100 (1977).

142. A. D. Martin and K. J. McLean, "The Effect of Adsorbed Gases on the Surface Conductivity of Quartz," J. Appl. Phys. 48, 2950-2954 (July 1977).

143. J. J. Mazenko, "The Effect of MIL-STD-883 Screening and Stress Upon Beam Lead IC's," Proc. 25th Electronic Components Conf., pp. 65-75 (May 1975).

144. J. J. Mazenko, "How Reliable Are Plastic Encapsulated/Polymer Sealed Hybrids?", Proc. Symp. Plastic Encapsulated/Polymer Sealed Semiconductor Devices for Army Equipment (US Army ERADCOM, Fort Monmouth, NJ), pp. 213-224 (1978).

145. W. J. McGarvey, "Autoclave vs. 85°C/85% R. H. Testing - A Comparison," 17th Ann. Proc. Reliab. Phys., pp. 136-142 (1979).

146. P. S. McLeod and J. L. Hughes, "Effects of Sputter Etching and Process Techniques on the Properties of Sputtered Aluminum Films," J. Vac. Sci. Technol. 16, 369-376 (Mar./Apr. 1979).

147. P. H. Melville, "Variation of Potential in Stress Corrosion Cracks," Br. Corrosion J. 14(1), 15-19 (1979).

148. C. G. Messenger, "Improved Reliability Through Dry and Hermetic Microcircuit Packaging," Proc. 27th Electronic Components Conf., pp. 172-174 (1977).

149. C. G. Messenger, "Moisture Syndromes in Microcircuit Packaging," Proc. 1978 Int. Microelectron. Symp., pp. 142-145, ISHM (1978).

150. K. W. Michael and R. C. Antonen, "The Properties of Silicone-Epoxy Electronic Grade Molding Compound," Proc. Tech. Program Int. Microelectron. Conf. (Anaheim, CA/New York, NY), pp. 246-252 (1978).

151. G. Milazzo and S. Caroli, Tables of Standard Electrode Potentials, John Wiley & Sons, Ltd., Chichester, England, 1978.

152. K. L. Mittal et al., Proc. Symp. Surface Contamination: Its Genesis, Detection and Control, Pergamon Press, New York, 1979.

153. R. Y. Moss, "Comparative Field Warranty Experience with Unscreened Plastic and Hermetic Semiconductors in Electronic Instruments," Proc. Symp. Plastic Encapsulated/Polymer Sealed Semiconductor Devices for Army Equipment (US Army ERADCOM, Fort Monmouth, NJ), pp. 33-41 (1978).

154. K. Mukai, A. Hiraiwa, S. Muramatsu, S. Takahashi, and S. Harada, "Mechanical Properties of Plasma-CVD Silicon Nitride Film," Electrochem. Soc. Ext. Abstr. 79-1, 268-269 (May 1978).

155. A. W. Mullendore, G. C. Nelson, and P. H. Holloway, "Surface Sensitive Analytical Techniques: An Evaluation," Proc. Advanced Techniques in Failure Analysis, pp. 236-245 (Sept. 1977).

156. I. L. Muller and J. R. Galvele, "Pitting Potential of High Purity Binary Aluminum Alloys - I. Al-Cu Alloys, Pitting and Intergranular Corrosion," Corrosion Sci. 17, 179-193 (1977).

157. C. R. Murphy and D. E. Mitchell, "Investigation of RGA Test Results for Hybrids with Epoxy Die/Substrate Attachment," Proc. 1978 Int. Microelectron. Symp., pp. 107-113, ISHM (Sept. 1978).

158. F. Neighbour and B. R. White, "Factors Governing Aluminum Interconnection Corrosion in Plastic Encapsulated Microelectronic Devices," Microelectron. Reliab. 16, 161-164 (1977).

159. D. A. L. Nicklen and D. R. Gabe, "A. C. Anodizing of Aluminum in Sulphuric Acid," Surface Technol. 7, 353-359 (1978).

160. K. Nisancioglu and H. Holtan, "Measurement of the Critical Pitting Potential of Aluminum," Corrosion Sci. 18, 835-849 (1978).

161. K. Nisancioglu and H. Holtan, "The Protection Potential of Aluminum," Corrosion Sci. 18, 1011-1023 (1978).

162. K. Nisancioglu and H. Holtan, "Correlation of the Open-Circuit and Electrochemical Measurements for the Pitting Corrosion of Aluminum in Chloride Media," Werkstoffe u. Korrosion 30, 105-113 (1979).

163. N. W. Nurnberg, ed., Electroanalytical Chemistry, Wiley-Interscience, New York, 1975.

164. A. E. O'Keefe and G. C. Oitman, "Primary Standards for Trace Gas Analysis," Anal. Chem. 38(6), 760-763 (1966).

165. R. C. Olberg and J. L. Bozarth, "Factors Contributing to the Corrosion of the Aluminum Metal on Semiconductor Devices Packaged in Plastics," Microelectron. Reliab. 15(6), 601-611 (1976).

166. R. G. Oswald, J. M. Montante, and W. R. Rodrigues de Miranda, "Automated Tape Carrier Bonding for Hybrids," Proc Symp. Plastic Encapsulated/Polymer Sealed Semiconductor Devices for Army Equipment (US Army ERADCOM, Fort Monmouth, NJ), pp. 143-167 (1978).

167. W. M. Paulson and R. W. Kirk, "The Effects of Phosphorus-Doped Passivation Glass on the Corrosion of Aluminum," 12th Ann. Proc. Reliab. Phys., pp. 172-179 (1974).

168. W. M. Paulson and R. P. Lorigan, "The Effect of Impurities on the Corrosion of Aluminum Metallization," 14th Ann. Proc. Reliab. Phys., pp. 42-47 (1976).

169. D. S. Peck, "New Concerns about Integrated Circuit Reliability," 16th Ann. Proc. Reliab. Phys., pp. 1-6 (1978).

170. D. S. Peck and C. H. Zierdt, Jr., "Temperature-Humidity Acceleration of Metal-Electrolysis Failure in Semiconductor Devices," 11th Ann. Proc. Reliab. Phys., pp. 146-152 (1973).

171. K. L. Perkins and J. J. Licari, "Investigation of Moisture Effects on Selected Microelectronic Devices," Proc. 1978 Int. Microelectron. Symp., pp. 125-127, ISHM (Sept. 1978).

172. P. W. Peterson, "The Performance of Plastic Encapsulated CMOS Microcircuits in a Humid Environment," Proc. 29th Electronic Components Conf., pp. 360-365 (May 1979).

173. G. F. Piacentini and G. Minelli, "Reliability of Thin Film Conductors and Air Gap Crossovers for Hybrid Circuits: Tests, Results and Design Criteria," Microelectron. Reliab. 15, 451-458 (1976).

174. D. C. Porter and M. Bahan, "Failure Analysis of Plastic Encapsulated Custom LSI Circuits," Proc. Symp. Plastic Encapsulated/Polymer Sealed Semiconductor Devices for Army Equipment (US Army ERADCOM, Fort Monmouth, NJ), pp. 42-53 (1978).

175. M. Pourbaix, Atlas of Electrochemical Equilibria in Aqueous Solutions, Pergamon Press, Oxford, England, 1966.

176. M. Pourbaix, Lectures on Electrochemical Corrosion, translated by J. A. S. Green, Plenum Press, New York, 1973.

177. M. Pourbaix, "Some Applications of Potential-pH Diagrams to the Study of Localized Corrosion," J. Electrochem. Soc. 123, 25C-36C (Feb. 1976).

178. J. L. Prince, Jr., "Investigation of Factors Involved in Reliability Assurance of Plastic-Encapsulated Integrated Circuits," Dept. Electrical and Computer Eng., Clemson Univ., SC, Feb. 8, 1978.

179. J. L. Prince, D. B. Bullard, and R. A. Hartman, "Investigation of Accelerated Testing of Plastic-Encapsulated CMOS Integrated Circuits," GOMAC-78, Monterey, CA, Nov. 14, 1978, pp. 143-144.

180. A. Quach and W. L. Hunter, "A Study of Properties of Plastics Used for Semiconductor Encapsulation," J. Electronic Mater. 6, 319-331 (May 1977).

181. B. Reich, "Life Characteristics of Plastic Encapsulated Semiconductor Devices," Microelectron. Reliab. 17(5), 513-515 (1978).

182. B. Reich, "A Study of Accelerated Storage Test Conditions Applicable to Semiconductor Devices and Microcircuits," IEEE Trans. Reliab. R-27, 178-180 (Aug. 1978).

REFERENCES (Continued)

183. B. Reich, "Reliability of Plastic Encapsulated Semiconductor Devices and Integrated Circuits," Solid State Technol. 21(9), 82-88 (Sept. 1978).

184. Reliability Analysis Center, "Microcircuit Reliability Bibliography," MRB-78, RADC, Griffiss AFB, NY, April 1978.

185. Reliability Analysis Center, "Search and Retrieval Index to IRPS Proceedings - 1968 to 1978," TRS-2, RADC, Griffiss AFB, NY, 1979.

186. F. H. Reynolds and J. W. Stevens, "Semiconductor Component Reliability in an Equipment Operating in Electromechanical Telephone Exchanges," 16th Ann. Proc. Reliab. Phys., pp. 7-13 (1978).

187. L. T. Romankiw, "Technique For Measuring pH at Electrodes During Electrolysis," Preprint rec. Nov. 2, 1978.

188. R. Rosenberg, M. J. Sullivan, and J. K. Howard, "Effect of Thin Film Interactions on Silicon Device Technology," in J. M. Poate, K. N. Tu, and J. W. Mayer, eds., Thin Films - Interdiffusion and Reactions, Wiley-Interscience, New York, 1978.

189. R. S. Rosler, W. C. Benzing, and J. Baldo, "A Production Reactor for Low Temperature Plasma-Enhanced Silicon Nitride Deposition," Solid State Technol. 19(6), 45-50 (June 1976).

190. W. H. Safranek, The Properties of Electrodeposited Metals and Alloys, American Elsevier Publishing Co., New York, 1974, pp. 153-178.

191. A. N. Saxena and R. A. Powell, "Chemical State of Phosphorus in Deposited SiO_2 (P) Films," in S. T. Pantelides, ed., The Physics of SiO_2 and Its Interfaces, Pergamon Press, New York, 1978, pp. 195-199.

192. N. L. Sbar, private communication, 1978.

193. N. L. Sbar, "Bias-Humidity Performance of Encapsulated and Unencapsulated Ti-Pt-Au Thin-Film Conductors in an Environment Contaminated with Cl_2," IEEE Trans. Parts Hybr. Pkg. PHP-12, 176-181 (Sept. 1976).

194. N. L. Sbar, "Environmental Testing to Study Circuit Failure Mechanisms and Acceleration Factors," Electrochem. Soc. Ext. Abstr. 78-2, 668-669 (Oct. 1978).

195. N. L. Sbar and L. G. Feinstein, "Performance of New Copper Based Metallization Systems in an 85°C 80 Percent RH Cl_2 Contaminated Environment," IEEE Trans. Parts Hybr. Pkg. PHP-12, 208-218 (1976).

196. N. L. Sbar and R. P. Kozakiewicz, "New Acceleration Factors for Temperature, Humidity, Bias Testing," 16th Ann. Proc. Reliab. Phys., pp. 161-178 (1978).

REFERENCES (Continued)

197. G. M. Schmid and M. E. Curley-Fiorino, "Gold," in Vol. 4 of A. J. Bard, ed., *Encyclopedia of Electrochemistry of the Elements*, Marcel Dekker, Inc., New York, 1975, pp. 87-178.

198. G. L. Schnable, "Reliability of MOS Devices in Plastic Packages," Proc. Tech. Program Int. Microelectron. Conf. (West/East), pp. 82-91 (1976).

199. G. L. Schnable, "State of the Art in Semiconductor Materials and Processing for Microcircuit Reliability," Solid State Technol. 21(10), 69-73 (Oct. 1978).

200. G. L. Schnable, L. J. Gallace, and H. Pujol, "Reliability of CMOS Integrated Circuits," Computer 11(10), 6-17 (Oct. 1978).

201. G. L. Schnable, W. Kern, and R. B. Comizzoli, "Passivation Coatings on Silicon Devices," J. Electrochem. Soc. 122, 1092-1103 (Aug. 1975).

202. G. L. Schnable, E. M. Reiss, and M. Vincoff, "Reliability of Hermetically-Sealed CMOS Integrated Circuits," EASCON (Electronics and Aerospace Systems Convention) '76 Record, pp. 143-A to 143-G, Sept. 1976.

203. G. L. Schnable and P. F. Schmidt, "Applications of Electrochemistry to Fabrication of Semiconductor Devices," J. Electrochem. Soc. 123, 310C-315C (Sept. 1976).

204. P. wh Schuessler, "Polymer Sealed Devices in IBM Military Products," Proc. Symp. Plastic Encapsulated/Polymer Sealed Semiconductor Devices for Army Equipment (US Army ERADCOM, Fort Monmouth, NJ), pp. 240-249 (1978).

205. R. A. Schwartz, "Plastic Encapsulated Semiconductor Field Removal Data for Commercial Test and Measurement Equipment," Proc. Symp. Plastic Encapsulated/Polymer Sealed Semiconductor Devices for Army Equipment (US Army ERADCOM, Fort Monmouth, NJ), pp. 1-16 (1978).

206. S. Shabde, J. Edwards, and W. Meuli, "Moisture Induced Failure Mode in a Plastic Encapsulated Dynamic Timing Circuit," 15th Ann. Proc. Reliab. Phys., pp. 33-36 (1977).

207. S. P. Sharma, J. H. Thomas III, and F. E. Bader, "Development of a Gentle Accelerated Corrosion Test," J. Electrochem. Soc. 125, 2002-2004 (Dec. 1978).

208. T. Shirasu and Y. Kosa, "Electrical Instability of Water-Absorbed CVD PSG Films," Electrochem. Soc. Ext. Abstr. 79-1, 462-463 (May 1979).

209. A. Shumka and R. Haack, "Moisture and Other Contaminants in Hybrid Packages," Proc. 1978 Int. Microelectron. Conf., pp. 128-133, ISHM (Sept. 1978).

210. A. Shumka and R. R. Piety, "Migrated-Gold Resistive Shorts in Microcircuits," 13th Ann. Proc. Reliab. Phys., pp. 93-98 (1975).

211. D. W. Siitari and R. C. Alkire, "Experimental and Theoretical Modeling Studies on the Initiation of Crevice Corrosion," Electrochem. Soc. Ext. Abstr. 79-2, 618-619 (Oct. 1979).

212. L. G. Sillen and A. E. Martell, "Stability Constants of Metal-Ion Complexes," Spec. Publ. No. 17, The Chemical Society, London, 1964.

213. S. P. Sim and R. W. Lawson, "The Influence of Plastic Encapsulants and Passivation Layers on the Corrosion of Thin Aluminum Films Subjected to Humidity Stress," 17th Ann. Proc. Reliab. Phys., pp. 103-112 (1979).

214. J. D. Sinclair, "An Instrumental Gravimetric Method for Indexing Materials, Contaminants, and Corrosion Products According to Their Hygroscopicity," J. Electrochem. Soc. 12[illegible], [illegible]34-742 (May 1978).

215. A. K. Sinha, H. J. Levinstein, and T. E. Smith, "Thermal Stresses and Cracking Resistance of Dielectric Films (SiN, Si_3N_4 and SiO_2) on Si Substrates," J. Appl. Phys. 49, 2423-2426 (April 1978).

216. A. K. Sinha, H. J. Levinstein, T. E. Smith, G. Quintana, and S. E. Haszko, "Reactive Plasma Deposited Si-N Films for MOS-LSI Passivation," J. Electrochem. Soc. 125, 601-608 (April 1978).

217. A. K. Sinha and T. T. Sheng, "The Temperature Dependence of Stresses in Aluminum Films on Oxidized Silicon Substrates," Thin Solid Films 48, 117-126 (1978).

218. J. M. Smith and S. M. Stuhlbarg, "Hybrid Microcircuit Tape Chip Carrier Materials/Processing Trade-Offs," IEEE Trans. Parts Hybr. Pkg. PHP-13, 257-268 (Sept. 1977).

219. P. J. Smith, H. S. Wildman, and A. Leighton, "Pitting Corrosion in Al-Cu Thin Films," Electrochem. Soc. Ext. Abstr. 79-2, 640-642 (Oct. 1979).

220. D. T. Somerville, "The Role of Hybrid Construction Techniques on Sealed Moisture Levels," 15th Ann. Proc. Reliab. Phys., pp. 107-111 (1977).

221. N. A. Soos and D. Jaffe, "Encapsulation of Large Beam Leaded Devices," Proc. 28th Electronic Components Conf., pp. 213-216 (April 1978).

222. R. W. Staehle, "Marcel J. N. Pourbaix - Palladium Award Medalist," J. Electrochem. Soc. 123, 23C-25C (Feb. 1976).

223. Staff Article, "Quality Control for Epoxy Encapsulants," Circuits Manufacturing 18(3), 18-19 (March 1978).

224. Staff Article, "Fairchild Molds MOS Devices Faster, Better with Silicone/Epoxy Compound," Dow Corning Material News, p. 3 (Mar./Apr. 1979).

225. H.-H. Strehblow and C. J. Doherty, "Examination of Aluminum Copper Films During Anodic Oxidation - I. Corrosion Studies," J. Electrochem. Soc. 125, 30-33 (Jan. 1978).

226. R. E. Sulouff, "A Study of Leak Rate Versus Reliability of Hybrid Packages," Proc. 1978 Int. Microelectron. Symp., pp. 121-124, ISHM (Sept. 1978).

227. M. E. Sweet, "Assessment of Moisture Permeation of an Epoxy Sealed Test Module," Proc. 28th Electronic Components Conf., pp. 33-37 (April 1978).

228. C. H. Taylor, "Just How Reliable Are Plastic Encapsulated Semiconductors for Military Applications and How Can the Maximum Reliability Be Obtained?", Microelectron. Reliab. 15(2), 131-134 (1976).

229. C. H. Taylor and B. C. Roberts, "Evaluation of a UK Specification for the Procurement of Plastic Encapsulated Semiconductor Devices for Military Use," Proc. Symp. Plastic Encapsulated/ Polymer Sealed Semiconductor Devices for Army Equipment (US Army ERADCOM, Fort Monmouth, NJ), pp. 55-66 (1978).

230. R. E. Thomas, V. Winchell, K. James, and T. Scharr, "Plastic Outgassing Induced Wire Bond Failure," Proc. 27th Electronic Components Conf., pp. 182-187 (May 1977).

231. R. W. Thomas, "Moisture, Myths and Microcircuits," IEEE Trans. Parts Hybr. Pkg. PHP-12, 167-171 (Sept. 1976).

232. P. A. Totta, "Abstract: In-Process Intergranular Corrosion of Al Alloy Thin Films," J. Vac. Sci. Technol. 13, 26-27 (Jan./ Feb. 1978).

233. R. K. Traeger, "Organics Used in Microelectronics: A Review of Outgassing Materials and Effects," Proc. 27th Electronic Components Conf., pp. 408-420 (May 1977).

REFERENCES (Continued)

234. H. H. Uhlig, Corrosion and Corrosion Control, John Wiley & Sons, Inc., New York, 1963.

235. H. H. Uhlig, "Advances in Corrosion Over the Past 25 Years," J. Electrochem. Soc. 125, 58C-61C (Feb. 1978).

236. T. Valand and G. Nilsson, "The Influence of F^- Ions on the Electrochemical Reactions on Oxide-Covered Al," Corrosion Sci. 17, 449-459 (1977).

237. M. Vandenberg, "Properties of Plasma Deposited Silicon Oxide," Electrochem. Soc. Ext. Abstr. 79-1, 262-264 (May 1979).

238. M. Vandenberg and M. S. Hassan, "Cracking of Plasma Deposited Si-N Films After Subsequent Anneal," Electrochem. Soc. Ext. Abstr. 79-1, 234-235 (May 1979).

239. E. P. G. T. van de Ven and H. Koelmans, "The Cathodic Corrosion of Aluminum," J. Electrochem. Soc. 123, 143-144 (Jan. 1976).

240. R. W. Vasofsky, "Water Vapor Sorption of Package Sealants," 17th Ann. Proc. Reliab. Phys., pp. 91-96 (1979).

241. Vasofsky, A. W. Czanderna, and K. K. Czanderna, "Abstract: Water Vapor Sorption by Cured Commercial Epoxies," J. Vac. Sci. Technol. 16, 716 (March/April 1979).

242. J. L. Vossen et al., "Bibliography on Metallization Materials and Techniques for Silicon Devices, I to V," Thin Film Div., American Vacuum Society, New York, NY, 1974-1979.

243. J. L. Vossen and W. Kern, eds., Thin Film Processes, Academic Press, New York, 1978.

244. J. L. Vossen, G. L. Schnable, and W. Kern, "Processes for Multilevel Metallization," J. Vac. Sci. Technol. 11, 60-70 (Jan./Feb. 1974).

245. B. L. Weigand, J. J. Licari and I. H. Pratt, "Detection of Conductive Condensates Resulting from Adhesive Outgassing in Hybrid Microcircuits," Proc. 28th Electronic Comp. Conf., pp. 217-222 (April 1978).

246. J. K. Whittington, G. T. Malloy, A. R. Mastro, and R. D. Hutchens, "Internal Conformal Coatings for Microcircuits," IEEE Trans. Components, Hybr. Mfg. Technol. CHMT-1, 416-422 (Dec. 1978).

247. R. E. Williams, "Improvements in Plastic Integrated Circuits - Molding Compounds, Assembly Techniques and Reliability," Proc. Symp. Plastic Encapsulated/Polymer Sealed Semiconductor Devices for Army Equipment (US Army ERADCOM, Fort Monmouth, NJ), pp. 184-196 (1978).

REFERENCES (Continued)

248. D. B. Willmott, "Investigation of Metallization Failures of Glass Sealed Ceramic Dual Inline Integrated Circuits," 15th Ann. Proc. Reliab. Phys., pp. 158-162 (1977).

249. J. C. Wright, "Reliability Improvements of Plastic Semiconductors Using Gold Metallization," 11th Ann. Proc. Reliab. Phys., pp. 224-229 (1973).

250. K. D. Zastrow, "Artillery Fuze Experience with Plastic Encapsulated Semiconductor Devices," Proc. Symp. Plastic Encapsulated/Polymer Sealed Semiconductor Devices for Army Equipment (US Army ERADCOM, Fort Monmouth, NJ), p. 54 (1978).

251. C. H. Zierdt, Jr., "Procurement-Specification Techniques for Plastic-Encapsulated Semiconductor Devices and Integrated Circuits," Proc. Symp. Plastic Encapsulated/Polymer Sealed Semiconductor Devices for Army Equipment (US Army ERADCOM, Fort Monmouth, NJ), pp. 84-96 (1978).

252. C. H. Zierdt, Jr., "Accelerated Life Testing for LSI Failure Mechanisms," 16th Ann. Proc. Reliab. Phys., pp. 76-78 (1978).

MISSION
of
Rome Air Development Center

RADC plans and executes research, development, test and selected acquisition programs in support of Command, Control Communications and Intelligence (C^3I) activities. Technical and engineering support within areas of technical competence is provided to ESD Program Offices (POs) and other ESD elements. The principal technical mission areas are communications, electromagnetic guidance and control, surveillance of ground and aerospace objects, intelligence data collection and handling, information system technology, ionospheric propagation, solid state sciences, microwave physics and electronic reliability, maintainability and compatibility.